NORTHWESTERN UNIVERSITY

FUNCTIONAL CHARACTERIZATION OF THE MULTI-DOMAIN HERPESVIRUS ESSENTIAL TEGUMENT PROTEIN VP1/2: AT THE CORE OF INFECTIOUS PROCESSES

A DISSERTATION

SUBMITTED TO THE GRADUATE SCHOOL
IN PARTIAL FULFILLMENT OF THE REQUIREMENTS

for the degree

DOCTOR OF PHILOSOPHY

Field of Microbiology and Immunology

Northwestern University Interdepartmental Neuroscience Program (NUIN)

By

Joy I-Hsuan Lee

EVANSTON, ILLINOIS

DECEMBER 2007

ABSTRACT

FUNCTIONAL CHARACTERIZATION OF THE MULTI-DOMAIN HERPESVIRUS ESSENTIAL TEGUMENT PROTEIN VP1/2:
AT THE CORE OF INFECTIOUS PROCESSES

Joy I. Lee

The neurotropic alphaherpesviruses infect and spread trans-synaptically within the vertebrate nervous system. Recurrent diseases are often manifested at the periphery of the host organism but occasional dissemination of the virus to the brain results in fatal encephalitis. Interactions between viral and host cellular proteins are integral to the success of a life-long infection. While inside the host cell, the most accessible viral component may include the DNA-enclosing capsid and the tegument layer, a collection of ~15 proteins that mediate a wide range of functions. This dissertation work investigates the largest virally encoded protein within the tegument, VP1/2, which is essential for viral propagation. A VP1/2-null virus was used to first establish the importance of VP1/2 in capsid intracellular transport during infection. A domain-specific mutational analysis was then used to correlate essential functions to VP1/2 regions. We find that the amino terminus of VP1/2, encompassing the deubiquitinase activity, is not essential for viral propagation but required for neuroinvasion. The carboxy terminus of VP1/2 can exist as a cleaved form to function independently of the full-length protein to

mediate capsid nuclear egress. The direct interaction of VP1/2 with capsid proteins, both cytoplasmic and nuclear, was examined and the binding domain identified. In all, this work unravels the very large, essential tegument protein VP1/2 to reveal novel functions of its multiple domains.

ACKNOWLEDGEMENTS

I would like to thank my thesis advisor and mentor, Dr. Greg Smith, for exemplifying the foundations of success: integrity, perseverance and a commitment to excellence. From passionate descriptions of project rationales, to fierce intellectual challenges, to feigned disappointment, to the interminable store of constructive criticisms, Dr. Smith has been effective as well as inspirational. I could not have developed my skills as fully under the guidance of another advisor.

I would also like to express my gratitude to all members of my thesis committee: Dr. Pat Spear, Dr. Richard Miller, and Dr. Peter Penzes. Every meeting with my committee was positive and productive. In particular, I am thankful to Dr. Spear for often times knowing my projects better and myself.

Another group of people instrumental to my training are my labmates. Working long hours in close quarters with Sarah Antinone and Kelly Coller has been a blessing and a necessary component to my professional development. Many scientific insights over the years were the direct result of our discussions. And more importantly, the companionship during hardship was what helped me stay the course.

Outside of the work environment, my emotional well-being was nurtured by these following friends: Tess Aman, Katie Drerup, Adam Stocker, Emi Nomura, and Sonia Bhangoo.

Lastly, I would like to acknowledge the support of my family. My father taught me to be proactive in all my undertakings but stay conscious of how my actions impact those around me. My mother taught me the importance of deriving happiness from my chosen endeavors and how to be compassionate to the less fortunate. My brother is always ready to listen and share insights even at the most wicked hours of the day. Finally, I would not be as motivated to dash to the finish line without my fiancé, Richard Tsai. I am forever indebted to Richard for his love, patience, and immovable faith in me.

LIST OF ABBREVIATIONS

aa	Amino acid
ARR	Alanine-rich region
ß-ME	Beta-mercaptoethanol
BGS	Bovine growth serum
BSA	Bovine serum albumin
bp	Base pair
C	Celsius
CBD	Capsid-binding domain
cm	Centimeter
CMV	Cytomegalovirus
CNS	Central nervous system
DIC	Differential interference contrast
DMEM	Dulbecco’s modified Eagle medium
DNA	Deoxyribonucleic acid
EGTA	Ethylenebis tetraacetic acid
EM	Electron microscopy
EW	Edinger-Westphal nucleus
FRT	Flp recombination target
g	Gram (as in 100 g)
g	Gravity (as in 10,000 × g)

GFP	Green fluorescence protein
h	Hour
hpi	Hours post infection
hrs	Hours
HSV-1	Herpesvirus Simplex Type 1
HSV-2	Herpesvirus Simplex Type 2
IE	Immediate early
kbp	kilobase pair
kD	kilodalton
L	Liter
LGN	Lateral geniculate nucleus
M	Molar
$MgCl_2$	Magnesium chloride
μg	Microgram
μl	Microliter
μm	Micrometer
μM	Micromolar
mg	Miligram
ml	Milimeter
mM	Milimolar
ms	Milisecond
mRFP1	Monomeric red fluorescence protein

MOI	Multiplicity of infection
NA	Numerical aperture
NaCl	Sodium chloride
NP-40	Nonidet P-40
nt	Nucleotide(s)
ORF	Open reading frame
rpm	Revolutions per minute
p	Plasmid (as in pGS1324)
PAGE	Polyacrylamide gel electrophoresis
PBS	Phosphate-buffered saline
PCR	Polymerase chain reaction
PEI	Polyethylenimine
PFU	Plaque forming unit(s)
PIPES	PIPES sodium salt
PK15	Pig kidney epithelial cells
PNS	Peripheral nervous system
PRR	Proline-rich region
PRV	Pseudorabies virus
PVN	Paraventricular nucleus
Rev	Revertant (virus)
RGC	Retinal ganglion cell
s	Second(s)

SCN	Suprachiasmatic nucleus
SDS	Sodium dodecyl sulfate
T	Time (time post-infection)
UL	Unique long region (as in UL36)
Us	Unique short region (as in Us3)
UV	Ultraviolet (wavelength)
v	Virus (as in vGS909)
VP	Viral protein (as in VP1/2)
WT	Wild-type

TABLE OF CONTENTS

LIST OF FIGURES

LIST OF TABLES

CHAPTER 1: INTRODUCTION

HUMAN HERPESVIRUS DISEASES

Herpesviruses are divided into three subfamilies: *alphaherpesviridae, betaherpesviridae,* and *gammaherpesviridae*. All neurotropic herpesviruses belong to the alpha-herpesvirus subfamily. Human infections by alpha-herpesviruses result in conditions that range from mild recurrent skin lesions, to the excruciating pain of neuralgia, to fatal encephalitis (28). A recent National Health and Nutrition Examination Surveys (NHAES) report states the prevalence of Herpes simplex virus type 1 (HSV-1) and type 2 (HSV-2) in the US adult population at 57.7% and 21%, respectively (113). There are eight human herpesviruses across all three *Herpesviridae* subfamilies : HSV-1, HSV-2, varicella-zoster virus (VZV), Epstein-Barr virus (EBV), human cytomegalovirus (HCMV), and human herpesvirus 6, 7, and 8 (HHV-6, -7, -8). HSV-1 infections most commonly result in the benign disease herpes labialis. However, the recurrent form of human herpesvirus disease can also result in ocular lesions, which is a leading cause of blindness, and severe disseminated infections in immunocompromised individuals. Sporadic infections of the CNS resulting from trans-synaptic spread of HSV-1 in otherwise healthy individuals are typically lethal. VZV causes chicken pox and shingles and may disseminate into generalized skin lesions and CNS neuralgia in immunocompromised individuals. Disease forms of human herpesviruses are summarized in Table 1.1. No cure is available for herpesvirus disease. Current treatment employs anti-viral dugs such as acyclovir or gancyclovir to target virally encoded thymidine kinase expressed in infected cells.

TABLE 1.1. HUMAN HERPESVIRUS DISEASES

Virus	Subfamily	Disease
Herpes simplex virus type 1 (HSV-1)	Alphaherpesviridae	Mucosal lesions, encephalitis
Herpes simplex virus type 2 (HSV-2)	Alphaherpesviridae	Genital lesions, encephalitis
Varicella-zoster virus (VZV)	Alphaherpesviridae	Chickenpox, shingles
Cytomegalovirus (HCMV)	Betaherpesviridae	Congenital defects; opportunistic pathogen in immunocompromised patients
Human herpesvirus 6 (HHV-6)	Betaherpesviridae	Roseola
Human herpesvirus 7 (HHV-7)	Betaherpesviridae	Orphan virus
Epstein-Barr virus (EBV)	Gammaherpesviridae	Infectious mononucleosis; associated with a variety of lymphomas
Human herpesvirus 8 (Kaposi's sarcoma-related virus)	Gammaherpesviridae	Kaposi's sarcoma rare B-cell lymphoma

Adapted from *Principles of Virology* 2nd edition.

HERPESVIRUS VIRION STRUCTURE

All herpesviruses share a common structure: 1) a linear, double-stranded DNA genome encoding 80-250 genes, 2) an icosahedral protein shell termed the capsid that encapsidates the large DNA genome, 3) a layer of proteins called the tegument surrounding the capsid, and 4) a host-derived lipid bilayer envelope containing membrane glycoproteins. All of these structures can be resolved using electron microscopy (EM) (Figure 1.1), in particular, recent advances in tomography techniques allow the preliminary identification of capsid surface electron densities as specific proteins. Such studies are beginning to bridge the knowledge gap between the capsid and tegument components of the virion.

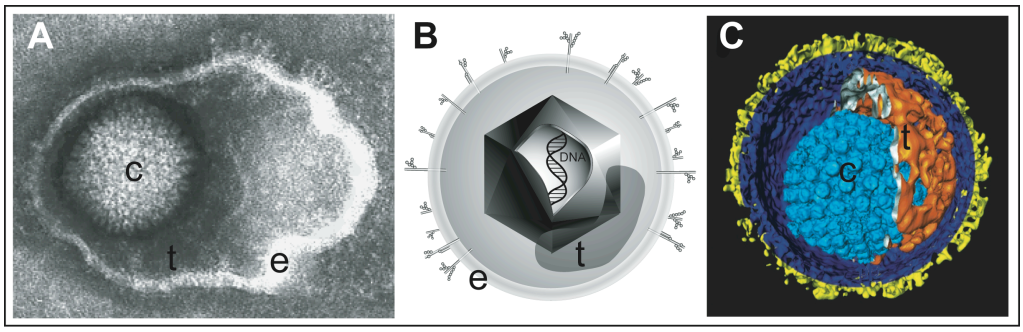

Figure 1.1. Herpesvirus virion structure.

Herpesvirus virion structure visualized as: (A) Negatively stained virion electron micrograph [99]. (B) illustration. (C) reconstruction of cryo-EM tomography [38]. c: capsid, t: tegument, e: envelope.

NEUROTROPISM AND INFECTIOUS CYCLE

Neurotropic herpesviruses belong to the alpha subfamily and are distinguished by their ability to establish latency in neurons, which requires the trans-synaptic spread from the peripheral nervous system (PNS) to CNS or within the CNS. Interestingly, transmission of virus from its natural host to other susceptible species generally ends in fatal encephalitis. Neuroanatomists have greatly benefited from these circuit-specific and self-amplifying tracers to map circuits in the CNS using PRV and HSV-1 in susceptible *dead-end* hosts. Another interest in herpesvirus neurotropism includes the development of target-specific vectors in anti-brain tumor therapies (2).

Herpesviruses infections typically begin in exposed epithelia, then disseminate through innervating axons to peripheral sensory ganglia where life-long, latent infections are established. Recurrent infections occur following reactivation from latency and progeny virions travel through axons in the anterograde direction back to the periphery. Another less common route of the virus is to enter the central nervous system (CNS) leading to devastating consequences. Notably, axonal transport underlies both primary and reactivated forms of alphaherpesvirus infections.

Herpesvirus infection begins when the viral envelope fuses with the host cell plasma membrane. At least four viral glycoproteins are required to mediate the initial attachment to cellular surface as well as the subsequent fusion via interactions with cellular receptors (97). The viral proteins that enter the cytosol include the DNA-containing capsid and the tegument. The capsid then transports along microtubules with a subset of tegument proteins towards the cell nucleus (55). The viral genome is

deposited through the nuclear pore complex (Figure 1.2).

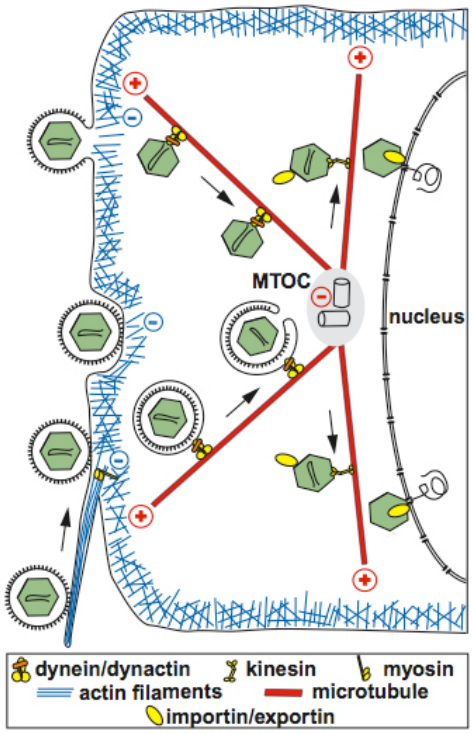

Figure 1.2. Infectious cycle: Entry

Herpesvirus infectious cycle begins with viral entry into host cells. Gradually components of the virion dissociate until final delivery of the viral genome into the nucleus. Infections in neurons are similar to the epithelial cell infections depicted here, with the exception that microtubule-based transport covers a longer distance. Two types of viral particles are shown to undergo microtubule-based transport. The unenveloped particles have entered the cell via membrane fusion and the enveloped particles transverse the plasma membrane through endocytosis.

Adapted from Radtke *et. al.*, 2006. *Journal of Virology* [79]

Upon reactivation newly replicated copies of the viral genome are packaged into the capsids assembled in the nucleus. For capsids to translocate from the nucleus into the cytosol, several events must take place. First the DNA-filled capsids move through the nuclear lamina network that has been locally dissolved by tegument proteins UL31 and UL34 (81). Once in close proximity to the inner nuclear membrane, capsids bud into the internuclear space, thus completing the first envelopment step. This enveloped particle is termed the primary virion. The budding event or vesicular formation at the inner nuclear membrane is also mediated by the tegument proteins UL31 and UL34 (45). Capsids cross the outer nuclear membrane by fusion (or deenvelopment) and enters the cytosol as an unenveloped particle. The envelopment-deenvelopment model of nuclear egress is widely accepted despite the recent report of an alternative mechanism. Wild et. al. proposed that the nucleus of infected cells swell and expand such that the pore diameter becomes large enough for the passage of capsids without involving the nuclear membranes (111). Once in the cytosol, at least a subset of tegument proteins are believed to assemble onto the capsid prior to acquisition of the glycoprotein-studded envelope. The precise location of the secondary envelopment has yet to be unequivocally determined. Particles transport along microtubules to the plasma membrane and are released as fully assembled virions (Figure 1.3).

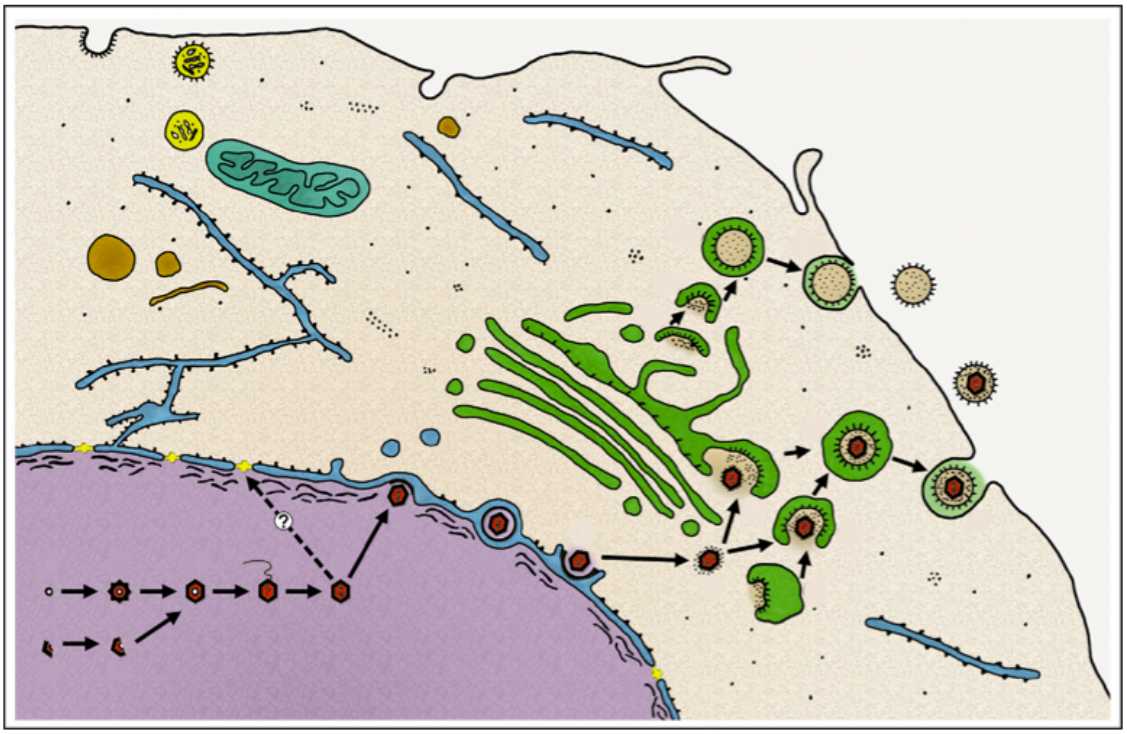

Figure 1.3. Infectious cycle: Egress.

Newly replicated viral genome is packaged into capsids that are assembled in the nucleus. The translocation of capsids into the cytosol involve the envelopment at the inner nuclear membrane and the deenvelopment at the outer nuclear membrane. Unenveloped capsids in the cytosol acquires tegument proteins and host-derived envelope with glycoproteins and transport to the plasma membrane for release. Adapted from Mettenleiter *et. al*., 2007. *Journal of Virology* [69]

HERPESVIRUS INTRACELLULAR TRANSPORT

During the herpesvirus infectious cycle, the successful translocation of viral genome into the nucleus of peripheral neuronal soma is a prerequisite for latency establishment. Once inside the cell, all envelope components dissociate from the capsid (57, 58, 60). Tegument proteins as well as capsid proteins travel as one major complex or further dissemble into smaller entities when traveling along the axon. During entry transport, a subset of tegument proteins (VP1/2, UL37, and Us3) remain associated with the capsid where as other tegument proteins (VP16, VP13/14, and VP22) are shed from the capsid surface (35, 55). Viral capsid complexes transporting inside axons move bi-directionally, exhibiting components of both anterograde and retrograde motility. During entry, when the net direction of travel is towards the nucleus, the retrograde component of the bi-directional travel (92) of viral protein complex dominates while the reverse is true for the net anterograde events during egress.

During both entry and egress, capsid transport is microtubule(MT)-based. High resolution electron microscopy (EM) studies have documented the colocalization of capsids with MTs and microtubule-depolymerizing drugs block infection (94). The cargos traveling on MTs typically utilize two classes of motors: dyneins and kinesins. The exact mechanism of herpesvirus axonal transport is currently unknown although numerous attempts have been made at identifying the cellular interacting partners of viral proteins (23, 24, 103, 114).

PSEUDORABIES VIRUS (PRV) AS A MODEL SYSTEM

Pseudorabis virus (PRV) is closely related to HSV and VZV (63, 64), and serves as a useful model virus to study the biology of neurotropic herpesviruses. The first advantage PRV offers over HSV and VZV arises from the broad host range susceptible to PRV infections. All vertebrates, except higher primates, are permissive for PRV infection that manifests as fatal encephalitis (25). The methods of the rat eye model system for studying neurovirulence and neuroinvasion will be presented in Chapter 4. Second, the full-length infectious clone of PRV is engineered into a self-excising bacterial artificial chromosome (BAC) in *E. coli*, which is advantageous to use over traditional plaque purification techniques as previously described (89). Together with a novel two-step recombination system of bacterial mutagenesis (101), the high degree of manipulation in the PRV infectious clone allows for the dissection of function in targeted regions of specific proteins. Third, PRV does not pose human safety concerns as it does not infect higher primates.

TEGUMENT PROTEINS INTRACELLULAR FUNCTION

The tegument layer is comprised of >15 different proteins, covering a wide array of functions, as summarized in Table 1.2. The herpesvirus infectious cycle is directed by viral interactions with host proteins, and different members of the tegument are believed to encode functions that adapt cellular machinery to the propagation of the virus. Most of the tegument proteins studied to date are dispensable for viral replication and therefore considered to play accessory roles to capsid delivery and association. Essential tegument proteins include VP1/2 and UL37 (in HSV-1), which are also two of the proteins transporting with the capsid complex (35, 55). VP1/2 and UL37 are known as the *inner tegument* due to their close association with the capsid (reviewed in 68). Outer tegument proteins are likely assembled through interactions with VP16 (encode by UL48 gene), which in turn directly interacts with VP1/2. Other protein-protein interactions such as UL37-UL37, UL47-UL48, and UL48-UL49 have been identified (107), refining the previous characterization of tegument being an amorphous layer. A complex organization is emerging as more interactions are identified and studied. An additional complication was put forth in a recent report suggesting the transience of previously compartmentalized protein-protein interactions (66), therefore raising even more combinatorial possibilities to how the tegument layer functions during infection.

TABLE 1.2. TEGUMENT PROTEIN FUNCTIONS

Genes	Gene Product	Functions
UL4		Enhances virion formation[30]
UL11		Myristoylated protein, involved in egress
		Interacts with UL16[107]
UL13	Protein Kinase UL13	Phosphorylates Us3, involved in nuclear egress[40]
UL14		Molecular chaperone function
UL21		Interacts with UL16[42]
UL36	VP1/2	Essential protein associated with transporting capsid[55]
		Interacts with UL37
UL37		Encodes nuclear export signal, important in egress, interacts with UL36 (VP1/2)[43] and itself (UL37)[107]
UL41	vhs (host shutoff protein)	Causes the degradation of mRNA; interacts with UL48 (VP16)[86]
UL46	VP11/12	Interacts with UL48 (VP16)
UL47	VP13/14	Enhances immediate early gene expression
		Interacts with UL48 (VP16)[107]
UL48	VP16	Stimulation of immediate early gene expression
		Interacts with VP22, vhs, VP11/12, VP13/14[86, 107]
UL49	VP22	Encodes intracellular trafficking activity, interacts with UL48 (VP16)[107]
UL51		Palmitoylated virion protein, associated with the Golgi
UL56		Type II membrane protein, associated with the Golgi and early endosome
ICP0		Promiscuous transactivator with E3 ubiquitin ligase domains
ICP4		Major regulatory protein
Us3	Protein Kinase Us3	Protein kinase with antiapoptotic activity, regulates UL31 and UL34 during nuclear egress[40]
Us10		Tightly associated with capsids
Us11		RNA-binding activity, intracellular trafficking activity

Adapted from Nishiyama 2004, with added references.

THE ROLE OF ESSENTIAL TEGUMENT PROTEIN VP1/2 DURING INFECTION

VP1/2 (Viral protein 1/2; also known as ICP1/2 or VP1-3) is encoded by the UL36 gene (65, 98). VP1/2 is essential for the propagation of HSV-1 and PRV(19, 32). In the absence of VP1/2, several steps of the infectious cycle are disrupted, including: capsid nuclear egress, secondary envelopment, and microtubule-based intracellular transport (19, 32, 56). A null mutation of the UL36 gene prevents virus replication, which limits its study. Propagation of the null mutant can be achieved using a complementing cell line; however, complemented viral stocks are unsuitable for study of initial events during infection because of the incorporation of VP1/2 in the complemented virion inoculum. No information is currently available for the requirement of VP1/2 during initial infection intracellular transport except for its association with the capsid (55). Another stage of infection suggested to be mediated by VP1/2 involves the delivery of the viral genome into the host nucleus. A temperature-sensitive mutation mapping to the UL36 gene failed to release the viral genome through the nuclear pore complex post docking of the capsid (5). VP1/2 may also encode for functions in the nuclear compartment of the cell as it is suggested to be involved in the packaging and cleavage of viral DNA (12). In addition to the possible nuclear functions, the site of VP1/2 assembly onto the capsid complex is an area of immense interest. Detergent extraction studies combined with ultrastructural analyses indicate that VP1/2, an inner tegument protein, is associated with pentons at the capsid surface (34, 106, 117). A newly identified capsid-binding domain on the extreme carboxy terminus of VP1/2 further piques the interest of potential nuclear tegumentation events prior to capsid nuclear egress (13). Finally, a collection of studies

has demonstrated the biochemical qualities of a VP1/2-encoded deubiquitinase (DUB) within the amino terminus of the protein (41, 82, 84), adding another activity to VP1/2 already impressive list of important functions.

PURPOSE

The goal of my dissertation work was to investigate the role of essential tegument protein VP1/2 in cells during infection. Based on work by others and my collaborative work with a former graduate student, I followed a top-down approach to studying VP1/2. The very large tegument protein (3084aa) VP1/2 was first characterized as a whole, then broken down into smaller domains and finally even more focused regions were analyzed. Studying an essential protein required the development of novel assays to circumvent the inability to propagate a non-viable virus. After identifying various conserved regions throughout VP1/2, mutagenesis studies in the majority of the protein have been carried out by numerous members of the lab while I performed carefully designed experiments to understand the function of the amino and carboxy termini during infection.

The aims of this thesis work were to:

1) Determine the impact on capsid transport of the absence of the associated VP1/2
2) Identify essential VP1/2 domains that mediate critical functions during infection
3) Investigate the function of the deubiquitinase-encoding amino terminus in neuroinvasion
4) Identify the naturally occurring VP1/2 fragments and characterize their functions

CHAPTER 2: THE PSEUDORABIES VIRUS VP1/2 TEGUMENT PROTEIN IS REQUIRED FOR INTRACELLULAR CAPSID TRANSPORT

(This chapter appeared as the published article, “The pseudorabies virus VP1/2 tegument protein is required for intracellular capsid transport”, by G.W.G. Luxton, J. I. Lee, S. Haverlock-Moyns, J. M. Schober, and G. A. Smith, 2006, *J Virol.* **80:** 201-209)

SUMMARY

Transport of capsids in cells is critical to alpha-herpesvirus infection and pathogenesis; however, viral factors required for transport have yet to be identified. Here we provide a detailed examination of capsid dynamics during the egress phase of infection in Vero cells infected with pseudorabies virus. We demonstrate that the VP1/2 tegument protein is required for processive microtubule-based transport of capsids in the cytoplasm. A second tegument protein that binds to VP1/2, UL37, was necessary for wild-type transport but was not essential for this process. Both proteins were also required for efficient nuclear egress of capsids to the cytoplasm.

INTRODUCTION

Viruses must overcome the diffusion barrier of the cytoplasm to effectively replicate in mammalian cells. This is most dramatically exemplified with neurotropic infections, such as those of the alpha-herpesviruses, during which virus particles may translocate several centimeters or more between axon terminals and neuronal cell bodies. Intracellular transport of alpha-herpesvirus particles to the nucleus in both neurons and non-neuronal cells is dependent on microtubules (51, 59, 72, 95).

The alpha-herpesvirus virion is composed of four structural elements. The viral genome consists of a linear double-stranded DNA (~120-230 kbp), that is housed within a proteinacious capsid having icosahedral symmetry (~120 nm diameter). The capsid is enclosed within a host-derived lipid envelope, and between the capsid and the envelope is a collection of viral proteins collectively referred to as the tegument. Upon entry into a cell the viral envelope fuses with the cellular plasma or endosomal membrane, depositing the capsid and tegument into the cytosol (33, 73, 74). At this phase, many tegument proteins are removed from the capsid. However, at least three tegument proteins (VP1/2, UL37 and US3) remain associated with capsids as they travel toward the nucleus (35, 55). Following replication and assembly of capsids in the nucleus, progeny capsids translocate to the cytosol where they are again found associated with the VP1/2, UL37 and US3 tegument proteins (31, 36). These capsid/tegument complexes ultimately bud into a component of the secretory pathway and egress from the cell (reviewed in 67). The dynamics of capsid transport and assembly in the

cytoplasm are poorly understood.

Although many alpha-herpesvirus proteins can interact with cellular microtubule-based motors, no herpesvirus proteins are currently known to be required for capsid transport (21, 22, 24, 50, 61, 76, 115). The presence of VP1/2, UL37 and US3 on cytosolic capsids makes them prime candidates as effectors of intracellular capsid transport. Of particular interest to the current study, cells infected with viruses lacking either VP1/2 or UL37 assemble genome-containing capsids in the nucleus, and these capsids egress to the cytoplasm similar to capsids of wild-type viruses. However, once in the cytoplasm, unenveloped capsids lacking either VP1/2 or UL37 accumulate, and re-envelopment is rare or non-existent (18-20, 32, 46, 47). One possible explanation of this accumulation is a failure of capsids to translocate to the site of secondary envelopment within the cytoplasm. We therefore set out to characterize capsid dynamics during the egress phase of infection, and to determine if either VP1/2 or UL37 is necessary for intracellular capsid transport.

RESULTS AND DISCUSSION

Isolation of fluorescent-capsid viruses lacking either the VP1/2 or UL37 tegument protein.

We have previously described infectious clones of PRV that encode the VP26 capsid protein fused to a fluorescent protein (i.e. GFP or mRFP1), and have wild-type growth properties in culture (55, 91, 92). To test the roles of VP1/2 and UL37 in intracellular capsid transport, recombination in *E. coli* was used to replace either nucleotides 4-8910 of the 9255 nt UL36 ORF, or nucleotides 46-2199 of the 2760 nt UL37 ORF, with a TAA stop codon followed by a 34 bp FRT site (Figure 2.1A). This was accomplished by RED-mediated insertion of a kanamycin cassette flanked by a pair of FRT sites, followed by Flp-mediated excision of the kanamycin cassette (Figure 2.1B).

VP1/2 is essential for herpesvirus growth in cultured cells, while UL37 is essential for the growth of herpes simplex virus type 1 and is necessary for wild-type growth of PRV (19, 20, 32, 49, 90). To verify that the ΔUL36 (VP1/2-null) and ΔUL37 mutations introduced into the PRV infectious clones impacted viral growth as expected, each clone was transfected into PK15 cells and capsid fluorescence was monitored (Figure 2.2A). A virus with intact UL36 and UL37 genes resulted in productive infections as noted by spread of capsid-fluorescence to all cells with corresponding cytopathic effects (i.e. cell rounding). In contrast, transfection of the ΔUL36 clone resulted in fluorescent-capsid expression in single cells only. The lack of viral spread from cell to cell was consistent with a lethal mutation. The ΔUL37 clone displayed minimal spread.

Figure 2.1. Description of VP1/2-null virus and VP1/2-complementing cell line.

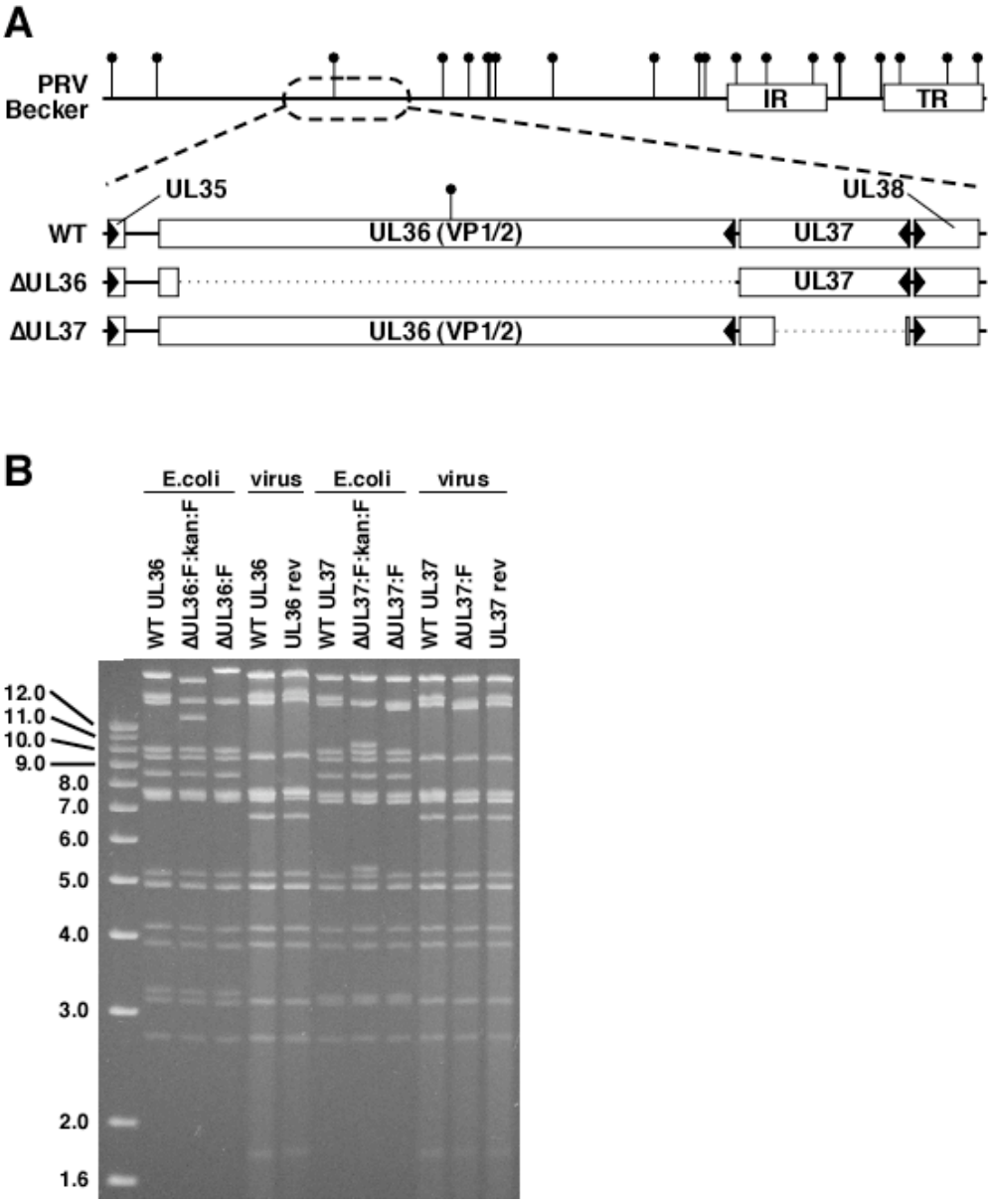

Figure 2.1: Description of VP1/2-null virus and VP1/2-complementing cell line.

A) Illustration of the PRV genome with characteristic internal and terminal repeats (IR and TR respectively) shown as white rectangles. *Bam*HI sites are indicated by vertical lollipops. The region of the genome relevant to this report is expanded to show the UL36 and UL37 ORFs, as well as the neighboring UL35 and UL38 ORFs (arrowheads indicate gene orientation). Below, dotted lines indicate regions deleted in the ΔUL36 (PRV-GS678) and ΔUL37 (PRV-GS993) viruses. B) EtBr-stained agarose gel of *Bam*HI digested infectious clone DNAs isolated from *E. coli* and corresponding viral DNA isolated from nucleocapsids. The UL36 gene overlaps the two largest *Bam*HI fragments of the viral genome, while the UL37 gene is exclusively on the second largest fragment. The FRT:kan:FRT insertion is ~ 1.5 kbp and encodes two *Bam*HI sites within the kanamycin-resistance cassette, resulting in the truncation of the two large fragments during the ΔUL36 construction, and split of the second largest fragment into two smaller fragments during the ΔUL37 construction. Removal of the kanamycin-resistance cassette and one FRT equivalent results in fusion of the remainders of the two largest fragments to produce the final ΔUL36 allele, and the reunion of the remainders of the second largest fragment to produce the final ΔUL37 allele. Additional fragment variations seen between the infectious clone plasmids and viral DNA result from loss of the *E. coli* vector backbone as described in (89).

To propagate the ΔUL36 and ΔUL37 virus for further study, complementing cell lines stably expressing either VP1/2 (PK15-UL36) or UL37 (PK15-UL37) were made. PK15-UL36 cells failed to fully complement growth of the ΔUL36 virus, as VP1/2-null virus produced small foci (Figure 2.2B). The inability of VP1/2-expressing cells to fully complement PRV lacking VP1/2 was previously noted by others (32). Trans-complementation of the ΔUL37 virus resulted in efficient viral spread throughout the cell culture.

To avoid reversion of the deletion viruses by recombination with the wild-type UL36 or UL37 genes in complementing cells, complemented viral stocks were examined by infection of non-complementing cells (Figure 2.2B). In one case, a spontaneous UL36 revertant was harvested from PK15 cells and further examined (not shown). The revertant virus grew with wild-type growth kinetics, and was saved for use as a control in subsequent experiments (Figure 2.3A). A spontaneous UL37 revertant was never observed; however, a UL37 revertant was isolated following infection of PK15 cells transiently transfected with a full-length UL37 construct. Unlike the ΔUL37 virus, which grew poorly, the revertant virus grew with wild-type kinetics (Figure 2.3B).

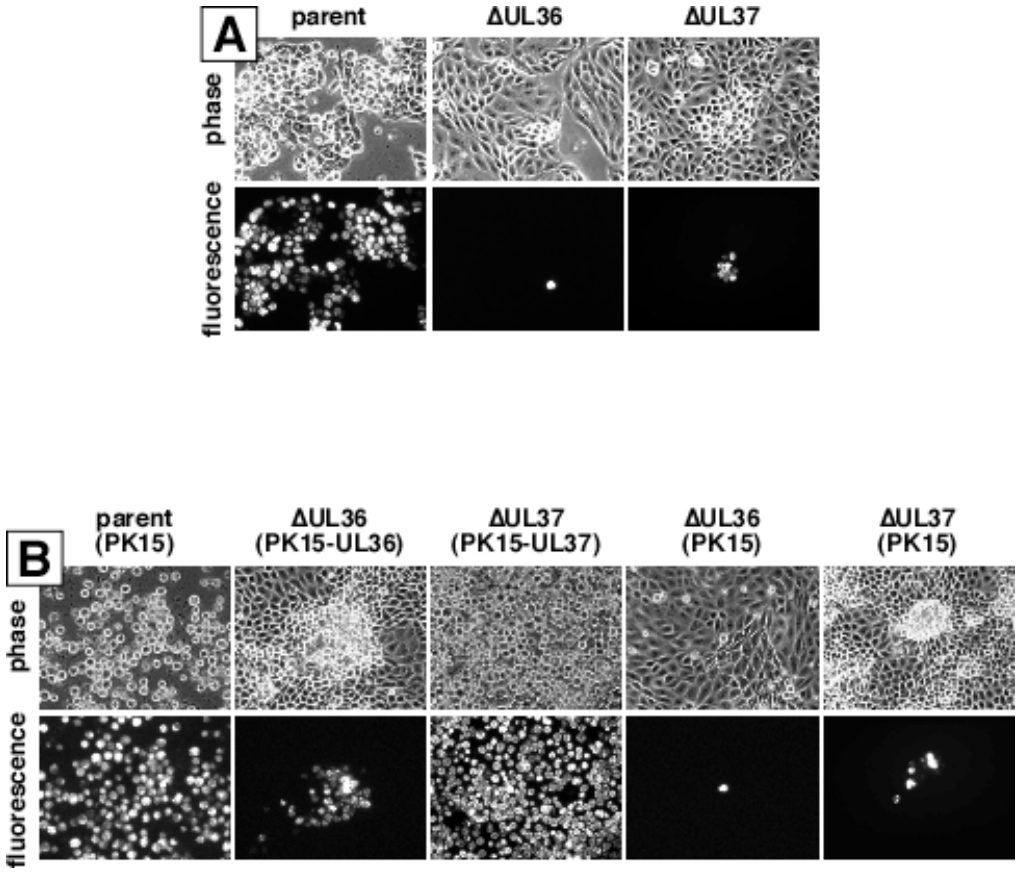

Figure 2.2. Initial characterization of VP1/2- and UL37-null viruses and complementing cell lines.

A) Images of living PK15 cells 2 days post transfection with infectious clones encoding fluorescent capsids (pGS575; "parent"), and clones carrying additional ΔUL36 (pGS678) or ΔUL37 (pGS993) mutations. B) Images of living PK15 or complementing cells (as indicated) 2 days post infection with viruses derived from the above three infectious clones (PRV-GS575, PRV-GS678 and PRV-GS993).

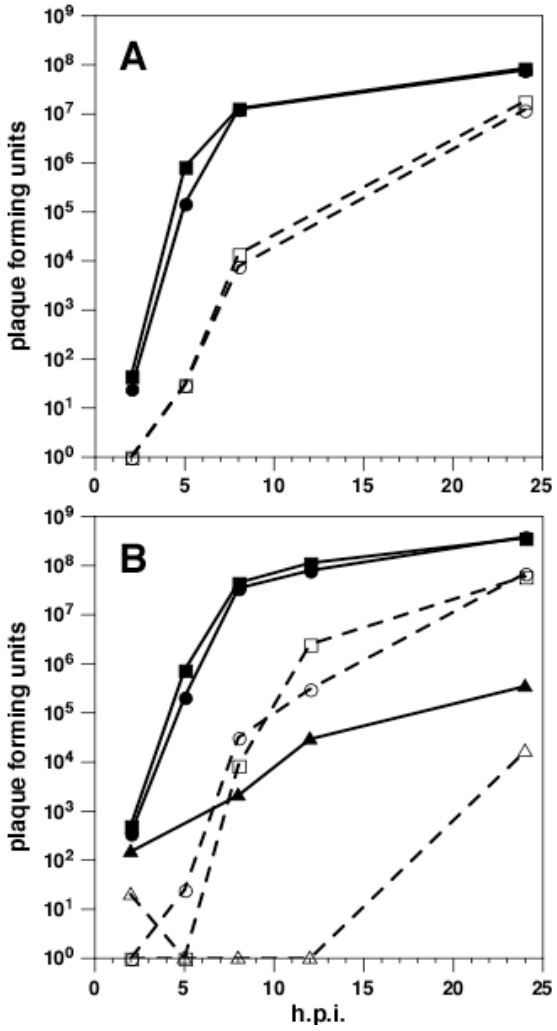

Figure 2.3. Single-step growth kinetics of fluorescent-capsid viruses.

A) Comparison of the growth of the parent virus (PRV-GS575; circles) with the UL36 revertant virus (PRV-GS678R; squares). The ΔUL36 virus was not viable and therefore could not be examined. B) Comparison of the growth of the parent virus (PRV-GS958; circles) with the ΔUL37 virus (PRV-GS993; triangles) and the UL37 revertant virus (PRV-GS993R; squares). Virions were harvested from the media (dashed lines; open symbols) and cells (solid lines; filled symbols) at indicated times.

VP1/2 and UL37 are required for efficient nuclear egress of PRV.

Cells infected with either HSV-1 or PRV harboring deletions in UL36 (VP1/2-null) are reported to accumulate unenveloped cytosolic capsids at late time points post-infection (19, 20, 32). To our surprise, our initial observations of cells infected with the ΔUL36 virus indicated that capsids were typically restricted to the nucleus. This observation was in contrast to a previous report of HSV-1 harboring a deletion in UL36 (19).

To further assess the role of VP1/2 in nuclear egress, Vero cells were infected with the fluorescent-capsid viruses harboring the wild-type UL36, ΔUL36 or the UL36-revertant alleles. Living infected cells were scored for the presence of cytoplasmic fluorescent capsids from 11-15 hours post infection (hpi) by fluorescence microscopy. Each virus produced capsids in the nuclei of infected cells as expected; however, only a fraction of infected cells were observed to have capsids that had translocated from the nucleus to the cytoplasm (Figure 2.4). Nearly half of cells infected with wild-type and revertant UL36 viruses had clear cytoplasmic capsid fluorescence (the fraction of cells with cytoplasmic capsids increased with time; data not shown). In contrast, capsids of the ΔUL36 virus egressed from nuclei at a significantly lower frequency. Examination of the ΔUL37 virus by this assay indicated a reduction in nuclear egress that was not as dramatic as the ΔUL36 virus, while the UL37-revertant virus behaved similarly to the "wild-type" and the UL36-revertant viruses.

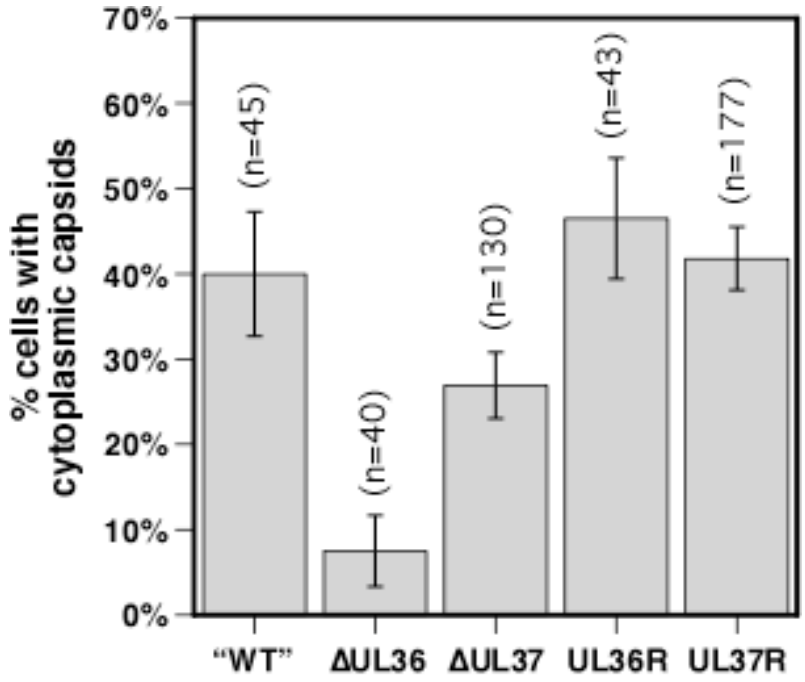

Figure 2.4. Nuclear egress of capsids into the cytoplasm.

The percentage of living cells displaying cytoplasmic capsids 11-15 hours post infection is shown. Vero cells were infected with PRV-GS575, having intact UL36 and UL37 genes ("WT"), PRV-GS678 (ΔUL36), PRV-GS993 (ΔUL37), the PRV-GS678R revertant virus (UL36R), or the PRV-GS993R revertant virus (UL37R) at an MOI ≤ 0.1. Because capsids near the nuclear rim could not be scored easily in this assay, cells were only counted as positive if at least 10 fluorescent-capsid punctae were observed in the cytoplasm. Error bars are standard error of the proportions (SEp). PRV-GS678 and PRV-GS993 were significantly different from each other and from each revertant virus ($z < 0.01$).

Microtubule-based transport of capsids requires VP1/2.

The dynamics of cytoplasmic fluorescent-capsids were examined by time-lapse microscopy in living Vero cells. Capsids of the parent virus (PRV-GS575) displayed three dynamic states: 1) static; 2) random non-processive motion; and 3) curvilinear processive motion (Supplementary Movie 1). The static capsids were observed around the margins of the cell and at the basal surface adjacent to the coverslip, consistent with this population of capsids having exited the cell as fully assembled viral particles (data not shown). Individual moving capsids were tracked for up to 20 seconds, or as long as they remained visible in the focal plane. An approximately equal number of PRV-GS575 capsids demonstrated processive (directed) and non-processive (random) movement (Figure 2.5A). The randomly oriented non-processive motion generally did not result in capsids diffusing more than 2 μm from the initially observed starting point during the course of recording. Processively transporting capsids moved greater distances (>10 μm in at least one instance) at rates comparable to that reported in axons of neurons (1-5 μm/s) (91, 92).

No curvilinear capsid transport from the ΔUL36 virus was observed; instead, motion was exclusively random and non-processive (Fig 5B & 5F; Supplementary Movie 2). Although transport of the ΔUL37 virus was reduced from wild type, directed transport could still be observed (Figure 2.5D & 5F). The UL36- and UL37-revertant viruses both had wild-type capsid transport dynamics (Figure 2.5C, 5E & 5F).

Figure 2.5. Transport of capsids in the cytoplasm.

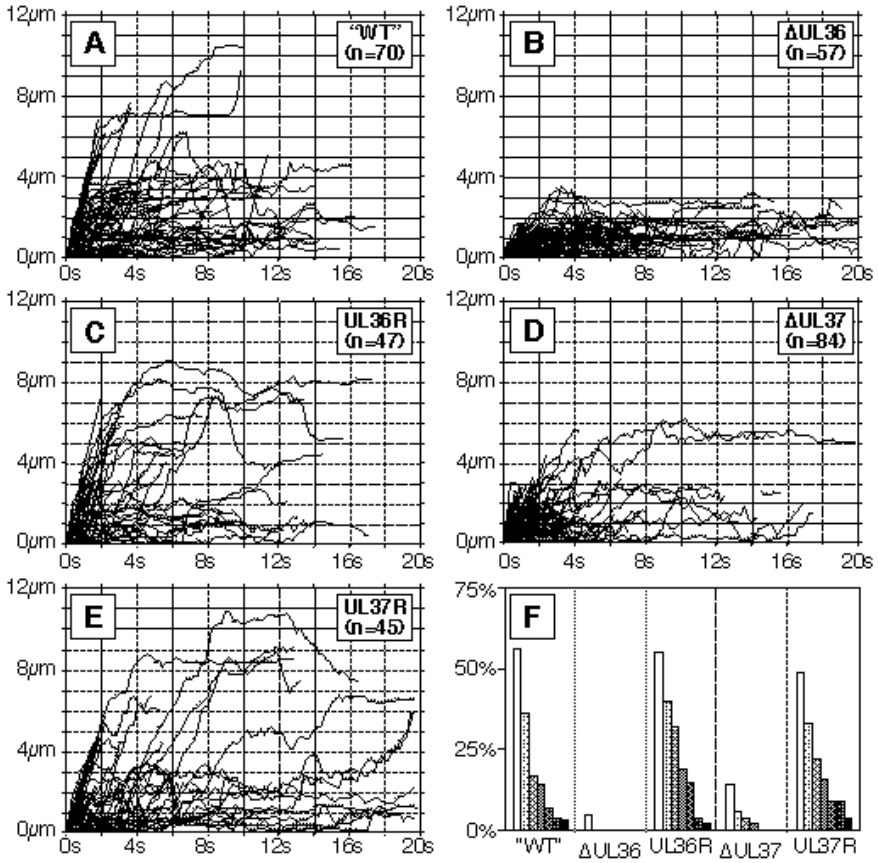

Figure 2.5. Transport of capsids in the cytoplasm.

Individual moving fluorescent capsids were tracked in the cytoplasm of Vero cells at 18 hpi. Tracking was performed on time-lapse fluorescence recordings collected from a single focal plane at 5 frames/s. A profile of transport for each infection is shown by plots of the individual capsids tracked as distance from starting position in the first frame (y-axis) versus time (x-axis). Vero cells were infected with the following viruses: A) PRV-GS575, B) PRV-GS678, C) PRV-GS678R, D) PRV-GS993, E) PRV-GS993R. F) Summary of data shown as percentage of tracked capsids that moved greater than 3 μm, 4 μm, 5 μm, 6 μm, 7 μm, 8 μm, and 9 μm from the origins for each infection (shown from left to right).

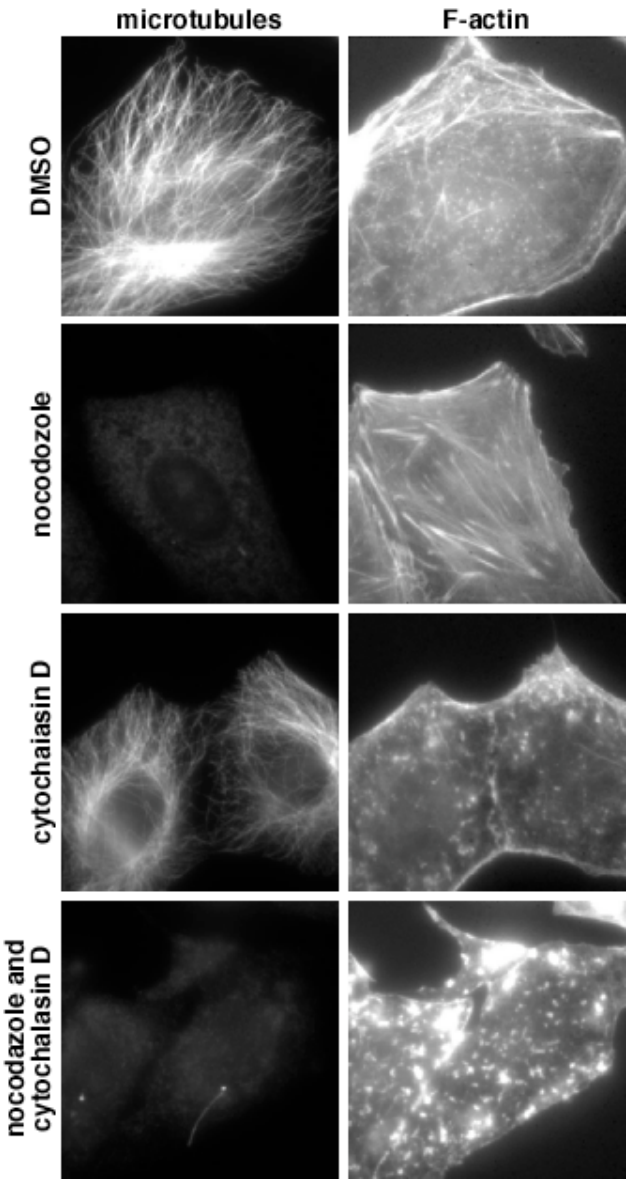

Figure 2.6. Vero cell cytoskeleton susceptibility to cytochalasin D and nocodazole. Uninfected Vero cells were treated for 1 hour with cytochalasin D, nocodazole, or both drugs together (or DMSO alone as control). Cells were fixed and processed for immunofluorescence imaging of filamentous actin and microtubules (image pairs).

To determine whether actin filaments or microtubules were required for capsid motion, cells were treated with cytochalasin D, nocodazole or both drugs in combination. Both drugs were effective at disrupting their respective cytoskeletal targets (Figure 2.6); however, in some cells isolated nocodazole-resistant microtubules were observed (for example, see the lower left panel in figure 2.6). In the presence of nocodazole the processive curvilinear transport of capsids was lost, while treatment with cytochalasin D or DMSO alone did not result in an obvious change in transport (Figure 2.7A-E). Non-processive motion was unaffected by cytochalasin D, nocodazole, or the combination of both drugs.

To further analyze the impact of cytoskeletal drugs on capsid motion, we examined the mean-square capsid displacement for each tracking experiment (Figure 2.7F). This analysis allows for an examination of the overall capsid diffusion in a sample. As expected for either passive or facilitated diffusion, mean-square capsid displacement was approximately linear with time (we note that this linearity was gradually lost as capsids progressed beyond ~ 5 μm, consistent with diffusion being caged by the plasma membrane; data not shown). Surprisingly, nocodazole did not completely disrupt capsid transport; wild-type capsid displacement in the presence of nocodazole was greater than that of ΔUL36 capsids. Cytochalasin D alone had no effect on capsid displacement (the cytochalasin D sample was indistinguishable from the DMSO control), but when cytochalasin D was added in combination with nocodazole capsid motion was reduced to that of the ΔUL36 virus. Co-treatment of ΔUL36 infected cells with cytochalasin D and nocodazole resulted in no further reduction in capsid diffusion. Addition of azide also

failed to further reduce capsid diffusion. Collectively, these results indicated that: (1) directed capsid motion was dependent on VP1/2; (2) random non-processive motion occurred by passive diffusion of capsids in the cytoplasm; (105) VP1/2-mediated capsid transport was primarily dependent on microtubules; and (4) residual capsid motion in the presence of nocodazole, relative to ΔUL36 capsids, was primarily dependent on intact actin filaments and not nocodazole-resistant microtubules.

Figure 2.7. Dependence of cytoplasmic capsid transport on cytoskeleton integrity.

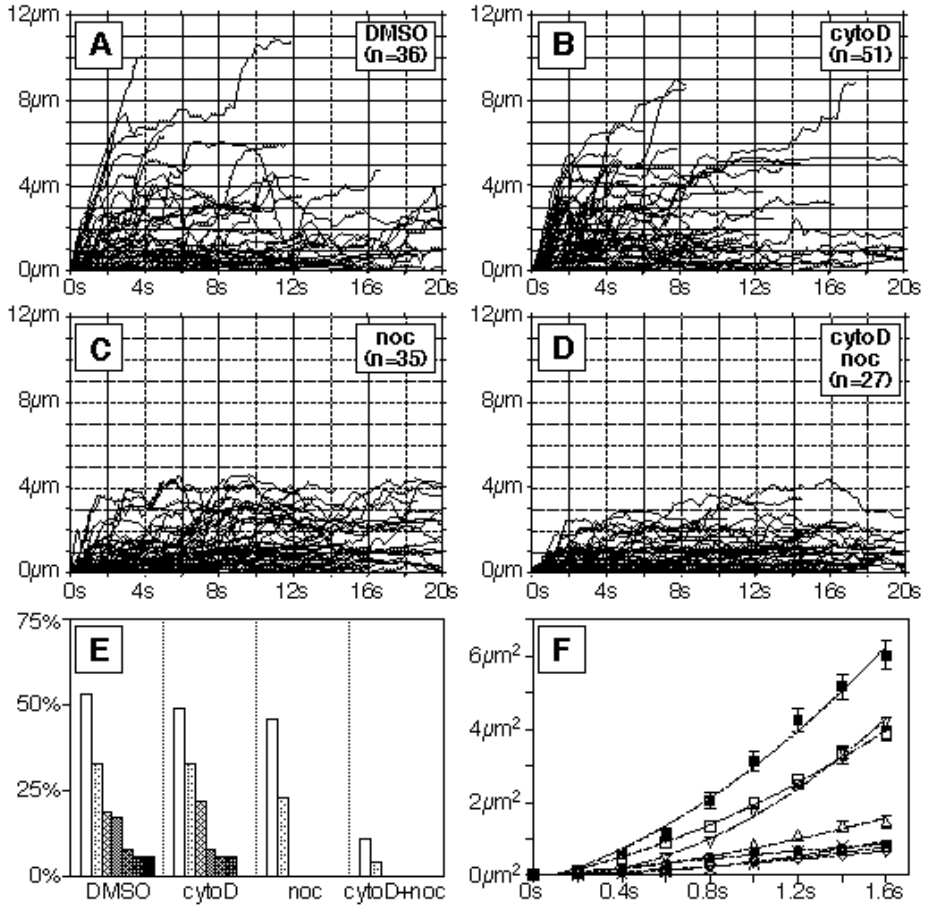

Figure 2.7. Dependence of cytoplasmic capsid transport on cytoskeleton integrity. Infected Vero cells were treated with cytochalasin D and nocodazole (or DMSO alone as control) at 17 hpi as indicated. (A-D) Individual moving cytoplasmic fluorescent capsids were tracked at 18 hpi and analyzed as described in the legend of figure 5. E) Summary of data shown as percentage of tracked capsids that moved greater than 3 μm, 4 μm, 5 μm, 6 μm, 7 μm, 8 μm, and 9 μm from the origins for each infection (shown from left to right). F) Diffusion profiles of moving cytoplasmic capsids. The mean squared displacement of the capsids from origin is shown over the first 1.6 s of the recordings. Symbols are as follows: (filled squares) PRV-GS575: "wild-type"; (filled circles) PRV-GS678: ΔUL36; (open squares) PRV-GS575 + DMSO; (open downward triangles) PRV-GS575 + cytochalasin D; (open upward triangles) PRV-GS575 + nocodazole; (open circles) PRV-GS575 + cytochalasin D + nocodazole; (open diamonds) PRV-GS678 + cytochalasin D + nocodazole; (cross hairs) PRV-GS575 + cytochalasin D + nocodazole + azide. Error shown is 95% confidence.

In summary, we find that capsid directional transport is disrupted in the absence of two capsid-associated tegument proteins VP1/2 and UL37. When deleted for either protein, capsids accumulate in the cytosol and are unenveloped (19, 32). Of the two null-mutant viruses, ΔVP1/2 mutant showed a dramatic abrogation of curvilinear, directional transport. Experiments using cytoskeleton-disruption drugs such as nocadozole and cytochalasin D further provided evidence of microtubule dependence in the capsid intracellular transport. An additional observation was made of the process of capsid nuclear egress. We detected a lower level of capsid translocation from the nucleus into the cytosol in both the ΔVP1/2 and ΔUL37 viruses, with ΔVP1/2 showing a more severe reduction. Unlike ΔUL37 mutation, ΔVP1/2 mutation was not previously reported to impact capsid nuclear egress (17, 19). The implications of this defect shall be examined further in later chapters. The next set of studies will begin the identification of conserved domains in VP1/2 that mediate important functions inside the host cell.

CHAPTER 3: IDENTIFICATION OF AN ESSENTIAL DOMAIN IN THE HERPESVIRUS VP1/2 TEGUMENT PROTEIN: THE CARBOXY TERMINUS DIRECTS INCORPORATION INTO CAPSID ASSEMBLONS

(This chapter appeared as the published article, “Identification of an essential domain in the herpesvirus VP1/2 tegument protein: The carboxy terminus directs incorporation into capsid assemblons”, by J. I. Lee, G.W.G. Luxton, and G. A. Smith, 2006, *J Virol.* **80:** 12086-12094)

SUMMARY

The herpesvirus tegument is a layer of viral and cellular proteins located between the capsid and envelope of the virion. The VP1/2 tegument protein is critical for the propagation of all herpesviruses examined. Using an infectious clone of the alpha-herpesvirus, pseudorabies virus, we have made a collection of truncation and in-frame deletion mutations within the VP1/2 gene (UL36) and examined the resulting viruses for spread between cells. We find that the majority of the VP1/2 protein was either essential for virus propagation or did not tolerate large deletions. A recently described amino terminal deubiquitinase-encoding domain was dispensable for alpha-herpesvirus propagation, but the rate of propagation in an epithelial cell line and the frequency of transport in axons of primary sensory neurons were both reduced. We map one essential domain to a conserved sequence at the VP1/2 carboxy terminus and demonstrate this domain sufficient to redirect the green fluorescence protein to capsid assemblons in nuclei of infected cells.

INTRODUCTION

All herpesviruses share a common structure that consists of an icosahedral capsid surrounded by a layer of additional proteins, collectively called the "tegument". The capsid and tegument are enclosed in an envelope consisting of a lipid bilayer and membrane-associated proteins. Although the capsid and envelope are similar to components found in many virus families, the herpesvirus tegument is rather unique.

The tegument is composed of both virally-encoded proteins as well as proteins derived from the host cell (16, 71, 104, 112, 118). Herpesviruses encode a dozen or more tegument proteins, and a fraction of these are conserved in the alpha-, beta- and gamma-herpesvirus sub-families (these are sometimes referred to as the "ancient" tegument proteins (14, 15)). Among the conserved tegument proteins is a large protein of >300 kD. In the alpha-herpesviruses, herpes simplex virus (HSV) and pseudorabies virus (PRV), the large tegument protein is referred to as VP1/2 (although the names ICP1, ICP1/2 and VP1-3 are also used), and is encoded by the UL36 gene (65).

VP1/2 is essential for alpha-herpesviruses propagation and is suggested to participate in a diverse array of functions (49, 90). Based on studies done with PRV in epithelial cells and sensory neurons, after entering a cell capsids shed the majority of the tegument layer but notably retain the VP1/2 protein during translocation from the plasma membrane to the nucleus (35, 55). Studies using HSV in epithelial cells demonstrate that once capsids are docked at nuclear pores, viruses encoding a temperature-sensitive form of VP1/2 fail to deliver the viral DNA into the nucleus at non-permissive temperatures (5). HSV VP1/2 isolated from infected epithelial cell nuclear extracts binds

to viral DNA probes and is suggested to participate in viral genome cleavage and packaging, and nuclear capsids in PRV infected epithelial cells have a reduced ability to exit the nucleus in the absence of VP1/2 (12, 56). In the cytoplasm, VP1/2 is required for the transport of capsids along microtubules in PRV infected epithelial cells (56). Finally, VP1/2 is required for the envelopment of cytosolic HSV and PRV capsids into mature virions (19, 20, 32).

The specific activities that VP1/2 performs in the above pathways are poorly understood. To date, VP1/2 is recognized to have two activities. First, the N-terminus of the protein is a cysteine protease that can function as a deubiquitinase, and this activity is conserved throughout the herpesvirus family (41, 83, 108). Second, VP1/2 binds at least two other tegument proteins: UL37 (shown with HSV and PRV) and VP16 (shown with HSV) (44, 107). UL37 and VP16, in turn, appear to recruit additional tegument proteins onto capsid surfaces, which leads to efficient cytoplasmic capsid envelopment (31, 47). However, VP1/2 binding to UL37 is not essential for propagation of PRV (32).

Using an infectious clone of PRV, we have made a collection of viruses harboring truncation and in-frame deletion mutations within the UL36 gene. The majority of mutants failed to propagate; however, the N-terminus of VP1/2 showed decreased growth kinetics indicating that the deubiquitinase is an important, but non-essential activity in the alpha-herpesviruses. Finally, we map one essential domain to a small conserved 62 aa sequence in the C-terminus of the VP1/2 protein and show that this domain is targeted to nuclear sites of capsid assembly, referred to as assemblons (109).

RESULTS AND DISCUSSION

Analysis of viruses encoding VP1/2 truncation mutations.

As a first step to identifying regions of the VP1/2 protein that are important for the alpha-herpesvirus infectious cycle, we aligned the predicted amino acid sequences of ten different herpesvirus VP1/2 homologues. Although the sequences were largely conserved, two regions were notably divergent between viruses. These two regions, aa226-299 and aa2026-2970 in the PRV VP1/2 sequence, had high proline content (33.78% and 28.15% respectively), and are referred to here as proline-rich regions #1 and #2 (PRR1 and PRR2). Within the remainder of VP1/2, we noted an alanine-rich region (ARR) from aa397-1293 that was conversely low in proline content (25.64% alanine; 3.68% proline). Because VP1/2 has no significant homologies to other proteins, the proline- and alanine-rich regions were used as the basis for mutational design.

A series of four stop codons were independently introduced into the UL36 gene of the PRV infectious clone, positioned at either the beginning or the end of a PRR or the ARR coding sequences (Figure 3.1A). The infectious clone used in these studies encodes a GFP-VP26 fusion protein, which produces the GFP-capsid virus described previously (91). To examine the impact of each mutation on viral propagation, each clone was transfected into PK15 cells and GFP fluorescence and cytopathic effects were monitored. Although transfected cells became evident based on GFP-capsid emissions, viral spread to neighboring cells was absent with each of the mutant viruses. This is in contrast to the parent GFP-capsid virus which spread to all cells within 3 days post-

transfection (Figure 3.1B). These findings indicated that the carboxy terminal 114 amino acids of VP1/2 were essential for viral propagation.

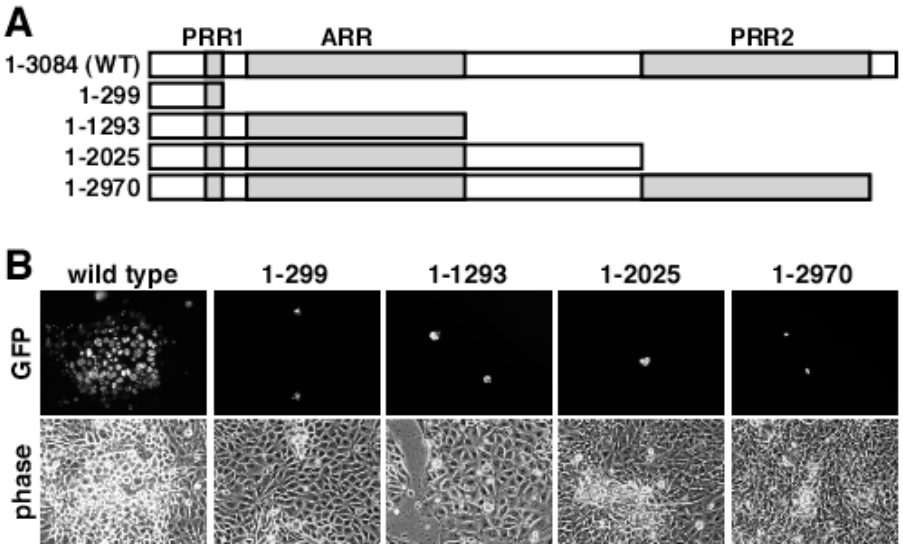

Figure 3.1. Propagation of PRV encoding VP1/2 truncations.

(A) Illustrations of predicted VP1/2 truncations expressed from recombinant PRV carrying stop codons in the UL36 gene. (B) Detection of infected cells by GFP-capsid fluorescence 2 days post-transfection with the corresponding infectious clone. Isolated fluorescent cells in the mutants indicate a lack of virus spread from the initially transfected cells.

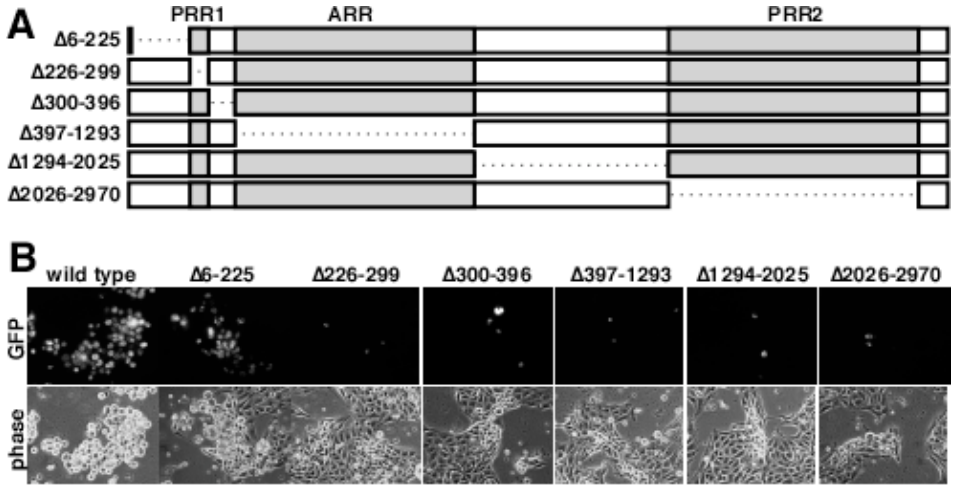

Figure 3.2. Propagation of PRV encoding VP1/2 deletions.

(A) Illustrations of predicted VP1/2 deletions expressed from recombinant PRV carrying in-frame deletions in the UL36 gene. (B) Detection of infected cells by GFP-capsid fluorescence 3 days post-transfection with the corresponding infectious clone.

Analysis of viruses encoding VP1/2 in-frame deletion mutations.

To determine if other regions of the VP1/2 tegument protein are required for viral propagation, a series of in-frame deletions were introduced into the UL36 gene (Figure 3.2A). Viruses carrying deletions resulting in expression of VP1/2 proteins lacking either PRR1, PRR2, ARR or the regions between PRR1 and ARR or ARR and PRR2 all failed to propagate in PK15 cells (Figure 3.2B). In contrast, a virus encoding VP1/2 lacking the amino terminus (∆6-225aa) was found to be viable.

Characterization of a virus lacking the amino terminus of VP1/2.

We noted that the ∆6-225aa virus propagated poorly relative to the parent virus. To confirm that this defect was not due to the FRT sequence present at the deletion site, a new virus, PRV-GS1651, was made that encoded a seamless in-frame deletion of codons 6-225 using a recently described two-step recombination protocol (101). PRV-GS1651 grew to a typical titer of $1x10^5$ PFU/ml (approximately 3 logs reduced from the parent virus). Single-step growth analysis showed a substantial decrease in both cell-associated and extracellular virus production. A revertant of PRV-GS1651 propagated with wild-type kinetics (Figure 3.3A). The decrease in viral propagation did not impact the ability of viral particles to move intracellularly in axons of sensory neurons upon entering a cell: retrograde transport kinetics were indistinguishable from the VP1/2 wild-type virus (Figure 3.3B). However, we noted a defect in the localization of progeny viral particles in axons following replication. In the majority of infected neurons, no capsids were detected egressing in axons of sensory neurons (Figure 3.3C) (91). Overall, we observed a 50%

reduction in egressing axonal capsids at a late time point post infection (20 hpi).

Based on our previous observations, the deletion in PRV-GS1651 may decrease upstream UL37 expression, which in turn may contribute to the defects seen with this virus (56). Western blot analysis of UL37 expression confirmed UL37 expression was reduced: UL37 expression levels in cells infected with Δ6-225aa were 54% that of the wild type. This decreased expression resulted in a corresponding drop in the amount of UL37 incorporated into released viral particles (43% relative to the wild type) (Figure 3.3D). Nevertheless, these results indicate that, similar to beta-herpesviruses, the alpha-herpesviruses cysteine protease present in the amino terminus of VP1/2 is dispensable for viral propagation in cell culture (41, 83, 108).

Figure 3.3. Characterization of PRV lacking the VP1/2 amino terminus.

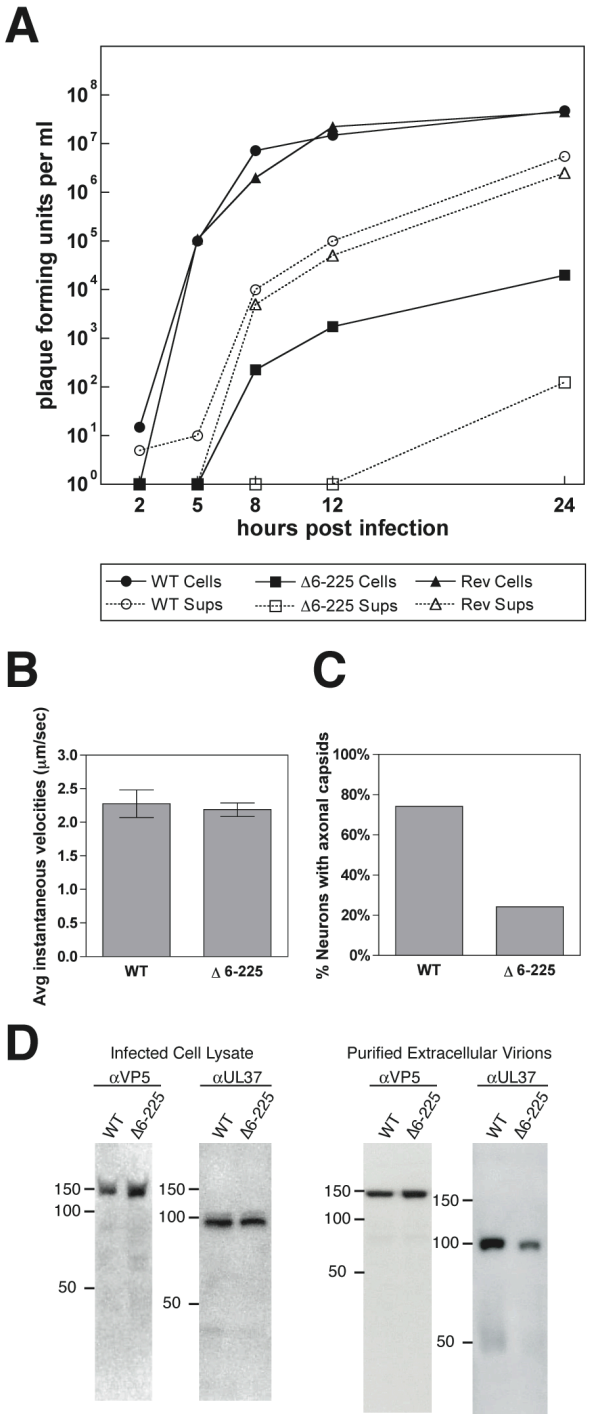

Figure 3.3. Characterization of PRV lacking the VP1/2 amino terminus.

(A) Single-step propagation kinetics. Plaque forming units were harvested from the media (dashed lines; open symbols) and PK15 cells (solid lines; filled symbols) at indicated times. PRV-GS847 (WT VP1/2; squares); PRV-GS1651 (Δ6-225 VP1/2; triangles); PRV-GS1651R (revertant VP1/2; circles). (B) Rates of retrograde capsid transport in axons following infection of primary sensory neurons in culture. Error bars are standard error of the means. (C) Frequency of *de novo* assembled capsids observed in axons of cultured sensory neurons follow replication (20 hpi). (D) Western blot analysis of the level of expression of the UL37 tegument protein in infected cells and released extracellular virions.

A conserved carboxy terminus of VP1/2 is targeted to nuclear capsid assemblies.

To further map the carboxy terminal essential domain, three additional stop codons were inserted into the 3' end of the UL36 gene (Figure 3.4B). The last 62 amino acids of VP1/2 are reasonably conserved; therefore, the stop codons were positioned at the beginning, middle and near the end of this region. Following transfection of the infectious clones into PK15 cells, only the clone encoding aa1-3078 resulted in a productive infection (Figure 3.4B). These results confirm that the carboxy terminus performs an essential function, as removal of only the last 6 amino acids allowed for a productive infection (which produced a viral stock with a $1x10^7$ PFU/ml titer). The essential domain was further confirmed by introducing two small in-frame deletions in the UL36 gene to produce viruses that express VP1/2 lacking either aa3024-3052 or aa3053-3077. Upon transfection into PK15 cells, both mutants failed to spread from cell to cell (data not shown).

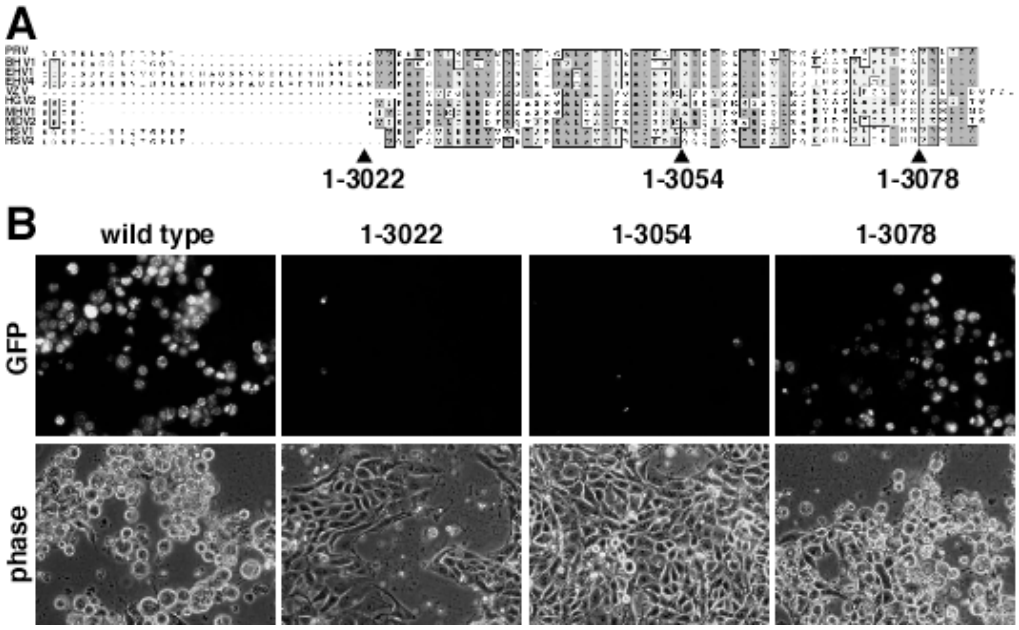

Figure 3.4. Propagation of PRV encoding carboxy terminal truncations in VP1/2.

(A) Alignment of the predicted amino acid sequences of the VP1/2 carboxy terminal from 10 alpha-herpesviruses. Sites of three PRV truncation mutations are indicated. (B) Detection of infected cells by GFP-capsid fluorescence 3 days post-transfection with the corresponding infectious clone.

Attempts to propagate viruses encoding truncations or deletions in the UL36 gene using a previously described VP1/2-complementing cell line were unsuccessful due to a high frequency of recombination leading to repair of the viral genomes (data not shown) (56). As an alternative approach to examining the function of the carboxy terminal domain, the 3' end of the UL36 gene was subcloned in-frame into a GFP-expression vector. The resulting construct encoded GFP fused to the amino terminus of the VP1/2 aa3023-3084 fragment.

In Vero cells transiently transfected with the GFP-VP1/2(aa3023-3084) construct, fluorescence was exclusively cytoplasmic and was localized to long tubular structures (Figure 3.5A). These structures were determined to be mitochondria, based on a MitoTracker fluorescence counter stain (Molecular Probes; data not shown). The relevance of this localization was not clear. GFP fused to the full-length VP1/2 protein, GFP-VP1/2(aa2-3084), never displayed mitochondrial localization and was instead diffuse throughout cells often showing a enriched nuclear localization (Figure 3.5A). However, infection of the GFP-VP1/2(aa3023-3084) transfected cells with a virus that encodes red-fluorescent capsids but is otherwise unaltered (PRV-GS847), resulted in a dramatic redistribution of GFP fluorescence to capsid assemblies within the nucleus, previously termed "assemblons" (Figure 3.5B & 3.6) (29, 92, 109). All infected cells containing capsid assemblons displayed this redistribution of GFP-VP1/2(aa3023-3084), whereas the fusion was never observed in the nucleus of uninfected cells. All mRFP1-capsid assemblies emitted detectable GFP-VP1/2(aa3023-3084) fluorescence, although the amount of GFP fluorescence associated with capsid assemblies varied. When

examined by confocal microscopy, the nuclear GFP- and mRFP1-emissions were confirmed to colocalize and were noted to be predominantly clustered near the nuclear rim, consistent with previous observations of HSV capsid assemblons (Supplemental Movie) (109). Unlike cells transfected with the GFP-VP1/2(aa3023-3084) construct, we noted that the majority of GFP-V1/2(aa2-3084) transfected cells were not permissive for infection. In those that were infected, the full-length GFP-VP1/2(aa2-3084) did not localize to assemblons upon infection and was in fact excluded from the nucleus altogether (Figure 3.5). GFP protein alone (not fused to VP1/2 sequences) was diffuse throughout the cytoplasm and nucleus of transfected cells, and did not relocalize upon infection with PRV.

Figure 3.5. Expression of the VP1/2 fused to GFP in Vero cells.

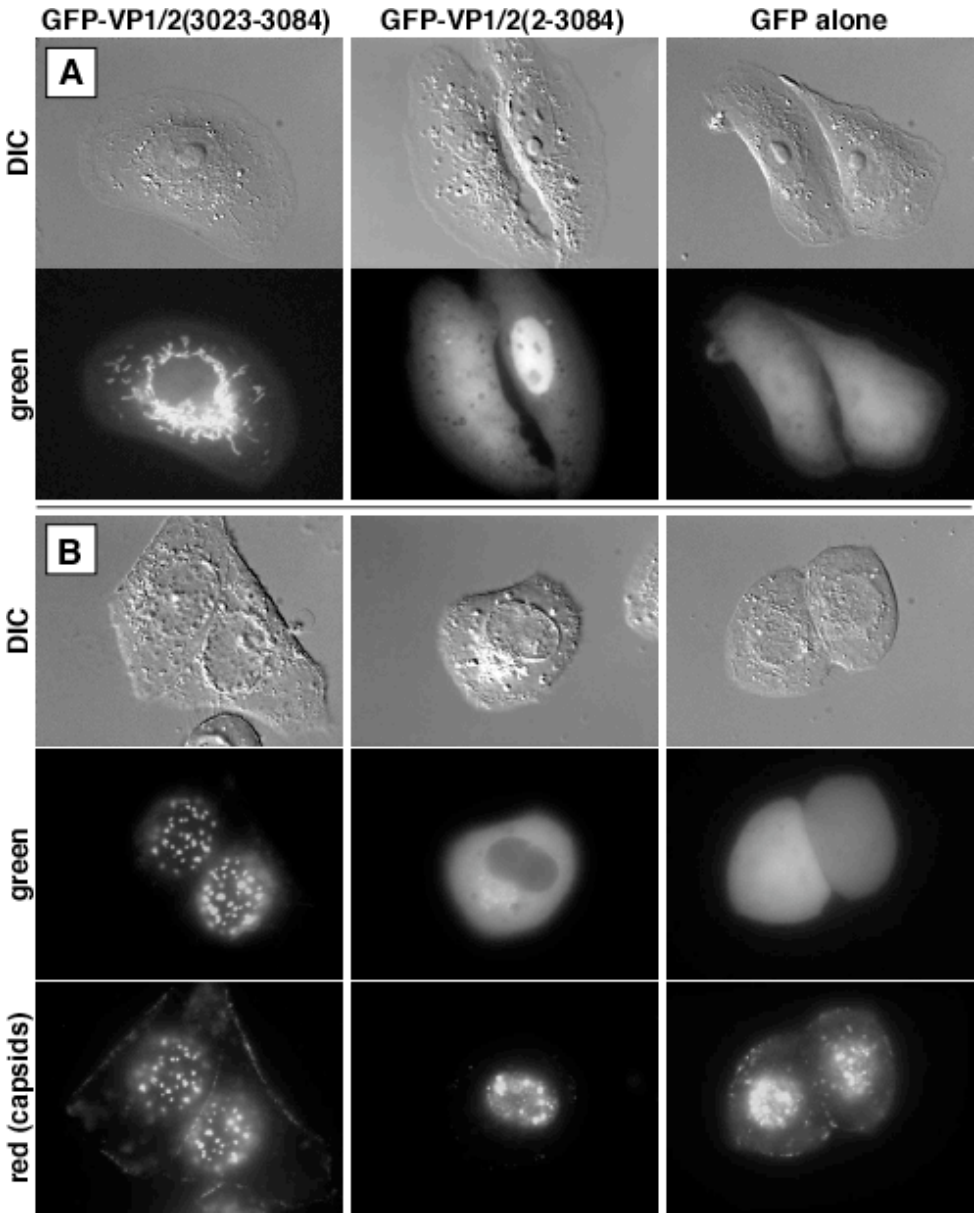

Figure 3.5. Expression of the VP1/2 fused to GFP in Vero cells.

Cells transfected with either GFP-VP1/2(aa3023-3084), GFP-VP1/2(aa2-3084) or unfused GFP are shown in (a) uninfected cells or, (b) cells subsequently infected with PRV expressing red-fluorescent capsids. Images were captured from a basal focal plane of the cells, thereby revealing capsid assemblies near the bottom of the nucleus.

Figure 3.6. Time course of GFP-VP1/2(aa3023-3084) redistribution.

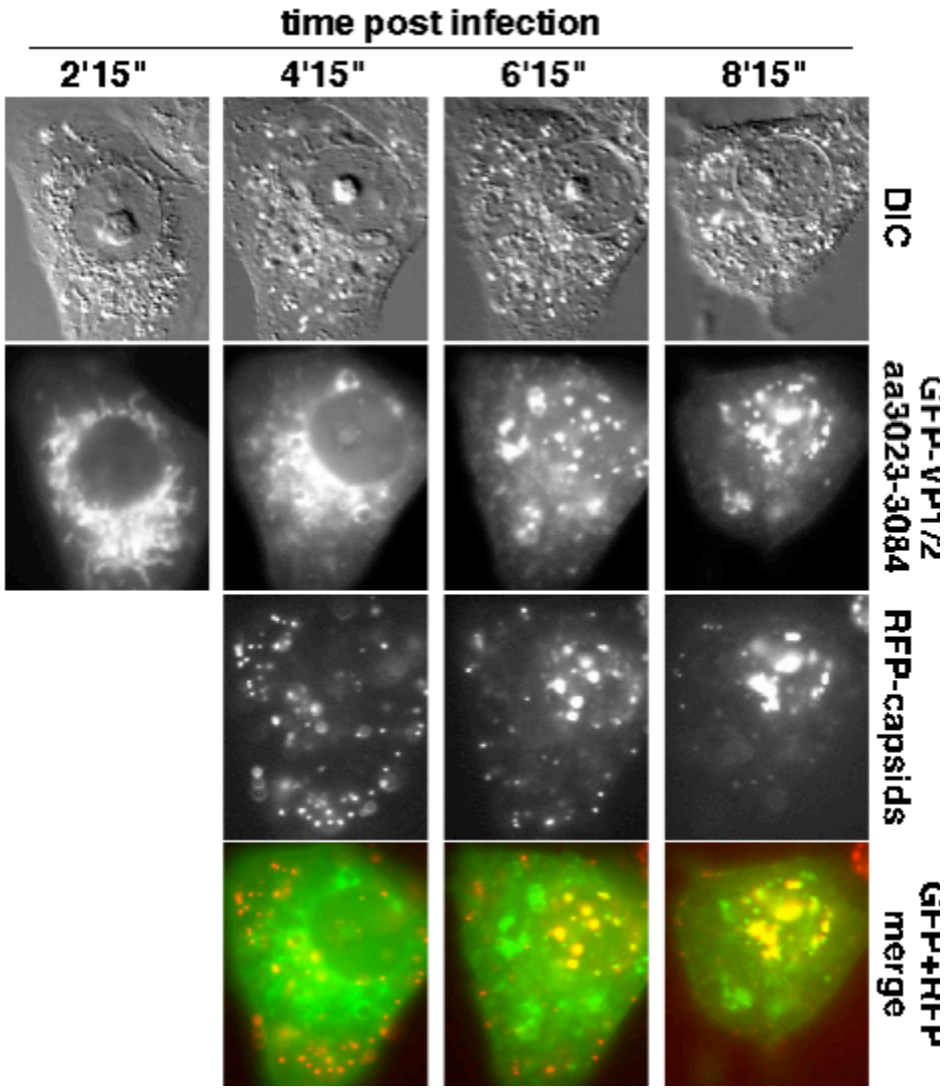

Figure 3.6. Time course of GFP-VP1/2(aa3023-3084) redistribution.

A Vero cell transiently transfected with the GFP-VP1/2(aa3023-3084) construct was infected with PRV-GS847 (expresses mRFP1-capsids) and imaged for GFP emissions at 2 hours intervals beginning at 2 hours 15 minutes post-infection. RFP-capsid images were captured beginning at 4.25 hpi.

The domain-specific analysis of VP1/2 revealed the large proportion of sequences that are essential for viral propagation. Of the 13 in-frame deletion and truncation recombinant VP1/2 mutant viruses investigated, only two were viable. A deletion of either aa 6-225 on the amino terminus or the last 6 amino acids on the carboxy terminus left the virus replication competent, all other manipulations were detrimental. The Δaa6-225 region encodes the recently reported deubiquitinase activity (41, 82, 108), which this study determined to be not required for viral propagation. However, the additional defects we observed in the amino terminal deletion, including reduction in viral titer and reduction in capsid axonal targeting during egress, may be attributed to polar effect that resulted in the decreased expression of upstream gene UL37.

Here we also report the finding that fusion of the carboxy terminal 62 aa of VP1/2 to GFP is sufficient to redirect GFP from the cytoplasm to the nucleus and for it to associate with dynamic sites of capsid assembly, referred to as assemblons, during infection (29, 109). The colocalization of the carboxy terminus of VP1/2 with nuclear capsid assembly sites led to the hypothesis that VP1/2 directly interact with the capsid proteins. A study was designed to test for such interaction. The collaboration between myself and another graduate student in the lab cumulated in a publication appended below with a selected figure.

ADDITIONAL STUDY

(results published as cited below)

Coller, K. E., **J. I. Lee**, A. Ueda, and G. A. Smith. 2007. The capsid and tegument of the alpha herpesviruses are linked by an interaction between the UL25 and VP1/2 proteins. *J of Virol*. **81:** 11790-11797.

Key finding

A capsid assemblon association assay was developed to identify the capsid protein partner for tegument. In the absence of protein(s) required for the association between the VP1/2 C-terminal 62aa and nuclear capsid assemblons, no colocalization would be detected. The VP1/2 C-terminal 62aa mCherry construct was transfected into cells, which displayed a mitochondria localization pattern. A panel of recombinant viruses each lacking one single viral protein was used to infect the transfected cells and the process of VP1/2 C-terminus relocalization into the nuclear capsid assemblons was scored. One mutant virus deleted for the UL25 gene emerged as the functionally important strain. The UL25 protein encoded by the UL25 gene is capsid-associated. In its absence, the VP1/2 C-terminus failed to redistribute into the nuclear capsid assemblons, indicating the potential interaction between the VP1/2 C-terminus and capsid-associated protein UL25. A more direct test was performed using the co-immunoprecipitation approach. Cells transfected with UL25 and VP1/2 cbd showed a clear interaction between the two proteins (Figure 3.7). Together with other control experiments described in (13), we now conclude the 62aa on the C-terminus of VP1/2 as the capsid-binding domain (or cbd).

Figure 3.7. VP1/2cbd and UL25 interact in the absence of other viral proteins.

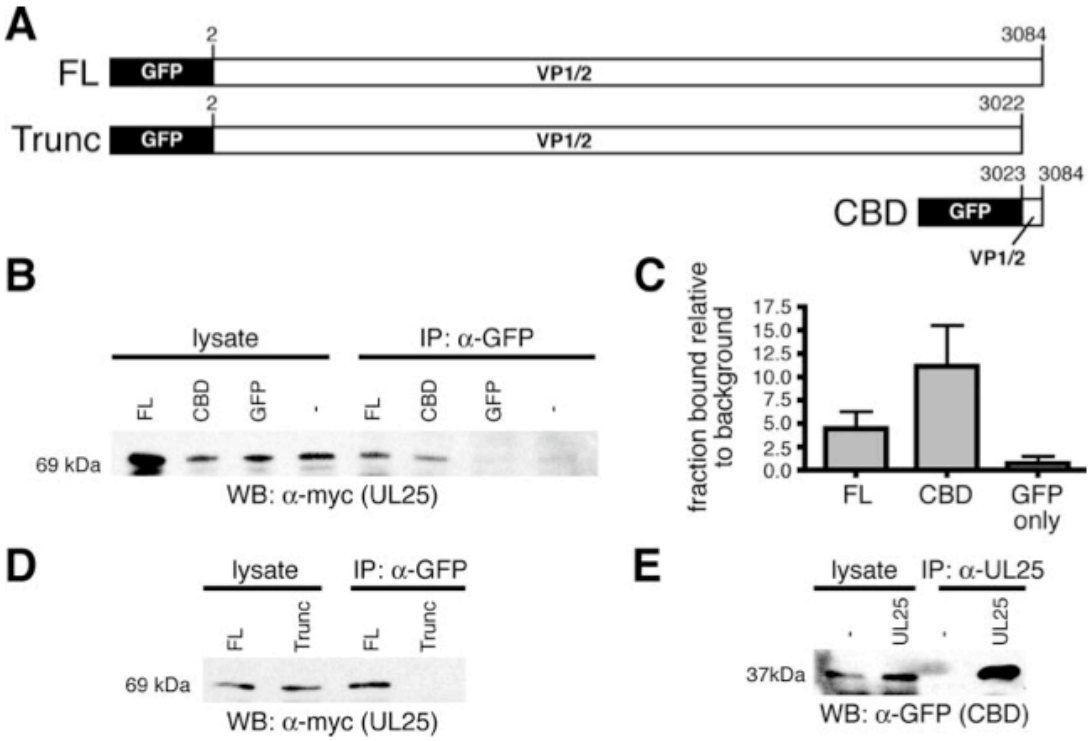

Figure 3.7. VP1/2cbd and UL25 interact in the absence of other viral proteins.

(A) Illustration of GFP-VP1/2 fusion proteins. (B and D) PRV UL25-myc detection by Western blotting either directly from cell lysates or after immunoprecipitation from lysates with an anti-GFP antibody. HEK-293 cells were cotransfected with PRV Ul25-myc and either PRV GFP-VP1/2 (FL, full-length), GFP-VP1/2Δcbd (Trunc, truncated), PRV GFP-VP1/2cbd (CBD), unfused GFP, or no additional construct. (C) Densitometry analysis of three duplicate experiments as documented in panel B. for each sample, the ratio of the amount of UL25-myc in the immunoprecipitate to the amount in the lysate is shown relative to the background (no GFP sample). Error bars are standard deviations. (E) HSV-1 VP1/2cbd detection by Western blotting from HEK-293 cells cotransfecteed with or without and HSV-1 UL25-mCherry fusion construct. Predicted molecular sizes of proteins are indicated at left, which were consistent with molecular size markers. α, anti; WB, Western blotting; IP, immunoprecipitation.

CHAPTER 4: THE DEUBIQUITINASE DOMAIN EMBEDDED IN A HERPESVIRUS TEGUMENT PROTEIN IS REQUIRED FOR VIRAL INVASION OF THE NERVOUS SYSTEM

(This chapter represents work in progress not yet submitted for publication. By J. I. Lee, P. J. Sollars, G. E. Pickard, M. Leelawong, and G. A. Smith, 2007)

SUMMARY

The neuroinvasive herpesvirus infectious cycle is delineated, in part, by stages of retrograde and anterograde transport in axons. These movements result in delivery of virus to sensory ganglia following primary infection and delivery back to the body surface following reactivated infection, respectively. During encephalitic spread, retrograde and anterograde transport misdirects viral dissemination to regions of the brain linked by neural circuits instead of peripheral body surfaces. Here we report that neuroinvasion by pseudorabies virus (PRV) depends upon a deubiquitinase domain embedded in the amino terminus of the large tegument protein, VP1/2. PRV carrying a single point-mutation in the deubiquitinase catalytic site (C26A) failed to invade the nervous system following inoculation of peripheral tissues, although replication at the site of injection occurred normally. Surprisingly, the mutant virus retained the ability to transport in axons in both the retrograde and anterograde directions, and was fully competent to spread trans-synaptically when inoculated directly into the brain or retina. The specific defect of the mutant virus to enter the nervous system from peripheral tissues was confirmed in autonomic circuits in two different models of infection. These findings demonstrate that the amino terminus of the VP1/2 tegument protein, which encodes a deubiquitinase domain, is a novel virulence determinant that is specifically required for transmission of PRV into the mammalian nervous system.

INTRODUCTION

Pseudorabies virus (PRV) is a neuroinvasive herpesviruses that is often used as a model for severe encephalitic infections, and as a consequence, as a self-amplifying tracer for mapping of the vertebrate neural circuitry (26). PRV is closely related to two human pathogens, varicella-zoster virus (VZV) and herpes simplex virus (HSV), sharing a common structure, similar genetic composition and a related neuroinvasive infectious cycle (62). Infections by these viruses consist of invasion of the peripheral nervous system (PNS), where life-long latent infections are established, followed by replication and spread back to exposed surface tissues. There are two key components to neuronal spread of the virus: retrograde axonal transport brings viral particles from sites of innervation to the neuronal cell bodies resident in peripheral ganglia, and anterograde transport moves newly replicated virions from the ganglia to axon nerve endings following reactivation from latency (102). On rare occasions, these viruses can spread from peripheral neurons to the central nervous system (CNS) trans-synaptically and cause severe encephalitic infections. With PRV, encephalitic infections occur at high frequency in many non-native hosts both in nature and in the laboratory (reviewed in 25). Identification of the molecular determinants that promote the neuroinvasive behavior of this class of herpesviruses would not only provide insights into the underlying mechanisms of viral dissemination within host tissues, but also into the relationship between tissue tropism and pathogenesis.

All herpesviruses express a large capsid-associated protein (Viral Protein 1/2; VP1/2) that is required for viral assembly and intracellular capsid transport on microtubules (13, 19, 32, 56). VP1/2 is encoded by the UL36 gene, which in PRV encodes for an approximately 330 kD protein (6, 43, 70). We recently determined that amino acids 6-225 of VP1/2 are dispensable for viral replication and spread in cell culture, but decrease the kinetics of viral propagation (54). To better understand the function of the VP1/2 amino terminus, we intended to study the mutant virus in an animal model of neuroinvasion and trans-synaptic spread (11). Unfortunately, the mutant virus propagated to titers that were reduced 3-logs relative to wild-type PRV, which were insufficient to allow for reproducible results in an *in vivo* study (9). However, the amino terminus of VP1/2 folds into a conserved deubiquitinase domain that is expressed and enzymatically active in infected cells (37, 41, 82, 84, 108). The role of the deubiquitinase during infection remains to be elucidated. By mutating a conserved catalytic cysteine residue in the deubiquitinase domain (C26A), a virus was isolated that displayed reduced kinetics of viral propagation in cultured cells, but could be prepared at a titer sufficient for study in the *in vivo* model.

We find that the C26A virus has a novel dissemination defect in the mammalian nervous system. Whereas wild-type virus transmits from innervated peripheral tissues to the PNS, and in turn into the CNS, the C26A virus lacks neuroinvasive ability. The phenotype was manifested specifically from a defect in accessing the nervous system from innervated peripheral tissues. The C26A virus was competent to replicate and spread within peripheral tissues and exposure of neurons directly, either by injecting

C26A virus into the brain or vitreous chamber of the eye, resulted in neuronal infection that subsequently spread to synaptically-linked second- and third-order CNS neurons in a manner similar to wild-type infections. Furthermore, neuroinvasion was restored upon co-infection with a virus competent to invade and spread in the nervous system.

RESULTS AND DISCUSSION

Isolation and initial characterization of the VP1/2 mutant virus

Ocular infections have proven to be an effective assay for PRV transmission in both retrograde (autonomic) and anterograde (visual) neural circuits (10, 11, 78, 80, 85, 110). However, attaining reproducible results in this model requires inoculation of 10^5 PFU in a 2 µl volume into the vitreous chamber of the eye (9). Because a virus carrying an in-frame deletion in the amino terminal-coding region of VP1/2 can only be propagated to a titer of 10^5 PFU/ml, assaying the role of the VP1/2 amino terminus in the ocular model of neuronal infection was not immediately practical. However, part of the reduction in titer may have resulted from a polar effect on expression of the neighboring UL37 gene, which is critical for viral propagation (19, 48, 53).

Because the amino terminus of VP1/2 is a conserved deubiquitinase domain, an alanine substitution for a conserved cysteine residue that is critical for the proteolytic activity responsible for deubiquitination (C26A) was expected to produce a VP1/2 protein lacking a functional amino terminus (37, 41, 82, 84, 108). Furthermore, a point mutation was not expected to have a polar effect on expression of the upstream UL37 gene (Figure 4.1A). To allow for monitoring of viral intracellular transport in cultured cells and spread in the mammalian nervous system, the C26A mutation was introduced into a virus previously made to encode a red-fluorescent protein fused to the viral capsid core (mRFP1-VP26) that itself has no impact on viral propagation in cell culture (55, 92).

Figure 4.1. Propagation of PRV with a mutated amino terminus in cultured cells

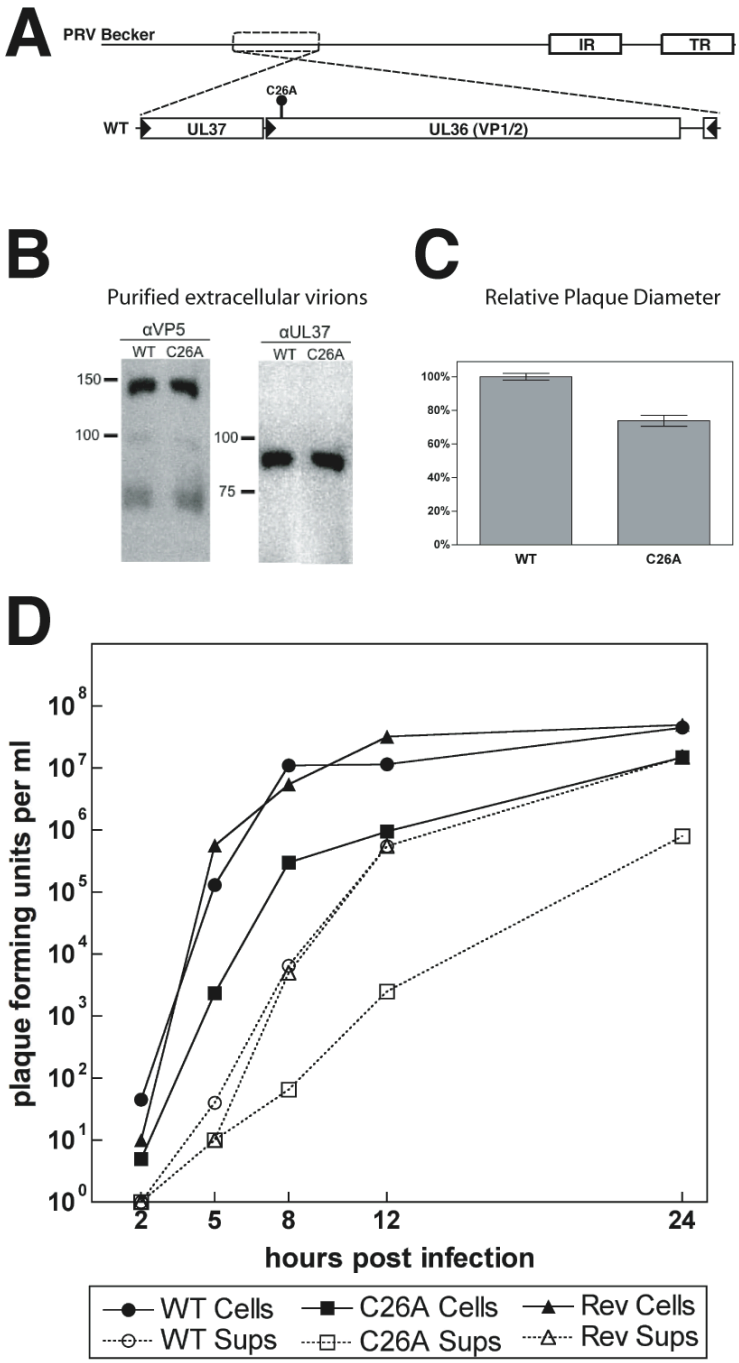

Figure 4.1. Propagation of PRV with a mutated amino terminus in cultured cells

(A) Illustration of the PRV-Becker genome with region encoding the UL36 gene (which encodes the VP1/2 protein) and UL37 gene expanded. The position of the codon change resulting in the C26A point mutation is indicated. Promoters are represented as black triangles. IR, internal repeat. TR, terminal repeat.

(B) Purified extracellular virions encoding mRFP1-capsids and either a wild-type UL36 allele (WT; PRV-GS847) or UL36 allele encoding the amino terminal point mutation (C26A; PRV-GS1652) were examined by Western blot analysis for the incorporation of the UL37 protein. The major capsid protein, VP5, was used as a loading control.

(C) Comparison of plaque diameters resulting from infection of Vero cells with the virus encoding wild-type UL36 (WT) or mutated UL36 (C26A) allele. Each virus also encodes the mRFP1-VP26 fusion (red capsids). Error bars are standard error of the means (SEM).

(D) Propagation kinetics of viruses encoding wild-type UL36 (WT), mutated UL36 (C26A), or a wild-type revertant of the C26A allele (Rev). All viruses also encode the mRFP1-VP26 fusion (red capsids). Infections virions were detected as plaque forming units harvested from either the cells (cells) or tissue culture media (sups).

Purified extracellular virions produced from Vero cells infected with the C26A virus incorporated wild-type levels of the UL37-encoded protein (Figure 4.1B). This is in contrast to the previously described virus encoding a mutant VP1/2 lacking amino acids 6-225, which showed an approximately 4-fold reduction in UL37 protein incorporation (53). In the absence of the UL37 polar effect, the C26A virus propagated to titers of 10^7 PFU/ml, and this was increased 10- to 100-fold to a titer equivalent to wild-type virus using a concentration protocol (53). The kinetics of propagation and cell-to-cell spread of the C26A virus were reduced relative to the virus encoding wild-type VP1/2, consistent with the previous finding that the amino terminal region of VP1/2 serves an important, but not essential, function in cell culture (Figure 4.1C&D) (53, 108).

Neuroinvasion in an intraocular model of infection

Viruses encoding RFP-capsids and either a wild-type VP1/2 allele (PRV-GS847) or the C26A allele of VP1/2 (PRV-GS1652) were injected into the vitreous body of the eye of adult rats. Of the nine animals infected with wild-type virus, 4 succumbed to infection between 60-74 hours post infection (hpi); the remaining 5 animals were killed between 70-72 hpi. The C26A virus was attenuated in this model, with animals showing little ill effect; animals were killed 47-264 hpi. Because several attenuated mutants of PRV display an inability to traverse anterograde circuits from retinal ganglion cells (RGCs) to visual centers in the brain, the brains of infected animals were examined for capsid fluorescence emissions (8, 10, 11, 78). The superior colliculus (SC), a primary target of RGC efferent projections, contained trans-synaptically labeled neurons in

animals infected with either the wild-type or mutant virus (Figure 4.2) in about 25% of the intravitreally injected animals (Table 4.1), similar to the proportion of animals showing anterograde infection of visual circuits following intravitreal injection with PRV152, and EGFP-expressing recombinant of the wild-type PRV Becker (78). Brains were also examined for evidence for infection via retrograde transneuronal labeling of the autonomic circuits innervating the iris and ciliary body, although the time course of infection and retrograde spread of PRV in these circuits following intravitreal injection is somewhat more variable due to gelatinous consistency of the vitreous body (compared to the aqueous humor of the anterior chamber). Nevertheless, in these experiments wild-type virus was reproducibly observed to have infected the Edinger-Westphal nucleus (EW) of the midbrain, preganglionic parasympathetic neurons that project to neurons in the ciliary ganglion via the oculomotor nerve, which in turn innervates the smooth muscles in the iris and ciliary body in the eye to mediate pupillary constriction and lens accommodation, respectively. In contrast, capsid fluorescence was never detected in the EW following C26A virus infection (Table 4.1). Wild-type virus also spread to the paraventricular nucleus (PVN) of the hypothalamus via a retrograde circuit of sympathetic origin (from iris, to superior cervical ganglion to thoracic spinal cord to paraventricular nucleus). Consistent with an inability to spread in retrograde circuitry, no labeled cells were observed in the PVN of C26A virus infected animals (data not shown). However, one animal that received an intravitreal injection of C26A virus showed clear signs of retrograde spread to the oculomotor nucleus, which innervates 4 of the 6 extraocular muscles of the eye (data not shown). Because this happened in only one

animal, and intravitreal injection requires puncture of the sclera (outer layer of the eye and point of insertion of the extraocular muscles on the globe) and surrounding extraocular muscles, we hypothesized that local tissue damage may have allowed for spread from the extraocular muscle to the oculomotor nucleus in the brain. Therefore, further examination of retrograde spread was necessary to determine the specific defect resulting from the C26A mutation.

	WT	C26A	50:50[c]	PRV-152
Anterograde (SC)[a]				
Intravitreal[b]	1/5 (20%)	4/15 (27%)	n/d	n/d
Retrograde (EW) [a]				
Intravitreal[b]	5/5 (100%)	0/15 (0%)	n/d	n/d
Anterior Chamber[b]	3/3 (100%)	0/4 (0%)	3/3 (100%)	4/4 (100%)
Retrograde (RGC) [a]				
SCN[b]	n/d	2/2 (100%)	n/d	n/d
Retrograde (CNS) [a]				
Eyelid[b]	n/d	1/11 (9%)	n/d	10/11 (91%)

TABLE 4.1. SUMMARY OF IN VIVO EXPERIMENTS.

Summary of different injection paradigms using different viruses.

[a] Structures in parenthesis are the representative sites examined for each pathway.

[b] Sites of virus injection.

[c] 50:50 mixture of PRV-152 (Bartha) and GS1652 (C26A).

n/d: no data.

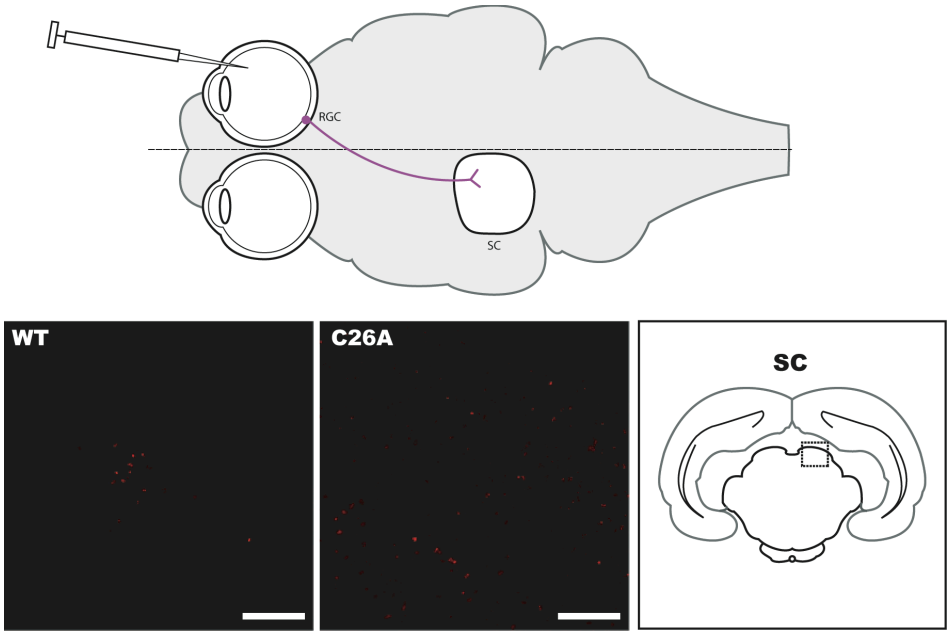

Figure 4.2. Anterograde transmission of viruses following intravitreal injection. Above illustration documents intravitreal injection route resulting in exposure of viral inoculum to retinal ganglion cells (RGC). RGC contralateral projection to the superior colliculus (SC) is also shown. Lower panels are representative images of virus fluorescence in the SC of coronal brain slices (doted box in bottom right panel). Scale bar = 10 μm. WT: 1/5 (20%) and C26A 4/15 (27%) animals showed detectable fluorescence.

The C26A virus is competent to spread in anterograde and retrograde circuits

To determine if the C26A virus was capable of intracellular transport in both the retrograde and anterograde directions, we examined axonal transport in cultured dorsal root sensory neurons by tracking red-fluorescence emissions from capsid particles by time-lapse microscopy. In these assays, the C26A virus behaved similar to the wild-type virus, having only small decreases in axon transport during both stages of infection (Figure 4.3). These findings demonstrate that intracellular transport of the C26A virus was intact, and suggests the defect observed after intravitreal injection was likely due to a change in intercellular viral spread in animals. These results did not immediately explain the defect observed in spread through retrograde sympathetic and parasympathetic circuits following intravitreal inoculation (i.e. to the EW and PVN), but were consistent with the one instance of C26A virus spread to the oculomotor region of the midbrain.

Figure 4.3. Viral transport dynamics in axons of cultured primary neurons.

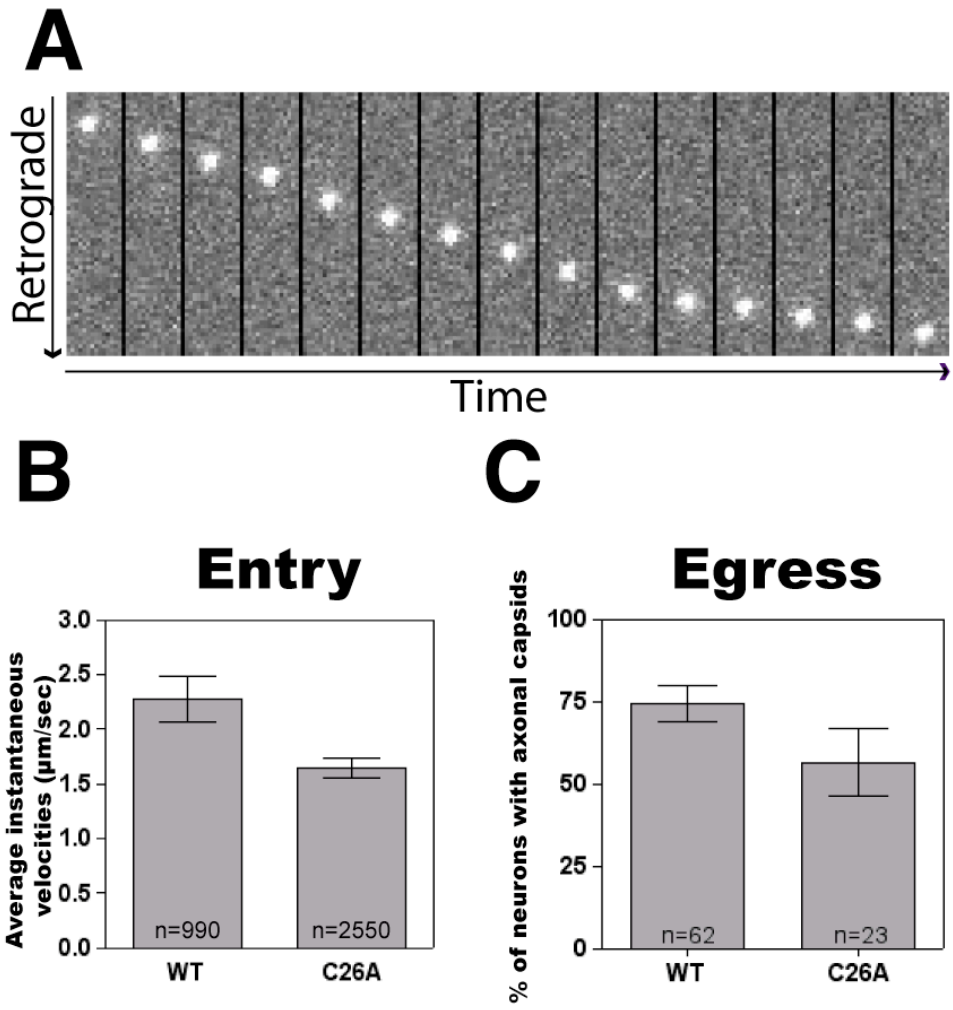

Figure 4.3. Viral transport dynamics in axons of cultured primary neurons.

(A) Representative example of retrograde transport of an individual capsid in a dorsal root sensory axon after infection with the C26A virus, shown as a time-lapse montage. All frames are 1.68 × 10.8 μm.

(B) Retrograde transport efficiency measured as frame-by-frame velocities of individual capsid particles in axons (as documented in panel A).

(C) Anterograde transport efficiency measured by accumulation of newly replicated capsids in axons.

To further examine trans-synaptic retrograde transport *in vivo*, stereotaxic injection of virus directly into the brain was employed. The suprachiasmatic nucleus (SCN), which receives axon projections from RGCs in the eye (77), was injected with the C26A virus. Although there is one SCN in each hemisphere of the brain, and both neighbor each other adjacent to the brain's midline, the stereotactic injection procedure allowed for delivery of virus to the SCN unilaterally. C26A virus infection was prominent in the injected SCN, but also to a lesser extent in the contralateral SCN. This spread is noteworthy, as the SCN are reciprocally innervated (77), and viral spread to the neighboring SCN provided further evidence that the C26A virus was competent to spread trans-synaptically in the CNS. Examining the retinas of the SCN-injected animals attained a definitive confirmation of retrograde transneuronal transmission; capsid fluorescence indicative of infected neurons was detected in neurons in the ganglion cell layer and also in bipolar and/or amacrine cells (neurons presynaptic to RGCs) located in the inner nuclear layer of the retina (Figure 4.4). This finding was consistent with the studies using cultured neurons, and unambiguously demonstrated that C26A virus is capable of multiple rounds of retrograde trans-synaptic spread (from SCN neurons to RGCs to bipolar/amacrine cells).

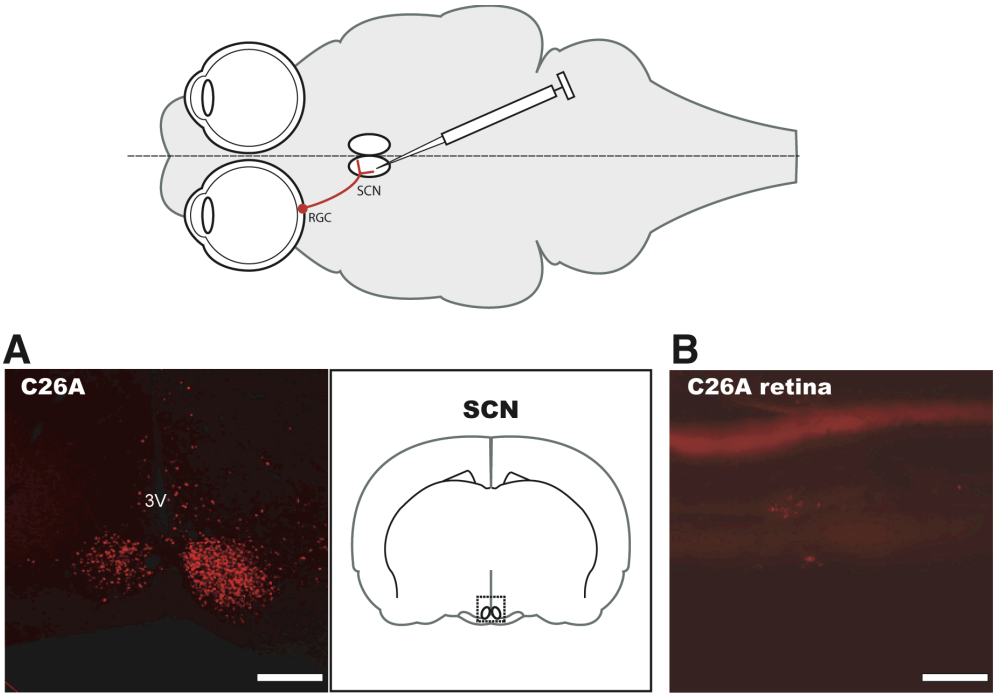

Figure 4.4. Retrograde transmission following CNS injection.

In the above illustration, the connection between the two SCNs are not shown. (SCN; suprachiasmatic nucleus).

(A) Dashed box indicates the zoomed in regions. 3V, third ventricle. Scale bar = 40 μm.

(B) Retrograde transmission of the viruses is detected by sectioning the retina. Scale bar = 10 μm. C26A: 2/2 (100%) animals showed detectable fluorescence.

The C26A defect occurs after virus reaches and replicates in peripheral sites of innervation

The data up to this point indicated that the C26A virus was incapable of spread in a subset of neural circuits, but the basis for the selective loss of function could not strictly be attributed to an inability to transport in either retrograde or anterograde circuitry. Because the C26A defect was observed only in retrograde circuits innervating tissues in the anterior chamber of the eye (i.e. iris and ciliary body), which are less efficiently infected following intravitreal injections, animals were next injected in the anterior chamber of the eye directly. This infection route immediately exposes the iris and neighboring ciliary body to the viral inoculum and provides a more reliable infection of the EW (96) with all neuroinvasive strains of PRV examined to date. Consistent with the intravitreal injections, the C26A virus again failed to spread to the brain; no infection was noted in the EW or any other area of the brain in all instances (Figure 4.5A).

As previously noted, the C26A virus typically propagated to titers 10-fold reduced relative to wild type. Preliminary studies indicated that the decrease in titer was due to an increase in the particle:PFU ratio of the C26A virus (data not shown). Therefore, by concentrating the C26A stocks to attain titers comparable to the wild-type virus that were necessary to initiate reproducible infections of the mammalian nervous system, we considered whether defective particles in the concentrated C26A viral stock may have interfered with infection of the retrograde circuits during intraocular infections. As an

initial test of interference, a stock of wild-type virus (PRV-GS847) was prepared as a concentrated stock and inoculated into the anterior chamber of the eye. Although 10-fold more PFUs were inoculated in this experiment than normal, retrograde transmission to the EW occurred unabated (data not shown). As a second test for interference, the C26A virus was mixed with an equal titer of PRV-152 virus, and co-injected into the anterior chamber of the eye. PRV-152 is a derivative of the PRV-Bartha strain, which is an attenuated PRV isolate that is incapable of spread in anterograde circuits but retains spread in all retrograde circuitry. PRV-152 encodes a GFP reporter cassette driven by a cytomegalovirus immediate early promoter, and therefore provides a fluorescent marker that is distinct both spectrally and spatially from the RFP-capsid emissions of the C26A virus (mRFP1-capsid fluorescence is most profound in the nucleus of an infected cell, whereas GFP diffuses throughout the cell body and neurites of an infected neuron). If the concentrated stock of C26A virus inhibited infection of the sympathetic and parasympathetic circuits from the eye, PRV-152 infection of the same circuits should also be blocked in a co-infection paradigm. Interference never occurred, and GFP fluorescence indicating presence of PRV-152 was readily detected in the EW. Furthermore, RFP-capsid fluorescence emissions indicative of the C26A virus were now also detected in the EW of these co-injected animals (Figure 4.5B).

Figure 4.5. Retrograde transmission following anterior chamber injection.

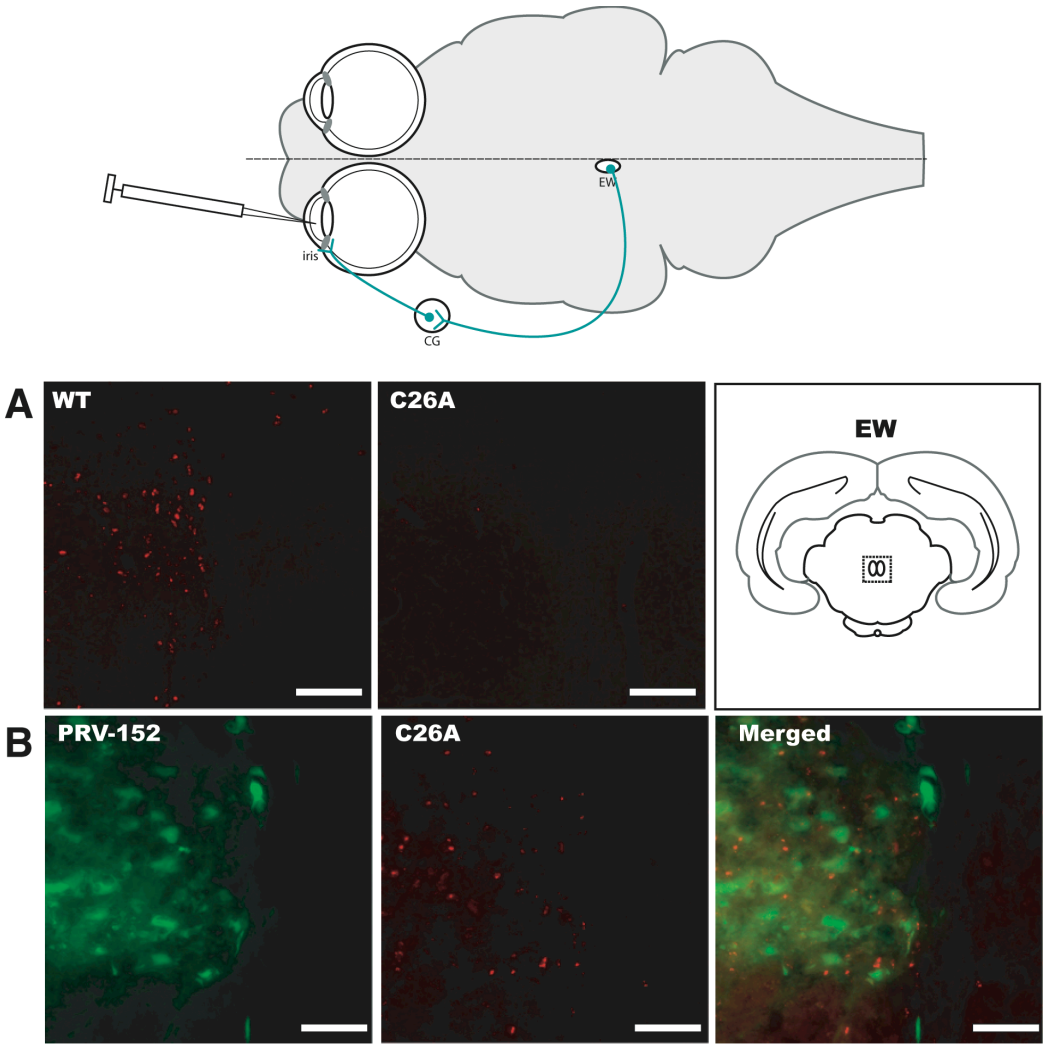

Figure 4.5. Retrograde transmission following anterior chamber injection. Representative coronal images of the Edinger-Westphal nucleus (EW; shown as a dashed box in coronal illustration) following anterior chamber injection or either wild type or C26A virus (panel A), or co-infection with PRV-152 and the C26A virus (panel B). Diffused GFP fluorescence and punctate RFP capsid signals are emitted from PRV-152 and the C26A viruses, respectively. Scale bars = 10 μm. In panel A) WT: 3/3 (100%) and C26A: 0/4 (0%) animals showed detectable fluorescence. In panel B) PRV-152: 4/4 (100%) and C26A: 3/3 (100%) animals showed detectable fluorescence.

Spread of C26A virus to the EW in the co-injection experiment indicated that PRV-152 had complemented the C26A defect. For this to occur, both viruses would have had to replicate in a common cell prior to entering the nervous system. This provided an incentive to examine the iris of the co-injected animals for infected cells (Figure 4.6A&B). Infection of the ciliary body near the junction of and with the iris by both PRV-152 and the C26A virus were observed and often appeared to be colocalized, indicating that initial replication in the iris prior to neuroinvasion provided an opportunity for the C26A virus to benefit from the unaltered VP1/2 protein expressed by PRV-152. In a subsequent experiment, the C26A virus was found to infect cells of the iris efficiently when injected alone into the anterior chamber of the eye (Figure 4.6C). Therefore, the C26A virus entered and replicated in the iris similar to a virus fully competent to spread into the nervous system (PRV-152), but in the absence of PRV-152 failed to invade the nervous system via the autonomic innervation of the iris/ciliary body.

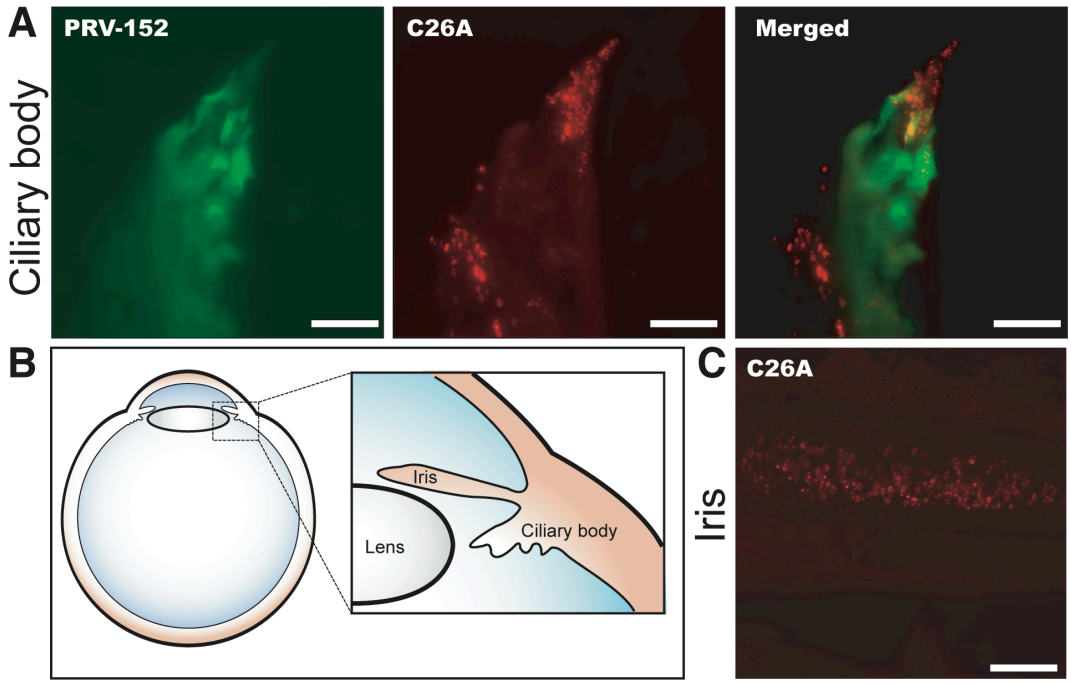

Figure 4.6. Viral infection in peripheral tissue of the eye.

(A) Images of the ciliary body following co-infection with PRV-152 (diffuse GFP signal) and the C26A virus (punctate RFP signal) in the anterior chamber. Cells infected with both viruses are evident in the merged image.

(B) Illustration of the peripheral tissues in the eye (iris and ciliary body) exposed to viral inoculum and imaged in these studies.

(C) C26A virus infection of the iris following anterior chamber injection. Scale bars = 10 μm.

The C26A virus is defective for neuroinvasion from peripheral tissues

To confirm that the C26A virus had a specific defect in neuroinvasion from tissues innervated by the PNS, PRV-152 and the C26A virus were independently injected into the skin of one upper eyelid each per animal; the smooth muscle of the eyelid receives both sympathetic and parasympathetic innervation (93). In this infection paradigm, PRV-152 consistently spread to several regions of the brain. Most notable was transmission to the locus ceruleus of the caudal pons (Figure 4.7). The C26A virus failed to spread to the locus ceruleus, and in fact was entirely absent from the brain in 10 of 11 animals (Table 4.1).

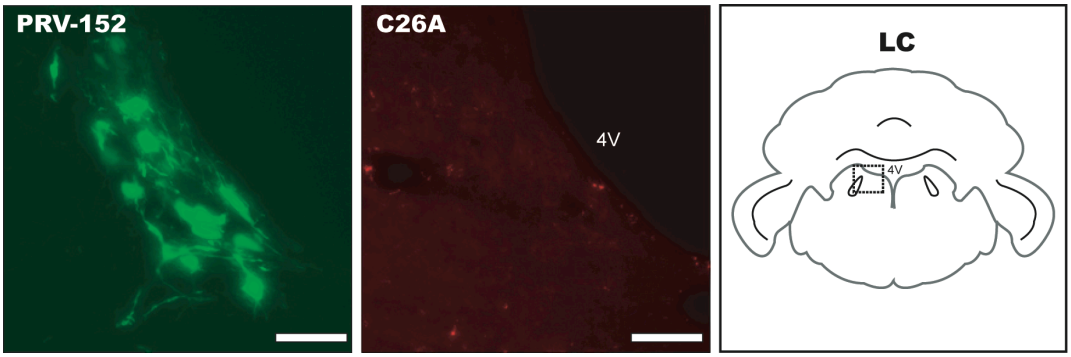

Figure 4.7. Eyelid infections.

Spread of virus injected into the eyelid to the locus ceruleus (LC). Region of brain imaged is illustrated as the dashed box in a coronal brain slice. 4V, fourth ventricle. Scale bar = 10 μm. PRV-152: 10/11 (91%) and C26A: 1/11 (9%) animals showed detectable fluorescence.

To explain how the C26A virus spread retrogradely in one animal, we again considered the possibility that injection into the eyelid might have caused local tissue damage that may have allowed direct exposure of the inoculum to innervating axon projections. We expect that a similar event likely occurred in the one intravitreal injected animal in which C26A virus spread specifically to the oculomotor nucleus. To determine if injection can, in some instances, allow for direct exposure of the inoculum to axons embedded within the peripheral tissue, cholera toxin (CTB) conjugated to Alexa Fluor 594 was injected in the eyelid model. CTB is a retrograde tracer, but unlike neuroinvasive herpesviruses which spread trans-synaptically, CTB labeling is restricted to the neuron cell body from which an axon projects. Furthermore, CTB must come into direct contact with the axon to label the distal neuronal cell body. Of 6 animals tested, only one showed CTB retrograde label into the brain. The absence of CNS labeling in the remaining five animals indicated that injection into the eyelid infrequently allowed for direct exposure to nerve endings. This finding was consistent with the conclusion that the C26A virus is specifically incapable of invading the mammalian nervous system from tissues innervated by the PNS, except in infrequent cases when nerve endings become exposed to the inoculum.

The role of VP1/2 amino terminus was studied using a recombinant virus encoding a codon change in a conserved cysteine residue critical for proteolytic activity (C26A) (41, 82). Although initial experiments produced results consistent with a selective loss of retrograde trafficking in the nervous system, retrograde transport with the C26A virus was unmasked by either infecting neurons directly in the retina or brain, or presumably by mechanical damage at the site of injection. The C26A mutation resulted in a virus that replicated in non-neuronal cells both in culture and in the iris, and also replicated and spread in cultured neurons and neural circuits *in vivo*, but failed to spread between the iris and the innervating neurons. Such a defect has never been observed for a neuroinvasive herpesvirus before. This novel phenotype reveals a biological function for the amino terminal deubiquitinase domain embedded in the VP1/2 protein, which previously had not been studied in the context of an animal infection model.

CHAPTER 5: CHARACTERIZATION OF VP1/2 DISTINCT FRAGMENTS DURING INFECTION: THE CARBOXY TERMINUS FUNCTIONS INDEPENDENT OF THE FULL-LENGNTH PROTEIN TO MEDIATE CAPSID NUCLEAR EGRESS

(This chapter represents work in progress not yet submitted for publication. By J. I. Lee and G. A. Smith, 2007)

SUMMARY

Alpha-herpesvirus infection of sensory neurons involves transport of capsid complexes inside the axon. There are two components of axonal transport: initial transmission of viral particles to the sensory ganglia and spread back to the periphery following reactivation. In both forms of transport, capsids are complexed with the essential tegument protein VP1/2. Recombinant pseudorabies viruses encoding fluorescent protein fusions to VP1/2 revealed a differential processing of the two terminal regions of the protein. During entry, both termini of the protein remain associated with the capsid but displayed distinct localization patterns during egress. The N-terminus of the protein was diffused cytoplasmic and the C-terminus preferentially associated with the nuclear envelope. The same intracellular localizations were observed in infections and transient transfections of subcloned fragments of VP1/2. The separation of two terminal regions of the protein was mapped to a site near amino acid 2025 (of 3084 total). The C-terminal fragment proved sufficient to mediate capsid nuclear egress during infection.

INTRODUCTION

Herpesvirus virions contain of four structural components. The ~150kB double-stranded DNA genome is packaged into the capsid of icosahedral symmetry (~120 nm). The capsid is surrounded by an amorphous layer of proteins collectively termed the tegument and all of the above are enveloped in a host-derived lipid bilayer, where glycoproteins reside. Virus entry requires the fusion of viral envelope with the host membrane such that the tegument and capsid are deposited into the cell. During egress, the nascent capsids translocate from the nucleus into the cytoplasm and the multiple components of the virion are assembled.

The largest tegument protein, VP1/2, is essential (19, 32) and involved in various stages of infection. VP1/2 is consistently associated with the capsid transporting complex after fusion entry (35, 55) and a temperature-sensitive mutation form prevents the DNA genome delivery into the nucleus once the capsid is docked onto the nuclear pore complex (5). In the absence of VP1/2, capsid nuclear egress post-replication is disrupted and the process of microtubule-based intracellular transport is abolished (56). The N-terminally encoded deubiquitinase (DUB) (37, 41, 82, 84, 108) may or may not function during egress and assembly but is at least required for the transmission across different cell types in an animal model (unpublished data). Recent work by Coller and colleagues identified the capsid-binding domain (CBD) as the carboxy terminal 62aa of VP1/2 (13). The VP1/2 cbd interacts with the capsid-associated protein UL25. The direct interaction between VP1/2 and a capsid-associated protein is consistent with the accepted

designation of VP1/2 as part of the inner tegument (69). However, it is unclear where within the cell tegumentation occurs. In addition, the intracellular site of association with other VP1/2-interacting tegument proteins (43, 107) remains unknown.

In this report, we examined the nuclear localization of VP1/2 using fluorescent protein fusions to either the amino terminus or the carboxy terminus. We analyze the separation of the two termini and detected the presence of the C-terminal region of VP1/2 on the nuclear envelope as well as inside the nucleus. This C-terminal region was mapped to approximately the carboxy one-third of the full-length protein. Supplementation of this C-terminal third of VP1/2 *in trans* is sufficient to restore the capsid nuclear egress defect previously reported in the null mutant (56).

RESULTS AND DISCUSSION

Isolation of fluorescent protein fusion VP1/2 viruses

We have previously reported a recombinant PRV virus that encodes a GFP fusion to the amino (N-) terminus of the UL36 gene. Together with the mRFP1 fusion to the capsid protein VP26, we were able to demonstrate the consistent association of VP1/2 with capsids during bidirectional intracellular transport (55). Here we characterize the isolation of additional recombinant viruses encoding fluorescence protein fusions to the UL36 gene. PRV-GS1903 carries a GFP fusion to the carboxy (C-) terminus of the UL36 gene and is otherwise the same as the previously described virus PRV-GS909 (55). PRV-GS1919 encodes no capsid fusion but carries a mCherry fusion and a GFP fusion to the N- and C-termini, respectively. Fluorescent protein fusions to the C-terminus or both ends of VP1/2 did not interfere with growth kinetics (Figure 5.1A). Next we examined the incorporation of fluorescence in the released virions. PRV-GS1903 released particles with colocalized capsid RFP and VP1/2-GFP signals similar to the PRV-GS909 (N-terminal GFP fusion) virus (Figure 5.1B). We then predicted that the intraaxonal retrograde transport of PRV-GS1903 and PRV-GS1919 would be unperturbed compared to the RFP capsid virus PRV-GS847.

Figure 5.1. Characterization of VP1/2 GFP fusion viruses.

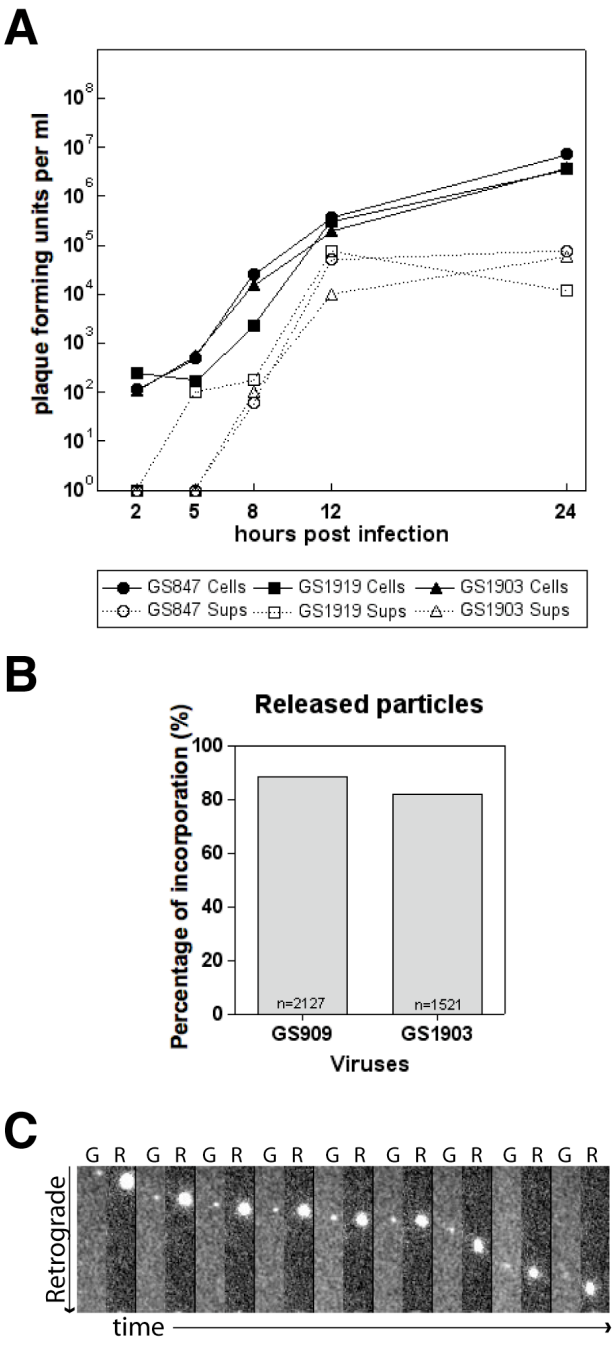

Figure 5.1. Characterization of VP1/2 GFP fusion viruses.

(A) Propagation kinetics of PRV-GS847 (WT parent), PRV-GS1919 (N-terminal mCherry fusion and C-terminal GFP fusion to VP1/2), and PRV-GS1903 (C-terminal GFP fusion to VP1/2). Both PRPV-GS847 and PRV-GS1903 encode the mRFP1-VP26 fusion (red capsids). Plaque forming units were detected in harvested either from tissue culture media (sups) or cells (cells).

(B) Released particles from infected cells on coverslips. Colocalization of GFP (VP1/2 fusion proteins) and RFP (red capsids) was compared between the N- (GS909) and C-terminal (GS1903) GFP fusions to VP1/2.

(C) Intraaxonal transport of PRV-GS1903 in embryonic chicken sensory neurons. VP1/2-GFP (green or G) and mRFP1 capsids (red or R) were captured in alternation. Frames shown represent retrograde (top to bottom) transport of VP1/2 and capsids in association. All frames are 2.52×9.12 μm.

In primary chicken dorsal root sensory neurons, both fluorescent protein fusion viruses transported with wild-type kinetics. PRV-GS1903 mirrored the amino terminus fusion PRV-GS909 result in that VP1/2 associates with transporting capsid complexes (Figure 5.1C). In PRV-GS1919, capsids do not contain fluorescent protein fusions but the mCherry (N-terminus) and the GFP (C-terminus) signals from VP1/2 are associated and exhibited the characteristic bidirectional and saltatory dynamics (data not shown).

Differential processing and function of VP1/2

After establishing the wild-type properties of the fusion viruses, we utilized the new viruses to investigate the possibility of differential processing and function of VP1/2 regions. The very large VP1/2 protein is ~330kD in size as a full-length protein but detected as multiple bands when visualized using Western blot analysis (7, 32, 43, 55, 70). In the case of GFP fusions to the distinct termini of VP1/2, the Western blot analysis of infected cell lysates revealed a very different migratory pattern for PRV-GS909 and PRV-GS1903 viruses (Figure 5.2A). The mono-clonal GFP antibody detected a common band in both lysates at ~330kD, consistent with the predicted full-length protein size in PRV. Each virus also produced additional bands that are distinct between the GFP-epitope on N- or C-terminus of the VP1/2 protein (Figure 5.2A). Aside from the nonspecific fragment migrating at ~100kD that's present in all samples (including the parent virus PRV-GS847, which does not encode GFP, data not shown), each distinct band is potentially functionally significant. However, the released virions appeared to

have incorporated predominantly the full-length form (Figure 5.2A). The observation of multiple protein forms led us to hypothesize that the multi-domain VP1/2 protein may not solely function as a full-length protein. Distinct populations of the protein could each play important roles during infection. We next examined the intracellular localization of the two terminal fusions using live cell fluorescence microscopy. If VP1/2 could function as a smaller protein, the N- and C-terminal fluorescent protein fusion virus may not localize to the same compartment of the cell. In Vero cells infected by PRV-GS1919, mCherry (N-terminal fusion) exhibited a diffused cytoplasmic pattern of fluorescence during egress (post-replication) while GFP (C-terminal fusion) showed a clear affinity to the nuclear envelope (Figure 5.2B). The differential intracellular localization of the N- and C-termini of VP1/2 was also observed using single fluorescent protein VP1/2 fusion viruses, PRV-GS909 and PRV-GS1903 (Figure 5.2B). The two termini of VP1/2 seemed to exist as separate proteins during egress.

Figure 5.2. Distinct profiles of amino and carboxy termini

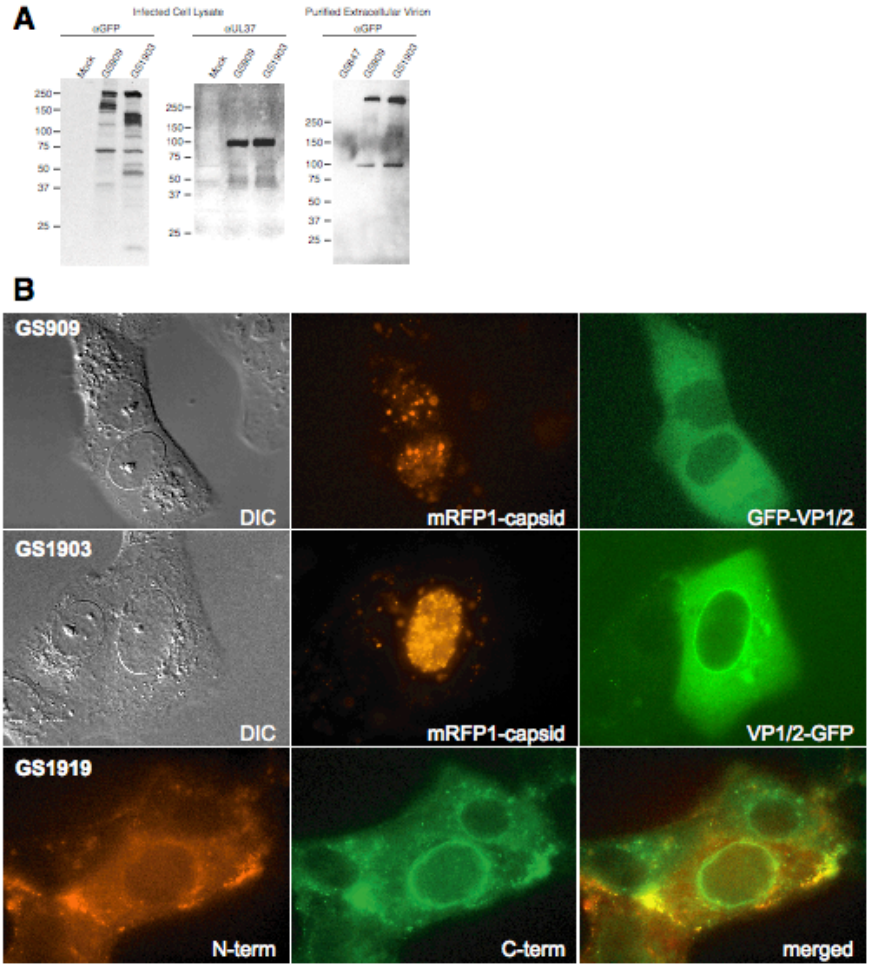

Figure 5.2. Distinct profiles of amino- and carboxy termini

(A) Infected Vero cell lysate or purified extracellular virions were blotted for VP1/2 proteins using an α–GFP antibody. UL37 levels was used to check for equal loading. Protein standard in kiloDaltons (kD)..

(B) Fluorescence emissions from amino- or carboxy terminal fusions to VP1/2 were detected in infected cells during egress (7-8 hrs post infection). GS909 and GS1903 also encode red capsids (mRFP1-VP26).

Cleavage site mapping

We have found that VP1/2 exists in distinct and separate forms during infection but the intracellular localization result was obtained independent of protein size information. To determine the size of VP1/2 proteins exhibiting distinct intracellular localization, we performed a comparative Western blot analysis. After the domain-specific mutational analysis yielded a collection of replication incompetent viruses (54), we subcloned out each domain of the VP1/2 protein into a GFP fusion construct and studied the intracellular functions of each domain (unpublished data). Amongst the collection, one construct pGS1952 (containing the second proline-rich region (PRR2) to the carboxy terminus; aa 2026-3084) consistently displayed a preferential localization to the nuclear envelope (Figure 5.3A). The intracellular localization of the VP1/2 C-terminal construct, pGS1952, and the C-terminally tagged virus PRV-GS1903 was virtually indistinguishable (Figure 5.2B and 5.3A). We then compared the migratory pattern of transfected pGS1952 to PRV-GS1903 infected Vero cell lysates. The predominant sub-full-length protein band in the PRV-GS1903 infected lysate migrated to the same position on the gel as the pGS1952 transfected sample (Figure 5.3B). The discrepancy between the predicted molecular weight of pGS1952 (108kD) and the detected molecular weight (~150kD) may be attributed to proline-rich nature in this region of the protein. When compared to the blot in Figure 5.2A not as many bands were resolved in the infected samples, suggesting a transience in the different forms of VP1/2 protein. There may be additional VP1/2 functions yet undiscovered. Taken together, the close approximation in

molecular weight and the same nuclear envelope affinity between the pGS1952 construct and the C-terminally tagged virus suggest the cleavage processing of the full-length VP1/2 protein targets at least one position neighboring the beginning of the VP1/2 PRR2 domain.

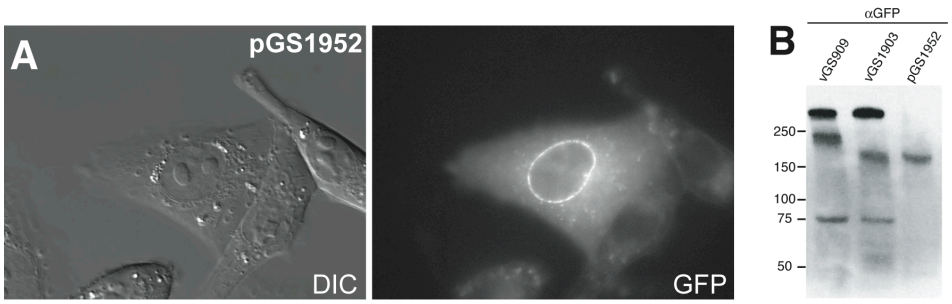

Figure 5.3. Cleavage site mapping

(A) Transient transfection of plasmid pGS1952 (C-terminal third of VP1/2 protein fused to GFP) in Vero cells.

(B) Western blot analysis was used to compare the molecular weight of pGS1952 to VP1/2 proteins detected in infected cell lysates by either PRV-GS909 or PRV-GS1903.

Characterization of the VP1/2 C-terminal domain function

The nuclear envelope localization of the C-terminal region of VP1/2 is suggestive of a perinuclear function of the capsid-associated, inner tegument protein. Even more strikingly, VP1/2 may play a nuclear role during infection. When we examined the GFP-tagged VP1/2 viruses in cells, the C-terminal region was detected in the nucleus superimposable onto the clusters of fluorescent capsid assemblons (Figure 5.4A). Nuclear GFP signal was only present in the C-terminally tagged VP1/2 virus, and not in the N-terminal fusion virus. The same nuclear capsid assemblon colocalization pattern could be seen using the pGS1952 construct. Vero cells transfected with pGS1952 that were subsequently infected with a RFP capsid virus showed the same GFP-RFP colocalization profiles in the nucleus (data not shown). We next check for the colocalization of RFP capsid and GFP VP1/2 fluorescence in purified intranuclear capsids. The C-terminally tagged VP1/2 GFP virus shows a higher percentage of capsid-VP1/2 colocalization than the N-terminally tagged virus (Figure 5.4B). In the ABC capsid preparation, only two of the three expected bands were resolved on the linear density gradient. They are likely B and C bands based on the relative position and light diffusion pattern compared to HSV-1 preparations (unpublished data).

Figure 5.4. Nuclear localization of the carboxy terminus

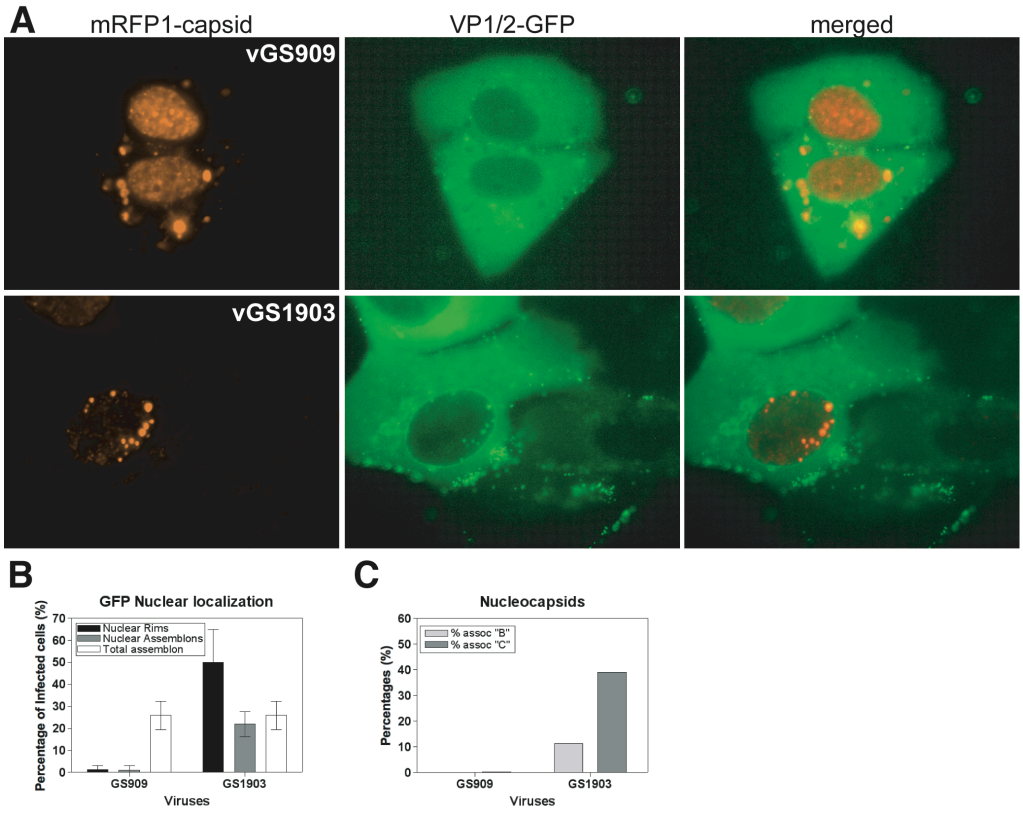

Figure 5.4. Nuclear localization of the carboxy terminus

(A) Nuclear fluorescence emissions from amino- or carboxy terminal fusions to VP1/2 were detected in infected cells during egress (7-8 hrs post infection).

(B) Quantitation of GFP nuclear rim (nuclear envelope) or nuclear assemblon signals in infected cells. Total assemblon indicates the number of infected cells with detectable nuclear capsid assemblons.

(C) Purified intranuclear capsids were separated into sub-populations. Putative “B” and “C” capsids were examined for red capsid and green VP1/2 colocalization.

Due to the lack of scaffold protein antibody, we could not state with certainty what the identity of these bands are but we could be sure that distinct populations of nucleocapsids were isolated and the difference between PRV-GS909 and PRV-GS1903 is statistically significant. The association of the C-terminal region of VP1/2 to nucleocapsids was stable enough to withstand extraction and purification procedures. To test if such association confers function, we used the capsid nuclear egress assay previously described (56). In the absence of VP1/2, viruses displays a great reduction in the nascent capsid nucleus-to-cytoplasm translocation, or nuclear egress. Here a set of cells are transiently transfected with pGS2213 (mCherry-VP1/2 [aa 2026-3084]) prior to infection by the ΔUL36 virus propagated on a complementing cell line (56). Compared to the untransfected cells, the supplementation of the pGS2213 construct significantly restores the nuclear egress defect (Figure 5.5). Furthermore, the level of nuclear egress complementation by pGS2213 seemed to increase over time. Therefore, the C-terminal region of VP1/2 (aa 2026-3084) that closely mimics the naturally liberated fragment during infection in its molecular weight and intracellular localization is important in mediating the process of capsid nuclear egress during infection.

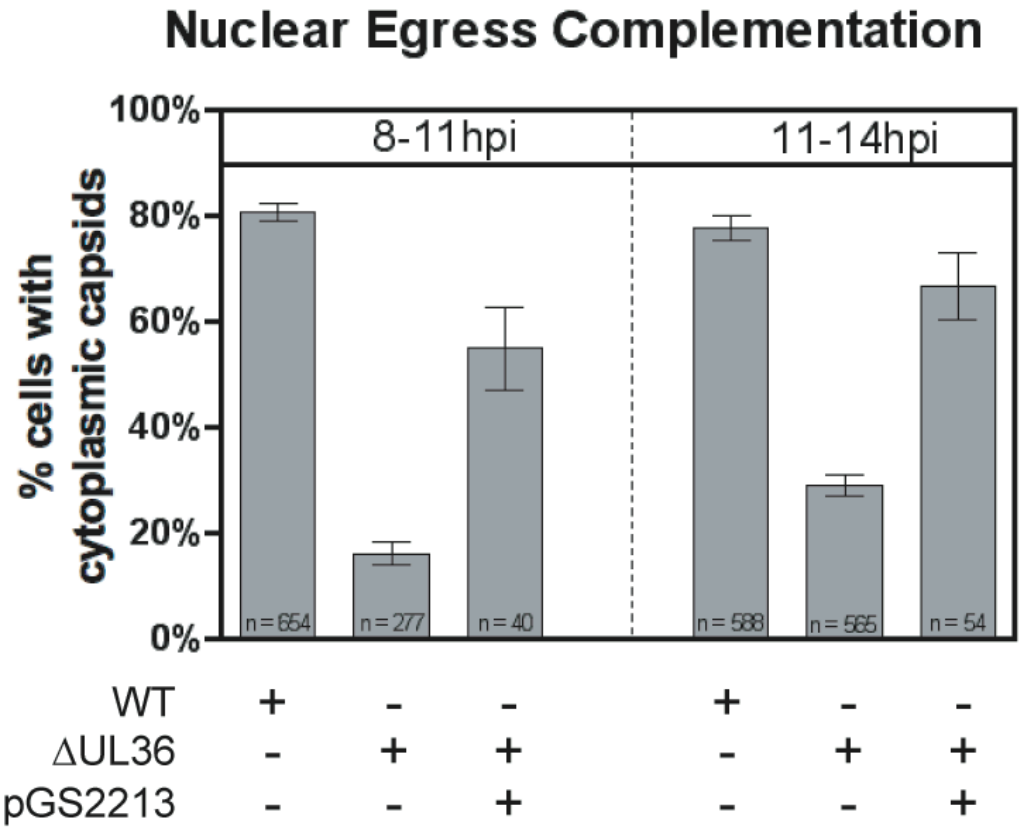

Figure 5.5. Nuclear egress complementation

Capsid nuclear egress was scored based on the presence of cytoplasmic capsids (positive if 10 or more cytoplasmic capsids per cell). Cells were either infected with WT virus or ΔUL36 virus, both encode GFP-capsid. A set of ΔUL36 virus infected cells were also transfected with pGS2213 (mCherry-VP1/2 [aa2026-3084]). Two separate time windows were examined (8-11 and 11-14 hrs post infection). Error bars are standar error of the proportions (SEp). PRV-GS678 infected, pGS2213 transfected cells and PRV-GS678 infected, untransfected cells are significantly different from each other, and from the wild-type virus infected, untransfected cells ($z < 0.01$).

Infection block and nuclear trafficking

In the process of investigating pGS2213 restoration of nuclear egress defect, we noted the low incidences of cells becoming infected. A closer examination of the infection incidence rate resulted in a surprising observation that cells are more resistant to infection in the presence of the carboxy terminal region of VP1/2. In these experiments, cells were first transfected with pGS2213 then infected with a wild-type virus that encodes a diffused mRFP reporter expression cassette. Only 36.6% of pGS2213 transfected cells become infected whereas 92% of control vector transfected cells are infected (Figure 5.6). An example of infection block is shown in Figure 5.6 with the reversed fluorescence colors. pGS1952 is the carboxy terminal VP1/2 fusion to GFP and PRV 616 is a virus that encodes diffused mRFP signal (4). The block is significant but not absolute.

Figure 5.6. VP1/2 carboxy terminus blocks subsequent infection.

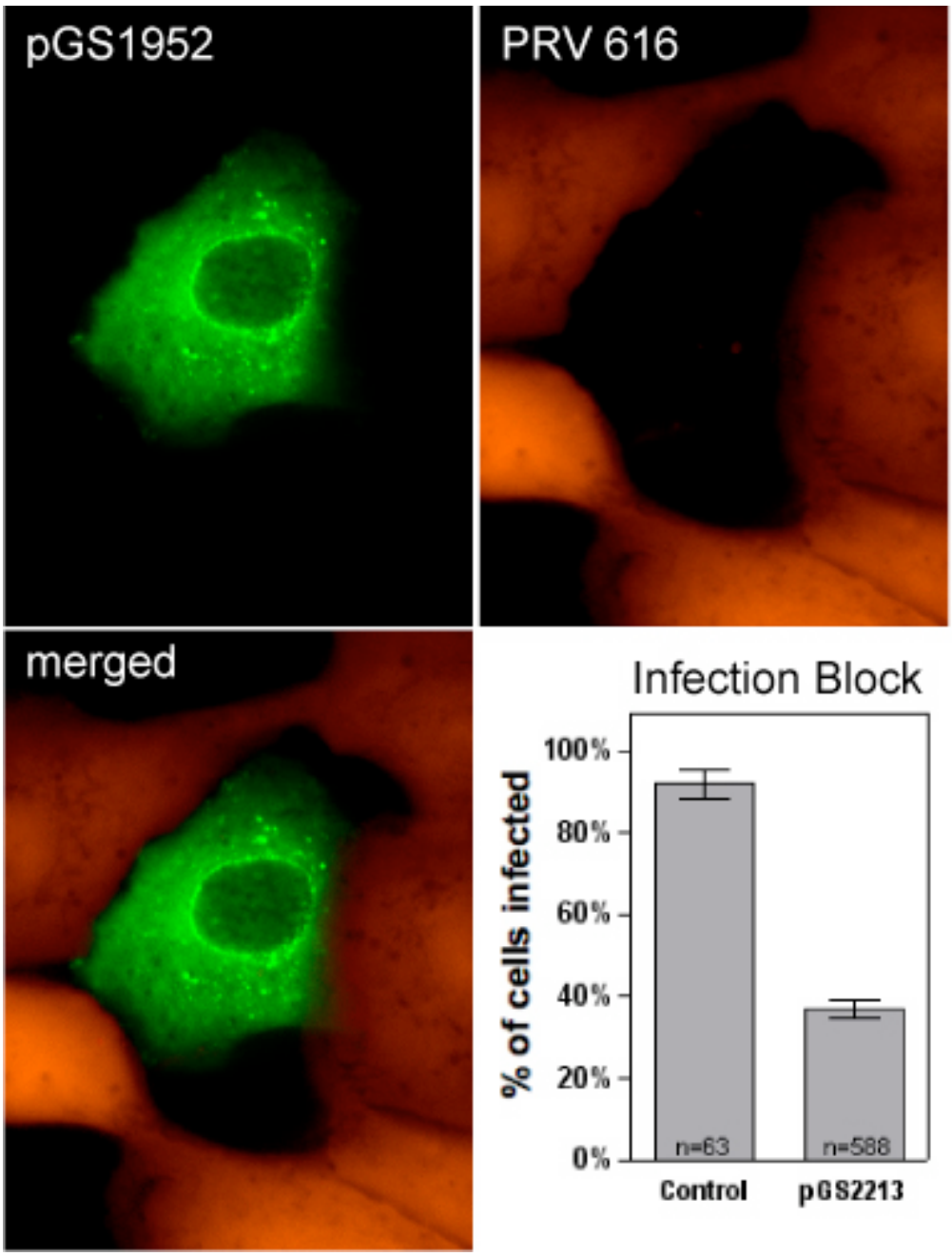

Figure 5.6. VP1/2 carboxy terminus blocks subsequent infection.

VP1/2 carboxy terminus fused to GFP (pGS1952) transfected cells showed the characteristic nuclear envelope localization. The diffused mRFP reporter gene expression in PRV 616 virus infected cells are less frequently observed in VP1/2 carboxy terminus transfected cells. The bar graph shown is based on an experiment using pGS2213 (mCherry fusion to VP1/2 carboxy terminus) and control vector encodes mCherry without fusion to other proteins. Error bars = SEp (Standard error of the population).

We next check to see if the nuclear envelope localization of VP1/2 carboxy terminus actively shuttles in and out of the nucleus such that the trafficking between subcellular compartments interferes the process of viral genome delivery into the nucleus. To do this, we treated pGS1952 transfected cells with Leptomycin B. Leptomycin B (LMB) inhibits CRM1 mediated function and thus halting specific protein nuclear export (39). A GFP-fusion TRIM 5α construct was included to show the efficacy of LMB treatment (unpublished data; Hope lab). The diffused cytoplasmic fluorescence pattern of TRIM 5α no longer showed a hollow nucleus post LMB treatment, indicative of the nuclear export disturbance. pGS1952 expression pattern, however, showed no discernible change when treatment with either DMSO or LMB. Thus, although VP1/2 carboxy terminus preferentially localizes to the nuclear envelop, we found that it is either not a true shuttling protein or at least not under the same regulation as the CRM1-dependent TRM 5α (Figure 5.7).

Figure 5.7. VP1/2 carboxy terminus nuclear envelope localization is independent of CRM1 nuclear receptor.

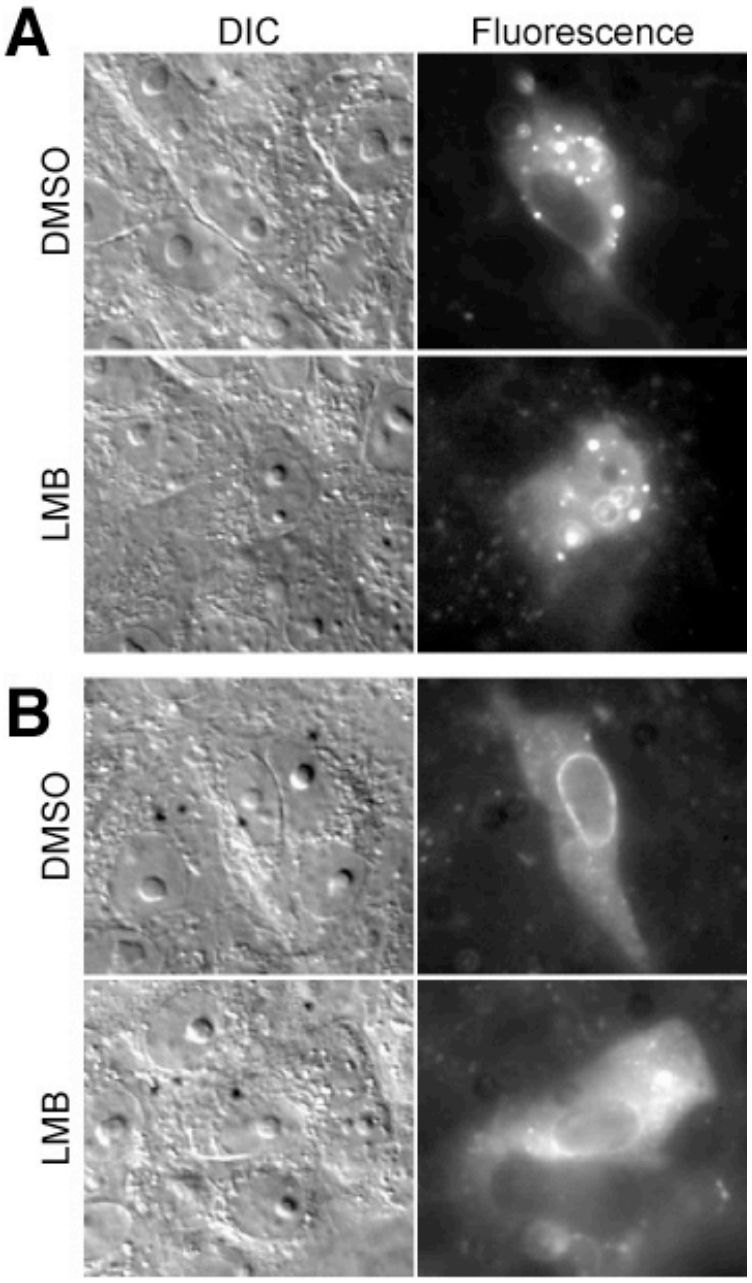

Figure 5.7. VP1/2 carboxy terminus nuclear envelope localization is independent of CRM1 nuclear receptor.

(A) Transfection of recombinant human TRIM 5α into Vero cells. At 24 hours post transfection (h.p.t), cells were either treated with DMSO or Leptomycin B (LMB). Export of TRIM 5α from the nucleus is disrupted in the LMB-treated sample.

(B) Transfection of VP1/2 carboxy terminus into Vero cells. At 24 h.p.t., cells were treated with DMSO or LMB. Intracellular fluorescence profile of pGS1952 is unaltered in the presence of LMB.

Using an infectious clone and a two-step recombination method, we constructed viruses carrying a single GFP fusion to either end of the VP1/2 protein. In studying the proteolytic processing and intracellular localization of the fusion proteins we observed the processing of the full-length protein into distinct fragments. In particular, the C-terminal third of VP1/2 showed clear affinity to the nuclear envelope, localizes with nucleocapsids, and is important in mediating capsid nuclear egress. Because the nuclear VP1/2 GFP signal colocalizes with the capsid assemblies, we further determined the structural coincidence of VP1/2 protein to capsids by studying the purified nucleocapsids. When purified nucleocapsids from PRV-GS909 and PRV-GS1903 infected cells were compared, GS1903 showed clear and high level of colocalization between GFP and RFP capsid signals, consistent with the observation in living cells. The nuclear VP1/2 signal we detected was associated with the capsids, suggesting the nucleus as the initial site for tegumentation. Furthermore, the assembly of VP1/2 C-terminal region (including the capsid-binding domain) onto capsids serves an important function, namely capsid nuclear egress. The essential tegument protein VP1/2 does not have to exist in its full-length form in order to mediate important infection processes.

CHAPTER 6: MATERIALS AND METHODS

Cells.

Derivatives of pseudorabies virus (PRV) strain Becker (PRV-GS443, PRV-GS678R, PRV-GS993R; see below) were propagated in pig kidney epithelial cells (PK15). PK15 cells were also used to determine viral titers and for single-step growth curve analysis as previously described (100). African green monkey kidney epithelial cells (Vero) were used for live cell imaging, as they had a flatter morphology than PK15 cells. Disruption of microtubules or actin filaments in Vero cells was achieved with 10 μm nocodazole or 0.5 μm cytochalasin D, respectively.

To grow the ΔUL36 virus (PRV-GS678; see below), PK15 cells were stably transfected with a fragment of the PRV genome that included the entire UL36 ORF and neighboring sequences (598 nt upstream and 798 nt downstream) containing portions of the UL35 and UL37 genes. The UL36-containing fragment was cloned into a neomycin phosphotransferase-encoding plasmid into which a monomeric red-fluorecent protein (mRFP1)-expression cassette was subsequently inserted, resulting in pGS901. Red-fluorescent cells were isolated by limiting dilution and subsequent expansion in the presence of 0.5 mg/ml G418. An isolate that expressed heterogeneous levels of red fluorescence provided the best complemented growth of PRV-GS678, and was saved as PK15-UL36 cells.

A UL37-complementing cell line was isolated to efficiently propagate the ΔUL37 virus (PRV-GS993; see below). The entire UL37 ORF and downstream 903 nt (which includes a portion of the UL36 gene), was subcloned into the CMV IE expression cassette of the pLPCX retroviral vector (Clontech), resulting in pGS1324. Co-transfection

of pGS1324 and pVSV-G into a retroviral packaging cell line, and subsequent isolation of retroviral particles, was done as recommended by the manufacturer (Clontech). The resulting retrovirus was used to transduce PK15 cells, which were then selected with 1 μg/ml puromycin. The resulting cell population was saved as PK15-UL37 cells.

Viruses.

Chapter 2:

Derivatives of PRV-Becker encoding either *egfp* or *mrfp1* fused in-frame to the UL35 capsid gene, PRV-GS443 and PRV-GS847 respectively, were previously described (91, 92). Deletions of the UL36 and UL37 genes were made by replacing each respective coding sequence with a kanamycin-resistance cassette flanked by Flp recombination target (FRT) sites, followed by removal of the kanamycin cassette by Flp mediated recombination.

To make the ΔUL36 virus, the pGS443 infectious clone was transformed into the EL250 *E. coli* strain, resulting in strain GS575 (52). A kanamycin cassette was amplified by polymerase chain reaction (PCR) from the pUCK4 plasmid (Pharmacia) using primers:

5'AAAGATTTTTCCCCCACGCGCGTGTGTTATTTCAGCCATG**TAA**
GAAGTTCCTATACTTTCTAGAGAATAGGAACTTCCCAGTCACGACGTTGTAAAACG
and
5'AGTCCTCCCGGGTGGGCCAGACGCGGCCGAGGCCGCCCAGGAAGTTCCTATTCT
CTAGAAAGTATAGGAACTTCGAAACAGCTATGACCATGATTACG.

Each primer encodes a single FRT site (underlined) and 3' homology to the pUC4K template. The 5' portions of the primers are homologous to the PRV UL36 gene (-37 nt to +3 nt and +8911 nt to +8950 nt relative to the UL36 ORF respectively). The first primer also encodes a stop codon (bold) fused downstream of the UL36 ATG initiation codon. The resulting PCR product was transformed into GS575 that was first induced to express the RED proteins (exo, beta and gam), and recombinants were selected with 20 μg/ml chloramphenicol and 50 μg/ml kanamycin (52, 116). One recombinant, GS674, was confirmed by restriction digest analysis. Arabinose-induced expression of Flp recombinase was used to remove the kanamycin cassette, resulting in GS678 (Figure 1). Sequencing of the pGS678 infectious clone plasmid confirmed the presence of a TAA stop codon and single FRT site in place of nucleotides 4-8910 of the UL36 ORF. The resulting allele has a stop codon fused immediately downstream of the endogenous UL36 start codon, and is deleted for the subsequent 2969 codons (the product of the UL36 ORF, VP1/2, is predicted to be a 3084 aa protein). Transfection of pGS575 into PK15 cells resulted in the GFP-capsid virus (PRV-GS575). Transfection of pGS678 into PK15-UL36 cells resulted in the ΔUL36 GFP-capsid virus (PRV-GS678). Transfection of infectious clones by electroporation into PK15 cells was performed as previously described (55).

The ΔUL37 virus was made by the same strategy as the ΔUL36 virus described above. The pGS847 infectious clone was transformed into the EL250 *E. coli* strain, resulting in strain GS958. The kanamycin cassette was amplified using a pair of FRT-encoding primers (FRT sequences are underlined) with 5' homologies to the PRV UL37

gene +6 nt to +45 nt and +2200 nt to +2239 nt relative to the UL37 ORF respectively):

5'GGCGCTCGTGCGCGCGCTCGAGGAGGCCGACCACGCCGTC**TAA**GAAGTTCCTATACTTTCTAGAGAATAGGAACTTCCCAGTCACGACGTTGTAAAACG

and

5'CCAGCGCCTCGCACTCGCGCAGCGCCTCCGTCGTCTGCGCGAAGTTCCTATTCTCTAGAAAGTATAGGAACTTCGAAACAGCTATGACCATGATTACG.

The resulting PCR product was recombined into GS958 and one recombinant, GS992, was confirmed by restriction digest analysis. Arabinose-induced expression of Flp recombinase was used to remove the kanamycin cassette, resulting in GS993 (Figure 1). The resulting allele has a stop codon fused 15 codons downstream of the endogenous UL37 start codon, and is deleted for the subsequent 718 codons (the product of the UL37 ORF is predicted to be a 919 aa protein). A deletion in UL37 that leaves the first 15 codons intact has no impact on expression of the upstream UL38 gene (47). Transfection of pGS993 into PK15-UL37 cells resulted in the ΔUL37 mRFP1-capsid virus (PRV-GS993).

Although PRV-GS678 could be propagated on PK15-UL36 cells, sequential passage of the virus ultimately resulted in repair of the ΔUL36 allele in the viral genome. PK15-UL36 cells provided less than wild-type growth kinetics of PRV-GS678, and only low titer stocks of PRV-GS678 could be isolated prior to the emergence of spontaneous revertant viruses. One spontaneous revertant virus, PRV-GS678R, was isolated from growth of PRV-GS678 on PK15 cells transfected with the UL36 gene. In contrast, we never observed spontaneous reversion of PRV-GS993 on PK15-UL37 cells, probably

due to the lack of flanking homology 5' of the transgene to the viral genome. Therefore, to make a revertant of the PRV-GS993 virus, the UL37 gene was subcloned with 800 nt of flanking sequence both upstream and downstream the UL37 ORF (pGS1522). This construct was transiently transfected into Vero cells, which were then infected with PRV-GS993 one day post-transfection. This resulted in many large foci of viral spread which were collectively harvested 3 days post-infection. The viral stock was expanded by two subsequent rounds of infection and harvest, resulting in the PRV-GS993R stock.

Chapter 3:

Viruses encoding either the green fluorescence protein (GFP) or monomeric red fluorescence protein (mRFP1) fused to the capsid VP26 protein (PRV-GS443 and PRV-GS847), and their respective infectious clones (pGS443 and pGS847) were previously described (91, 92). Truncations of the UL36 gene were made using a RED-GAM/Flp-recombinase protocol that we have previously described (56). RED-GAM mutagenesis was first used to insert a stop codon followed by a kanamycin-resistance cassette flanked by Flp recombination target (FRT) sites at the desired location within the UL36 coding sequence. The kanamycin-resistance cassette was then excised by Flp-mediated recombination, leaving behind a 37 nt insertion that consisted of the stop codon immediately followed by a single FRT site. In the case of truncations made after codons 3022, 3054 and 3078, the UL36 coding sequence downstream of the insertion was replaced by the 37 nt insertion. In-frame deletions within the UL36 gene were also made using the RED-GAM/Flp method. However, stop codons were not included in the primer

sequences, resulting in a single FRT site residing at the site of deletion, with two additional nucleotides present to maintain the reading frame. As a result, the following twelve amino acids are encoded at the site of each in-frame deletion: GSSYSLESIGTS. Primers sequences used for RED-GAM mutagenesis are available upon request. All RED-GAM/Flp recombinations were introduced into the pGS443 (GFP-capsid) full-length infectious clone.

A virus carrying the in-frame deletion lacking codons 6-225 of the UL36 gene was remade using a two-step RED-GAM recombination protocol (101). Using this protocol, the deletion was made without leaving behind an FRT site in the viral genome (codons 5 and 226 were abutted directly). The primers used for this protocol were:

5'-

‘CCCACGCGCGTGTGTTATTTCAGCCATGACGGCCGACGCGCCCTCCGTGCACCCG

ATGGCAGGATGACGACGATAAGTAGGG

and

5'-

CCGCCGGGTCCGGCGGCAGGGCCATCGGGTGCACGGAGGGCGCGTCGGCCGTC

ATGGCTGCAACCAATTAACCAATTCTGATTAG.

The primers contain homology to the UL36 gene both upstream and downstream the sequence to be deleted, and homology to the pEPkan-S template plasmid (underlined) (101). The recombination was used to modify the pGS847 infectious clone, which encodes the previously described mRFP1-VP26 (red capsid) allele (92). The resulting recombinant infectious clone, pGS1651, was confirmed by sequencing. Transfection of

pGS1651 into PK15 cells resulted in production of virus PRV-GS1651, which typically grew to a titer of $1x10^5$ PFU/ml. To make a revertant of the PRV-GS1651 virus, a segment of the UL36 gene was subcloned with 616 nt of flanking sequence upstream and 1822nt downstream the deletion (pGS765). This construct was transiently transfected into Vero cells, and the cells were subsequently infected with PRV-GS1651 the next day. Virus was harvested 3 days post-infection, passaged 2 additional times, and a single isolate was plaque purified. The resulting virus stock, PRV-GS1651R was confirmed to encode the full-length UL36 gene by restriction analysis and DNA sequencing.

Chapter 4:

Two recombinant viruses were made from a derivative of the PRV (Becker strain) infectious clone, pBecker3, that was previously made to encode an mRFP1-VP26 (red-fluorescent capsid) fusion allele (pGS847) (89, 92). A mutant derivative of pGS847 encoding a single codon change in the UL36 gene (C26A) was constructed using a two-step RED recombination protocol (101). The primers used for this protocol were

5´-

TCAGTATGACCCCGACCTGGGGCCCGGGTCGGGCGTCTCG**GCT**CTGCGCTCCTCC

CTCTCCTTAGGATGACGACGATAAGTAGGG

and

5´-

TCGTGAAGACCAGGCGCAGGAAGGAGAGGGAGGAGCGCAGAGCCGAGACGCCCG

ACCCGGGCCCAACCAATTAACCAATTCTGATTAG.

The primers encode the sequence to be mutated (bold) with surrounding homology to the UL36 gene, as well as homology to the pEPkan-S template plasmid (underlined). Transfection of the resultant infectious clone, pGS1652, into pig kidney epithelial (PK15) cells produced the PRV-GS1652 virus, which typically propagated to a titer of 1×10^7 plaque forming units (PFU) per ml. A revertant virus, PRV-GS1768, was constructed using the same methods. The primers used were

5´-

TCAGTATGACCCCGACCTGGGGCCCGGGTCGGGCGTCTCG**TGC**CTGCGCTCCTCC

CTCTCCTTAGGATGACGACGATAAGTAGGG

and

5´-

TCGTGAAGACCAGGCGCAGGAAGGAGAGGGAGGAGCGCAG**GCA**CGAGACGCCCG

ACCCGGGCCCAACCAATTAACCAATTCTGATTAG. All mutations were confirmed by restriction digests and sequencing.

PRV152 is a derivative of the PRV-Bartha vaccine strain that encodes a GFP-expression cassette driven by the CMV immediate early promoter inserted in the gG locus, and was described previously (87). PRV152 spreads through retrograde circuits efficiently, and served as a control for these studies.

Chapter 4:

Stocks of PRV-GS847 (WT), PRV-GS1652 (C26A), PRV-GS1768 (revertant) and PRV152 (Bartha-GFP) were harvested from infected PK15 cells grown in DMEM supplemented with 2% bovine growth supplement (Invitrogen). High titer virus stocks were prepared for a subset of animal studies as described previously (54).

Viral propagation kinetics, titers and plaque size analysis

Quantitation of viral propagation kinetics by single-step growth curve analysis was conducted as previously described, with the exception that Vero cells were substituted for PK15 cells in Chapters 3 & 4 (100). PK15 cells were infected at a multiplicity of infection (MOI) of 5 for each viral strain. Viral titers from cells or media supernatants harvested at 2, 5, 8, 12 or 24 hours post infection (hpi) were determined in duplicate by plaque assay. Plaque diameters were measured from images captured with a 10x objective with a 0.3 numerical aperture (NA). Two orthogonal diameter measurements of each fluorescent plaque were analyzed using the Metamorph software package (Molecular Devices). The reported plaque diameters represent an averaged of more than 50 plaques per virus, and were plotted using the Prism software package (GraphPad Software).

DNA Purification.

Infectious clone plasmids were isolated from *E. coli* strain EL250 by standard alkali lysis methods. Viral DNAs were isolated from nucleocapsids purified from infected PK15 cells, as previously described (90).

Viral stocks, transfection and infection.

Infectious clones of pseudorabies virus (PRV) were isolated following transfection of infectious clone plasmids into PK15 cells as previously described (55). A high-titer stock of the ∆6-225aa virus (PRV-GS1651) for use in single-step growth analysis (Chapter 3) was prepared by infecting $9.5x10^7$ PK15 cells in roller bottles at an MOI=0.01. Three days post-infection, the culture media was harvested, cleared of cells by centrifugation at 3950 x g for 30 minutes, and virions were concentrated by pelleting through a 10% Nycodenz cushion at 13000 rpm in a SW28 rotor (Beckman). Pellets were resuspended in approximately 150 µl Dulbecco's Modified Eagle's Medium (DMEM) supplemented with 2% bovine growth serum (HyClone), and titers were determined using African green monkey kidney epithelial cells (Vero) by plaque assay. This typically resulted in a PRV-GS1651 titer of $1x10^7$ PFU/ml.

Vero cells were used for subcellular localization studies, and were transfected with polyethylenimine (PEI; Polysciences, cat#23966) as follows: to 1 ml DMEM, 45 µl PEI solution (1 µg/ml) and 45 µl plasmid DNA (300 µg/ml) were added, mixed and incubated at room temperature for 10 minutes. The mixture was added to a subconfluent 10 cm dish of cells and incubated for 8-18 hours. The cells were then passaged onto coverslips for imaging. In a subset of experiments, the cells were infected with a RFP-capsid virus (PRV-GS847; see above) at an MOI = 10 prior to imaging between 10-12 hours post infection (hpi).

Human embryonic kidney epithelial cells (HEK293) were used in transient

transfections that were further made into cell lysates using 100 μL of 2× final sample buffer (see Western blot analysis section below) per well in a 6-well tray.

Chick embryonic dorsal root sensory neurons were isolated and cultured for studies of axonal transport, as previously described (88, 91). Neurons were infected after 2-3 days in culture. Time-lapse imaging of capsid transport following entry was captured between 0-1 hpi. Capsid transport velocities were measured as the instantaneous distance traveled between successive captured frames divided by the frame rate of 50 ms/frame. Capsid egress in axons following replication was imaged at 20 hpi, and axons were scored for the presence or absolute absence of capsids.

Subcloning.

Chapter 3:

The 3' end 189 nt of the UL36 gene (encoding the carboxy terminal 62 amino acids and stop codon of VP1/2) were amplified with primers:

5'-GCAGATCTCGCGTGGTGGAGTCG

and

5'-GCAAGCTTAACCGAGAATCAGGCG.

The resulting PCR product was subcloned into pEGFP-C1 (Clontech) using *Bgl*II and *Hind*III restriction sites (underlined in primers), resulting in pGS1163. The UL36 insert was confirmed by DNA sequencing. The full-length UL36 gene was isolated from the viral genome by using a variation of the RED-GAM recombination procedure, which allowed us to avoid the possibility of introducing PCR errors into the ~ 9.3 kbp open

reading frame. Briefly, a plasmid encoding an R6K origin of replication and beta-lactamase (ampicillin resistance) was PCR amplified with primers:

5'-

CCAAATAAAAAGATTTTTCCCCCACGCGCGTGTGTTATTTCAGCCGATTTTTATCGAATTCGTCATCCATATCACCACG

and

5'-

ACTGATTACGATAGCCGACGACCACCGCGTCGGCCGTCAAAGCTTCCACATGTGGAATTCCCAT

(underlined sequences encode *Bsa*BI, *Eco*RI and *Hind*III restriction sites). The resulting PCR product was recombined immediately upstream of the UL36 start methionine codon using RED-GAM as described above (the 5' ends of each primer encode the homology to the UL36 gene). A resulting ampicillin-resistant recombinant was digested with *Bsa*BI to liberate a viral genomic fragment containing the PCR product adjacent to the UL36 gene, as well as downstream sequences that include the UL35 gene and a small segment of the UL34 gene (which encodes a second *Bsa*BI restriction site). Self-ligation of the fragment resulted in a plasmid that was cloned into S17λpir *E.coli*, allowing for replication based off the R6K origin. The UL36 gene was then subcloned in-frame downstream the *egfp* open-reading frame within the pEGFP-C1 mammalian expression vector (Clontech) using the primer-encoded *Eco*RI and *Hind*III sites. The resulting plasmid, pGS1521, expresses GFP fused to aa2-3084 of VP1/2 (the entire protein minus the start methionine).

Western blot analysis, antibodies and densitometry.

Chapter 2:

Coverslips were incubated for 1 hour in fixation-extraction buffer (100mM PIPES, pH 6.9, 1mM EGTA and 1mM MgCl2 containing 0.1% glutaraldehyde and 1.0% Triton-X 100) at room temperature. Samples were washed in PBS and quenched with 1% sodium borohydride for 20 minutes at room temperature. Coverslips were then blocked with 1% BSA. For microtubule staining, samples were incubated with rat monoclonal anti-tubulin antibodies (clone YL1/2, provided by J.V. Kilmartin, Laboratory of Molecular Biology, Cambridge, UK) for 30 minutes at 37˚C followed by incubation with anti-rat secondary antibodies (1:200) conjugated to Cy5 fluorophore (Jackson Immunoresearch Laboratories). The actin cytoskeleton was visualized by staining with phalloidin conjugated to Alexa350 fluorophore (Molecular Probes).

Chapter 3&4:

VP5 and UL37 antigens were detected in PK15 cells infected with either PRV-GS847, PRV-GS1651 or PRV-1652 at an MOI < 0.1. Infections were carried out in confluent 10 cm dishes, which were harvested once all cells displayed cytopathic effect. Cells were lysed in 1 ml 2× final sample buffer (10 mM Tris, pH 7.4 / 150 mM NaCl / 1% Triton X-100) containing 10% β–mercaptoethanol, and the samples were boiled for 5 minutes prior to electrophoreses of 10 µl of each sample through a 8% SDS/polyacrylamide gel. Extracellular virions were purified from infected cell

supernatants by rate zonal ultracentrifugation in a 12-32% dextran gradient as described previously (3), then mixed with equal parts sample buffer and boiled for 5 minutes. Proteins were subsequently transferred onto a Hybond-P membrane (Amersham Biosciences), and Western blot analysis was performed as previously described (89). 3C10 is a mouse monoclonal antibody raised against the PRV VP5 protein that was used at 1:1000 dilution, and was a kind gift of Lynn Enquist. D1789 is a rabbit antisera raised against a peptide derived from the PRV UL37 sequence (REAADRVLGDYHE) that was used at 1:2500 dilution. The secondary goat anti-mouse and anti-rabbit horseradish peroxidase (HRP)-conjugated antibodies (Jackson ImmunoResearch) was used at a 1:10,000 dilution. HRP was detected with a luminol-coumeric acid-H_2O_2 chemiluminescence solution and exposed to film. For detection of VP5 and UL37 antigens in extracellular viroins, equal volumes of purified virions (see above) and 2× final sample buffer were mixed and boiled for 5 minutes. 15 µl of each sample was separated by electrophoresis on 4-20% SDS/polyacrylamide gel. Western blot analysis was carried out as described above.

Relative expression levels of UL37 protein were determined by digitizing exposed films with an EDAS 290 documentation system (Kodak). The intensity of UL37 and VP5 protein bands were quantitated using the ImageJ software package (1). UL37 protein expression was normalized using VP5 expression as a baseline, and the relative expression of UL37 was calculated as a percentage relative to virus encoding wild-type VP1/2.

Chapter 5:

GFP-fusion proteins were detected in Vero cells either infected with PRV-GS847, PRV-GS909, PRV-GS1903, or transfected with pGS1952. Cell lysis was as described in Lee et. al, 2006. Cells were lyzed and collected in 500 µL volumes in 2× sample buffer (10 mM Tris [pH 7.4], 150 mM NaCl, 1% Triton X-100) containing 10% β-mercaptoethanol, and the samples were boiled for 5 min prior to electrophoresis of 10-30 µL each sample through and 4-15% gradient sodium dodecyl sulfate-polyacrylamide gel (Bio-Rad Laboratories cat no. 161-1104). GFP is a mouse monoclonal antibody purchased from Santa Cruz Biosciences and was used at 1:1,000 dilution.

Live-cell fluorescence microscopy

Immunostained cells were observed with a Nikon Eclipse TE200 inverted microscope equipped with a 100X oil immersion objective (Chapter 2). Optimized Cy5 and UV filter sets (Chroma Technology Corporation) were used for Cy5 and Alexa350 fluorescence detection, respectively. Digital images were acquired with a CH250 charged coupled device (CCD; Photometrics) controlled by Metamorph imaging software (Molecular Devices).

All other static and time-lapse images were acquired from living cells using an inverted wide-field Nikon Eclipse TE2000-U microscope. The microscope was fitted with a Cascade:650 CCD (Roper Scientific) and was housed in a 37˚C environmental box (Life Imaging Services). Infected cells were imaged in sealed chambers as previously described (91). The Metamorph software package was used for image acquisition.

Fluorescent and phase contrast images of infected PK15 cells were captured using a 10X/0.3 numerical aperture (NA) objective, and time-lapse fluorescent imaging of infected Vero cells was performed with a 60X/1.4NA objective. Cytoplasmic fluorescent punctae observed in Vero cells were consistent with emissions from individual fluorescent-capsids (91, 92). Nuclear fluorescence was significantly brighter and not diffraction limited, and likely results from the formation of large nuclear capsid inclusions (27, 75).

Confocal image Z-series were acquired on a LSM510 Meta microscope using a 63X/1.4NA objective with 488 Argon, 543 HeNe and 405 diode laser lines. Cells were incubated in 5 μg/ml Hoechst 33342 (Molecular Probes) for 30 minutes prior to imaging. Imaging of entry and egress axonal transport events was performed using primary cultured neurons from embryonic chicken (E8-E10) dorsal root ganglia, as previously described (54). Metamorph and Prism software packages were used for the analysis of instantaneous velocities and quantitation of viral capsids in axons. Time-lapse images were captured as described above.

Image analysis.

Chapter 2:

Nuclear egress in Vero cells was analyzed by acquiring both fluorescence and DIC still images of infected cells. The DIC images were used to identify the location of nuclei. Because fluorescent-capsids in proximity of the nuclear membrane cannot be spatially resolved as cytoplasmic or nuclear, cells were only scored as positive if 10 or

more fluorescent-punctae were considered to be outside of the nucleus.

To examine cytoplasmic capsid dynamics, time-lapse fluorescence images were captured at 5 frames/s (continuous 200 ms exposures). The fluorescent punctae of individual fluorescent-capsids were subsequently tracked using the Metamorph "Track Points" application. Because many capsids displayed little or no motion during recording, only capsids that moved at least 1 μm were included in the data sets used for subsequent analysis. Statistical analysis of capsid transport velocities (in Chapter 3&4) was carried out using the Prism software package (GraphPad Software).

Released particles assay

Released viral particles were imaged on glass coverslips to determine the incorporation of fluorescence fusion proteins as previously described (55). Briefly, Vero cells were grown on coverslips and infected with fluorescent viruses at a low MOI (<1). Images were taken at 3 days post infection focusing on areas devoid of cell debris. Emissions from fluorescent proteins are of the *de novo* synthesized proteins. Colocalization quantitation was performed using Metamorph and Excel.

ABC nucleocapsid preparation

Vero cells were grown in 850 cm^2 roller bottles and infected with PRV-GS909 or PRV-GS1903 at an MOI of 3. Cells were resuspended in lysis buffer (150mM NaCl, 10mM Tris-Hcl [pH 7.2], 2mM $MgCl_2$, 1% NP-40, 5mM DTT, 0.2% protease inhibitor cocktail (Sigma cat. no. P8340). Cell nuclei were pelleted 1000×g for 10 min at 4°C and

subsequently lyzed by three cycles of freeze-thaw. Capsids were collected by discarding the nuclei pellet after 7000×g for 10 min at 4°C. The 100U DNase treated capsid fraction was first pelleted through a 35% sucrose cushion then overlayed onto a 20-50% sucrose gradient (both steps were 25,000 RPM for 1 hr at 4°C in a Beckman-Coulter SW41 rotor). Resultant A, B, and C bands were pulled from the gradient using a 27-gauge needle. Each fraction was diluted in PBS and placed on glass coverslips for imaging. Metamorph and Excel softwares were used to RFP and GFP signal colocalization analysis.

Infection block experiment

Vero cells were transfected with 2 µg of DNA in a 10 cm plate using Lipofectamine 2000 (Invitrogen) and split onto glass coverslips 24 hours post transfection. After another 12-16 hours, transfected cells were infected with a wild-type virus at MOI = 5.0. Transfected cells were scored for infection at 9-11 hpi. Statistically analysis was performed using Excel and plotted using the Prism software package (GraphPad Software).

Leptomycin B treatment

Vero cells were transfected with 250 ng of DNA on glass coverslips using PEI (Polyethylenimine). At 24 hours post transfection, DMSO or 20 ng/mL Leptomycin B (Sigma) was used to treat the transfected cells. Fluorescence microscopy was performed 3-4 hours post treatment.

Animals

Male Sprague-Dawley and Long Evans rats (Charles River Breeding Laboratories) were maintained under a light/dark cycle of 12 h light/12 h dark with food and water available ad libitum. Animals were at least 14weeks of age when used in experiments.

In vivo injection of virus

Intraocular injections: under isoflurane inhalation anesthetic (2.5-5%), animals received a unilateral intravitreal injection of PRV-GS847 or PRV-GS1652 (1 -14.5 X 10^8 plaque-forming units/ml) or a unilateral anterior chamber injection of 2µl of either PRV-GS847, PRV-GS1652, PRV152 or a 1:1 mixture of PRV-GS1652:PRV152, over a 1-min interval using a Nanoject II nanoinjector fitted with a glass micropipette (Drummond Scientific Co, Broomall, PA). A fresh stock of virus was thawed for each injection. Animals were maintained in a biosafety level 2 facility for up to 11 days post-inoculation. *Intracranial injections*: under isoflurane inhalation anesthetic (2.5-5%), animals were positioned in a Kopf stereotaxic apparatus (David Kopf Instruments, Tujunga, CA). A craniotomy was performed and the exposed dura mater was excised. A glass micropipette attached to a Nanoject II nanoinjector, angled laterally 10^o to the vertical to avoid the midline third ventricle, was lowered to a predetermined depth and 207 nl of PRV GS1652 $\text{of } 1 \times 10^8$ pfu/ml were ejected into the region of the hypothalamic suprachiasmatic nucleus (SCN). The micropipette was left in place for about 1 minute before slowing retracting. The craniotomy was packed with gelfoam and the incision was sutured.

Eyelid injections: under isoflurane inhalation anesthetic (2.5-5%), the skin of the upper eyelid of one eye was injected with 2 μl of GS1652 (1-4.25 × 10^8 pfu/ml) and the upper eyelid of the other eye was injected with 2 μl of PRV152 (1 × 10^8 pfu/ml). In a separate set of experiments, animals received a unilateral upper eyelid injection of 2 μl of cholera toxin-_ subunit conjugated to Alexa Fluor 594 (Molecular Probes, Eugene, OR) using a Nanoject II nanoinjector fitted with a glass micropipette.

Tissue preparation

After post-injection intervals ranging from 2-11 days, animals were deeply anesthetized with sodium pentobarbital (80 mg/kg, i.p.), and perfused transcardially with 0.9% saline followed by freshly prepared fixative consisting of 4% paraformaldehyde in phosphate buffer (0.1M), pH 7.3. Brains were removed, stored in the same fixative containing 30% sucrose at 4ºC overnight, and sectioned at 40 μm in the coronal plane on a sliding microtome equipped with a freezing stage (Physitemp Instruments Inc., Clifton, NJ). Sections were collected in phosphate buffer, mounted on subbed slides, blotted to remove excess buffer, and coverslipped with Vectashield mounting medium (Vector Laboratories, Burlingame, CA). Coverslips were sealed with fingernail polish to prevent dehydration, and slides were stored in the dark at 4ºC. EGFP and mRFP1 fluorescence is stable under these conditions for several months with minimal quenching. Slides were examined using a Leica (Nussloch, Germany) DMRA light microscope equipped with epifluorescence and fitted with a microstepping servomotor in the z–axis. Images were captured using a Hamamatsu (Hamamatsu City, Japan) C4742-95 CCD digital camera

under epifluorescence using either EGFP optics (412020 High Q narrow band EGFP filter; Chroma, Brattleboro, VT) or mRFP optics (#41004 HQ Texas Red filter, Chroma) and deconvolved using Openlab fluorescence deconvolution software (Improvision, Boston, MA) running on an Apple Macintosh G-4 platform. Digital images were pseudo-colored, and images were prepared using Adobe Photoshop version 6.0.1. Images were enhanced for brightness and contrast.

Statistical Analysis

All errors shown in figures were calculated using either of the following two statistical analysis methods: 1) standard error (SE), 2) standard error of the proportions (SEp). The decision to use either analysis is dependent on the nature of the scoring. If the experimental score represents a wide range of values, the standard error was used to average the data over 3 experiments. In experiments that yielded binary coding of results, on the other hand, standard error of the proportions was used. For example, analysis of capsid nuclear egress defect experiments were performed by examining a large number of cells, each with a score of either positive of negative. The significance of the percentage of cells scoring positive in one experiment may not be meaningfully assessed if no standard was applied to the overall sample size. The sample size of each experiment was included in the analysis. Standard error of the proportions test takes into account the deviation from the mean with respect to the size sampled and was therefore the analysis of choice. Calculations were done using Microsoft Excel software and Prism software package (GraphPad Software).

CHAPTER 7: CONCLUSIONS AND FUTURE DIRECTIONS

VP1/2, the largest herpesvirus-encoded protein, is conserved throughout the *Herpesviridae*, and is critical for the propagation of all herpesviruses examined. At the onset of my dissertation work, little was known regarding the specific functions performed by this protein. Null-deletion mutants of VP1/2 in both HSV-1 and PRV are nonviable and show abnormal accumulation of unenveloped capsids in the cytosol (19, 32). VP1/2 may be responsible for the delivery of viral genome into the nucleus and its involvement in cleavage and packing of DNA was suggested (5, 12). Our lab has reported the association of VP1/2 to the capsid complex during microtubule-based transport (35, 55). Through the work described in the preceding chapters, we now expand VP1/2 list of functions with the following: 1) VP1/2 is required for intracellular transport; 2) VP1/2 conserved domains are essential for virus propagation; 3) VP1/2 amino terminus, and the deubiquitinase encoded within, is dispensable for viral replication but required for neuroinvasion from peripheral innervated tissues; 4) the full-length protein is preferentially incorporated into the virion; 5) the protein is proteolytically processed during infection yielding a carboxy terminal fragment, which, 6) associates with the capsid inside the nucleus, and 7) mediates capsid nuclear egress; 8) the 62aa on the carboxy terminus directly interacts with the capsid-associated protein UL25. The significance of each finding will be examined below.

First, we conclude that VP1/2 is required for intracellular transport (Chapter 2). There are two likely explanations of the ΔVP1/2 mutant's abrogation of capsid intracellular transport. One involves the possibility of VP1/2 direct or indirect binding to a host motor complex. VP1/2 remains bound to capsids during intracellular transport and is

therefore a good candidate for a motor binding protein (55). This possibility is especially interesting in light of our recent publication on direct interaction between VP1/2 and the capsid-associated protein UL25 (13). Another explanation for the observed intracellular transport defect in the absence of VP1/2 is for VP1/2 to play a direct role in the re-envelopment process. Any residual capsid transport may represent cellular vesicles containing re-enveloped capsids (i.e. , virions) moving to the plasma membrane. We expect both explanations to be true and much work is needed to further identify the role of VP1/2 in capsid intracellular transport. Other members of the lab are actively pursuing the identification of VP1/2 regions responsible for host motor protein interaction, directly or indirectly through other proteins such as tegument or host cellular components. The role of UL37 in these transport processes are also being investigated. Novel assays are implemented to test for the requirement of UL37, the other capsid-associated protein, during entry intracellular transport. The search for motor protein interaction may be an arduous undertaking but one that will certainly yield important information. In addition to the investigation of VP1/2's involvement in capsid transport, we observed the disruption of capsid nuclear egress in the absence of VP1/2. This is in contrast to previous reports using both HSV-1 and PRV (19, 32). Together with data acquired in a subsequent study (to be discussed in a later section), we conclude VP1/2 to be directly involved in capsid nuclear egress.

Next, the large-scale analysis of specific conserved domains led to the finding that the amino terminus of VP1/2 is not essential for viral replication, despite the allure created by the deubiquitinase activity encoded within this region (41, 82). Our finding

using an alphaherpesvirus is consistent with recent findings obtained using a betaherpesvirus (108). Although the virus remains replication competent, the amino terminus deletion mutant (Δaa6-225) shows decreased propagation kinetics and reduction in capsid axonal targeting during egress. We next turned to an animal model of infection to gain insight into the functions of the amino terminus of VP1/2. The 1,000-fold reduction is indicative of important functions. Viruses with this deletion proves unusable in an *in vivo* study. In Chapter 4, we describe the study of the amino terminus using a single-codon replacement mutant. The C26A virus encodes an alanine in place of the catalytic cysteine at the core of the deubiquitinase activity. The C26A mutation resulted in a virus that replicated in non-neuronal cells both in culture and in the iris, and also replicated and spread in cultured neurons and neural circuits *in vivo*, but failed to spread between the iris and the innervating neurons. The revelation of this biological function has not been reported by other groups. An experiment to reproduce the *in vivo* findings in cultured cells would serve as a nice complement to our study. Future work for this project would entail the development of a co-culture system wherein neurons and epithelial cells are cultured in physically separated compartments and connected only through the neurite outgrowth across the barrier. Pathway dependence and cell type specificities could then be examined and the understanding of the deubiquitinase activity at the molecular level may be attained.

Unlike removal of the amino terminus, removal of other regions of the VP1/2 protein failed to result in productive viral infections (Chapter 3). Our conclusions differ from another group studying VP1/2 in PRV using a similar approach. In a previous

report, data from both our groups coincide at the carboxy terminus serving essential functions (7, 54). In a more recent report from the same group, authors Böttcher et. al. state that up to 45% of VP1/2 protein sequence is nonessential for viral replication (6). The emerging findings of VP1/2 mutagenesis studies point to the need for even more subtle manipulations of the protein sequences. Future work in this regard will parallel the motor-interaction search efforts such that smaller, conserved regions along the length of VP1/2 protein sequences will be mutated and examined. It is very likely that many more functions mediated by VP1/2 are yet undiscovered. Thus current findings help to prioritize the selection of potentially important regions for further analysis.

With little to no evidence from the literature, we were pleasantly surprised to find interesting functions mediated by the carboxy terminus of VP1/2. In Chapter 3, we describe the relocalization of the GFP-fused VP1/2 carboxy terminal 62aa to the nuclear capsid assembly sites during infection (54). Subsequent work led us to the demonstration of direct interaction between VP1/2 carboxy terminus and UL25 on the capsid (13). While these findings serve to advance the field, many questions remained: where is the intracellular site of tegumentation, how is this process regulated, and are tegumentation and capsid egress coupled? The next series of experiments we carried out resulted in findings that directly addressed these questions.

In our experiments designed to study the proteolytic processing of VP1/2 protein in cells, we constructed recombinant viruses that encode distinct fluorescent proteins on the ends of VP1/2. One virus encodes GFP on the carboxy terminus, which was otherwise identical to a previously characterized amino terminus GFP fusion virus, and

another virus simultaneously encodes mCherry and GFP on both ends of VP1/2. The approach resulted in the observation of distinct, processed forms of VP1/2 protein in infected cells. Western blot analysis revealed novel sub-full-length form species of the VP1/2 protein while fluorescence profile in living cells distinguished the intracellular localization of the amino terminus from the carboxy terminus. The propensity displayed by the carboxy terminus to localize at the nuclear envelope was further determined to contribute greatly to the process of nuclear capsid egress. Our ability to demonstrate a capsid nuclear egress defect restoration by the carboxy terminal region of VP1/2 reaffirms our previous report (Chapter 2) that ΔVP1/2 mutant virus is defective in capsid translocation from the nucleus into the cytosol (56). This is different from what other groups have reported (6, 19, 32). A ΔVP1/2 mutation made in HSV-1 did not result in nuclear egress defects (19). The same is true for a PRV ΔVP1/2 mutant virus (32). In the case of the HSV-1 ΔVP1/2 mutant virus, a large portion of the coding sequence was left intact in the mutant construction. The coding sequences analogous to our PRV carboxy terminal region (aa2026-3084) were not deleted. The possibility exists that the undeleted sequences in the HSV-1 ΔVP1/2 mutant virus may be expressed and are sufficient to confer nuclear egress function and therefore no defect was observed. The PRV ΔVP1/2 mutant virus described by Fuchs and colleagues, on the other hand, may have showed normal nuclear egress functions due to another reason. We detected deficient nuclear egress in the ΔVP1/2 mutant virus using fluorescence microscopy in living cells whereas Fuchs et. al. employed electron microscopy (EM) with fixed cells. It is likely that live-cell fluorescence microscopy allowed for a larger sample size than EM studies. Nuclear

egress is not completely abolished and that thin sections of cells examined using the EM approach may not provide full appreciation of a partial defect.

The detection of nuclear VP1/2 signal using the carboxy terminal GFP fusion virus also provided insight to egress stages of infection. Due to its tight association with the capsid (34, 98), VP1/2 is believed to constitute the inner most layer of tegument surrounding the capsid (69). When ultrastructural cryo-EM tomography was use to visualize the capsid at angstroms resolution, the protruding non-capsid density was suggested to be tegument protein (117). Taken together, VP1/2 is favored as a capsid-binding protein which is possibly added in the nucleus. Much effort has been devoted to the demonstration of VP1/2 nuclear presence to no avail; most notably, the use of immuno-gold particles electron microscopy (43). We attribute the difference between our result and previous reports to proteolytic processing of VP1/2. In the immuno-gold EM experiment, the detection method was dependent upon the antibody raised against the amino terminal region of the VP1/2 protein (43). It was an appropriate epitope choice under the assumption of VP1/2 functioning solely in the full-length form. In our approach, we have a GFP label on the capsid-binding region of VP1/2 that allowed for the direct detection of the carboxy terminal part of the protein. In addition, our observation using the dual-fluorescent labeled virus (43, 70) indicated the separation of the two termini during infection. Thus, we believe that the immuno-gold EM experiment failed to detect VP1/2 because the antibodies recognized an epitope that is physically separated from the carboxy terminus of VP1/2 and therefore absent in the nucleus. If an antibody recognizing the VP1/2 carboxy terminus were available, we predict the immuno-gold EM

technique would arrive at the same result as we have.

Although we have shown that VP1/2 may not be required to function in the full-length form during infection, there may still be an indispensable role played by the ~330kD protein (6, 43, 70). In the Western blot analysis using purified extracellular virions, we noted that the predominant structural form of VP1/2 was full-length and that both ends of the protein stay associated during intra-axonal retrograde transport. It is likely that after capsid nuclear egress, the full-length VP1/2 could either append to the capsid complex as an addition to or replacement of the carboxy terminal region that helped to deliver the capsids into the cytoplasm. VP1/2 is speculated to exist as an oligomer and the exact composition of such complex is worthy of future studies. We have yet to determine the possibility of intramolecular interactions within VP1/2 or intermolecular affinities between multiple copies of VP1/2, be it full-length or in smaller parts.

Another important future direction is to employ ultrastructural studies to examine the presence of VP1/2 carboxy terminal region in primary virions. As mentioned above, an antibody raised against the carboxy terminal region of VP1/2 would be useful in revealing the nuclear localization of VP1/2 as well as possible inclusion into the primary virion (in the internuclear space). Tegumentation of other proteins, in particular the ones that directly interact with VP1/2, shall be examined for the location of their addition onto the capsid complex.

In all, we have gained much understanding to the VP1/2 functions underlying its essential role to viral propagation. Many of the VP1/2 functions we have demonstrated

coincide with areas of intense interest in the field. To highlight one particular area, we now have strong evidence that VP1/2 (at least the carboxy terminal region) is directly involved in nuclear egress. The well-accepted envelopment-deenvelopment model of nuclear egress is quite complex and requires high expenditure of energy. In this model, capsids need to transverse two nuclear membranes by first budding then fusion. Tegument proteins UL31 and UL34 play important roles during this stage of infection but neither is structurally incorporated into the released virion.

Our finding that VP1/2, an integral component of the tegument, is sufficient to partially restore a nuclear egress defect serves as the first link between primary envelopment and the fully assembled virion. The mediation of capsid nuclear egress coupled with known interactions to other tegument proteins (UL37 and VP16) place VP1/2 at the core of assembly and egress. VP1/2 is potentially the thread that strings together distinct stages of infection. Based on our work and others, one could not help but wonder why a single protein alone, albeit very large, encodes for such a multitude of functions. There is an enzymatic activity (as a deubiquitinase) that is important for neuroinvasion, the interaction with capsid and tegument proteins, the requirement for intracellular transport, and the participation in nuclear egress. Why are so many functions assigned to one protein in a genome that encodes over 100? Perhaps in the evolution of herpesviruses, the necessary long-range travels (in axons) imposed limitations on cargo weight. But to take a light cargo, the content must be worthwhile. VP1/2 is maybe analogous to the carefully edited survival kit one takes into the wilderness; it provides all essential instruments to sustain life. By packing VP1/2 to travel with, capsids and the

enclosed genome may ensure the functions essential for viral propagation to be available. Other virally encoded proteins may serve functions redundant to VP1/2, which would be consistent with some of the partial defects observed in the VP1/2 mutants. Other proteins may be reliant on interaction to VP1/2 for tegumentation. Much work lay ahead but we are now much better poised to unravel the complicated infectious processes as events that are nucleated by VP1/2 tegumentation onto the capsid.

REFERENCES

1. **Abramoff, M. D., P. J. Magelhaes, and S. J. Ram.** 2004. Image Processing with ImageJ. Biophotonics International **11:**36-42.
2. **Andreansky, S. S., B. He, G. Y. Gillespie, L. Soroceanu, J. Markert, J. Chou, B. Roizman, and R. J. Whitley.** 1996. The application of genetically engineered herpes simplex viruses to the treatment of experimental brain tumors. Proc Natl Acad Sci U S A **93:**11313-8.
3. **Antinone, S. E., and G. A. Smith.** 2006. Two modes of herpesvirus trafficking in neurons: membrane acquisition directs motion. J Virol **80:**11235-40.
4. **Banfield, B. W., J. D. Kaufman, J. A. Randall, and G. E. Pickard.** 2003. Development of pseudorabies virus strains expressing red fluorescent proteins: new tools for multisynaptic labeling applications. J Virol **77:**10106-12.
5. **Batterson, W., D. Furlong, and B. Roizman.** 1983. Molecular genetics of herpes simplex virus. VIII. further characterization of a temperature-sensitive mutant defective in release of viral DNA and in other stages of the viral reproductive cycle. J Virol **45:**397-407.
6. **Bottcher, S., H. Granzow, C. Maresch, B. Mohl, B. G. Klupp, and T. C. Mettenleiter.** 2007. Identification of functional domains within the essential large tegument protein pUL36 of pseudorabies virus. J Virol.
7. **Bottcher, S., B. G. Klupp, H. Granzow, W. Fuchs, K. Michael, and T. C. Mettenleiter.** 2006. Identification of a 709-amino-acid internal nonessential region

within the essential conserved tegument protein (p)UL36 of pseudorabies virus. J Virol **80:**9910-5.

8. **Brideau, A. D., M. G. Eldridge, and L. W. Enquist.** 2000. Directional transneuronal infection by pseudorabies virus is dependent on an acidic internalization motif in the Us9 cytoplasmic tail. J Virol **74:**4549-61.
9. **Card, J. P., J. R. Dubin, M. E. Whealy, and L. W. Enquist.** 1995. Influence of infectious dose upon productive replication and transynaptic passage of pseudorabies virus in rat central nervous system. J Neurovirol **1:**349-58.
10. **Card, J. P., M. E. Whealy, A. K. Robbins, and L. W. Enquist.** 1992. Pseudorabies virus envelope glycoprotein gI influences both neurotropism and virulence during infection of the rat visual system. J Virol **66:**3032-41.
11. **Card, J. P., M. E. Whealy, A. K. Robbins, R. Y. Moore, and L. W. Enquist.** 1991. Two alpha-herpesvirus strains are transported differentially in the rodent visual system. Neuron **6:**957-69.
12. **Chou, J., and B. Roizman.** 1989. Characterization of DNA sequence-common and sequence-specific proteins binding to cis-acting sites for cleavage of the terminal a sequence of the herpes simplex virus 1 genome. J Virol **63:**1059-68.
13. **Coller, K. E., J. I. Lee, A. Ueda, and G. A. Smith.** 2007. The capsid and tegument of the alpha herpesviruses are linked by an interaction between the UL25 and VP1/2 proteins. J Virol.
14. **Cunningham, C., A. J. Davison, A. R. MacLean, N. S. Taus, and J. D. Baines.** 2000. Herpes simplex virus type 1 gene UL14: phenotype of a null mutant and

identification of the encoded protein. J Virol **74:**33-41.

15. **Davison, A. J.** 1993. Herpesvirus Genes. Rev Med Virol **3:**237-244.
16. **del Rio, T., C. J. DeCoste, and L. W. Enquist.** 2005. Actin is a component of the compensation mechanism in pseudorabies virus virions lacking the major tegument protein VP22. J Virol **79:**8614-9.
17. **Desai, P., G. L. Sexton, J. M. McCaffery, and S. Person.** 2001. A null mutation in the gene encoding the herpes simplex virus type 1 UL37 polypeptide abrogates virus maturation. J Virol **75:**10259-71.
18. **Desai, P., G. L. Sexton, J. M. McCaffery, and S. Person.** 2001. A null mutation in the gene encoding the herpes simplex virus type 1 UL37 polypeptide abrogates virus maturation. J Virol **75:**10259-71.
19. **Desai, P. J.** 2000. A null mutation in the UL36 gene of herpes simplex virus type 1 results in accumulation of unenveloped DNA-filled capsids in the cytoplasm of infected cells. J Virol **74:**11608-18.
20. **Desai, P. J.** 2000. A null mutation in the UL36 gene of herpes simplex virus type 1 results in accumulation of unenveloped DNA-filled capsids in the cytoplasm of infected cells. J Virol **74:**11608-18.
21. **Diefenbach, R. J., E. Diefenbach, M. W. Douglas, and A. L. Cunningham.** 2004. The ribosome receptor, p180, interacts with kinesin heavy chain, KIF5B. Biochem Biophys Res Commun **319:**987-92.
22. **Diefenbach, R. J., M. Miranda-Saksena, E. Diefenbach, D. J. Holland, R. A. Boadle, P. J. Armati, and A. L. Cunningham.** 2002. Herpes simplex virus

tegument protein US11 interacts with conventional kinesin heavy chain. J Virol **76:**3282-91.

23. **Diefenbach, R. J., M. Miranda-Saksena, E. Diefenbach, D. J. Holland, R. A. Boadle, P. J. Armati, and A. L. Cunningham.** 2002. Herpes simplex virus tegument protein US11 interacts with conventional kinesin heavy chain. J Virol **76:**3282-91.

24. **Douglas, M. W., R. J. Diefenbach, F. L. Homa, M. Miranda-Saksena, F. J. Rixon, V. Vittone, K. Byth, and A. L. Cunningham.** 2004. Herpes simplex virus type 1 capsid protein VP26 interacts with dynein light chains RP3 and Tctex1 and plays a role in retrograde cellular transport. J Biol Chem **279:**28522-30.

25. **Enquist, L. W.** 1994. Infection of the mammalian nervous system by pseudorabies virus (PRV). Seminars in Virology **5:**221-231.

26. **Enquist, L. W., P. J. Husak, B. W. Banfield, and G. A. Smith.** 1998. Infection and spread of alphaherpesviruses in the nervous system. Adv Virus Res **51:**237-347.

27. **Epstein, M. A.** 1962. Observations of the mode of release of herpes virus from infected Hela cells. JCB **12:**589-597.

28. **Flint, S. J., L. W. Enquist, R. M. Krug, V. R. Racaniello, and A. M. Skalka.** 1999. Principles of Virology, First ed. American Society for Microbiology, Washington DC.

29. **Forest, T., S. Barnard, and J. D. Baines.** 2005. Active intranuclear movement of herpesvirus capsids. Nat Cell Biol **7:**429-31.

30. **Fuchs, W., H. Granzow, R. Klopfleisch, B. G. Klupp, and T. C. Mettenleiter.** 2006. The UL4 gene of pseudorabies virus encodes a minor infected-cell protein that is dispensable for virus replication. J Gen Virol **87:**2517-25.

31. **Fuchs, W., H. Granzow, B. G. Klupp, M. Kopp, and T. C. Mettenleiter.** 2002. The UL48 tegument protein of pseudorabies virus is critical for intracytoplasmic assembly of infectious virions. J Virol **76:**6729-42.

32. **Fuchs, W., B. G. Klupp, H. Granzow, and T. C. Mettenleiter.** 2004. Essential function of the pseudorabies virus UL36 gene product is independent of its interaction with the UL37 protein. J Virol **78:**11879-89.

33. **Fuller, A. O., and P. G. Spear.** 1987. Anti-glycoprotein D antibodies that permit adsorption but block infection by herpes simplex virus 1 prevent virion-cell fusion at the cell surface. Proc Natl Acad Sci U S A **84:**5454-8.

34. **Gibson, W., and B. Roizman.** 1972. Proteins specified by herpes simplex virus. 8. Characterization and composition of multiple capsid forms of subtypes 1 and 2. J Virol **10:**1044-52.

35. **Granzow, H., B. G. Klupp, and T. C. Mettenleiter.** 2005. Entry of pseudorabies virus: an immunogold-labeling study. J Virol **79:**3200-5.

36. **Granzow, H., B. G. Klupp, and T. C. Mettenleiter.** 2004. The pseudorabies virus US3 protein is a component of primary and of mature virions. J Virol **78:**1314-23.

37. **Gredmark, S., C. Schlieker, V. Quesada, E. Spooner, and H. L. Ploegh.** 2007. A functional ubiquitin-specific protease embedded in the large tegument protein (ORF64) of murine gammaherpesvirus 68 is active during the course of infection.

J Virol **81:**10300-9.

38. **Grunewald, K., P. Desai, D. C. Winkler, J. B. Heymann, D. M. Belnap, W. Baumeister, and A. C. Steven.** 2003. Three-dimensional structure of herpes simplex virus from cryo-electron tomography. Science **302:**1396-8.

39. **Hutten, S., and R. H. Kehlenbach.** 2007. CRM1-mediated nuclear export: to the pore and beyond. Trends Cell Biol **17:**193-201.

40. **Kato, A., M. Yamamoto, T. Ohno, M. Tanaka, T. Sata, Y. Nishiyama, and Y. Kawaguchi.** 2006. Herpes simplex virus 1-encoded protein kinase UL13 phosphorylates viral Us3 protein kinase and regulates nuclear localization of viral envelopment factors UL34 and UL31. J Virol **80:**1476-86.

41. **Kattenhorn, L. M., G. A. Korbel, B. M. Kessler, E. Spooner, and H. L. Ploegh.** 2005. A deubiquitinating enzyme encoded by HSV-1 belongs to a family of cysteine proteases that is conserved across the family Herpesviridae. Mol Cell **19:**547-57.

42. **Klupp, B. G., S. Bottcher, H. Granzow, M. Kopp, and T. C. Mettenleiter.** 2005. Complex formation between the UL16 and UL21 tegument proteins of pseudorabies virus. J Virol **79:**1510-22.

43. **Klupp, B. G., W. Fuchs, H. Granzow, R. Nixdorf, and T. C. Mettenleiter.** 2002. Pseudorabies virus UL36 tegument protein physically interacts with the UL37 protein. J Virol **76:**3065-71.

44. **Klupp, B. G., W. Fuchs, H. Granzow, R. Nixdorf, and T. C. Mettenleiter.** 2002. Pseudorabies Virus UL36 Tegument Protein Physically Interacts with the UL37

Protein. J Virol **76:**3065-71.

45. **Klupp, B. G., H. Granzow, W. Fuchs, G. M. Keil, S. Finke, and T. C. Mettenleiter.** 2007. Vesicle formation from the nuclear membrane is induced by coexpression of two conserved herpesvirus proteins. Proc Natl Acad Sci U S A **104:**7241-6.

46. **Klupp, B. G., H. Granzow, and T. C. Mettenleiter.** 2001. Effect of the pseudorabies virus US3 protein on nuclear membrane localization of the UL34 protein and virus egress from the nucleus. J Gen Virol **82:**2363-71.

47. **Klupp, B. G., H. Granzow, E. Mundt, and T. C. Mettenleiter.** 2001. Pseudorabies virus UL37 gene product is involved in secondary envelopment. J Virol **75:**8927-36.

48. **Klupp, B. G., H. Granzow, E. Mundt, and T. C. Mettenleiter.** 2001. Pseudorabies virus UL37 gene product is involved in secondary envelopment. J Virol **75:**8927-36.

49. **Knipe, D. M., W. Batterson, C. Nosal, B. Roizman, and A. Buchan.** 1981. Molecular genetics of herpes simplex virus. VI. Characterization of a temperature-sensitive mutant defective in the expression of all early viral gene products. J Virol **38:**539-47.

50. **Koshizuka, T., Y. Kawaguchi, and Y. Nishiyama.** 2005. Herpes simplex virus type 2 membrane protein UL56 associates with the kinesin motor protein KIF1A. J Gen Virol **86:**527-33.

51. **Kristensson, K., E. Lycke, M. Röyttä, B. Svennerholm, and A. Vahlne.** 1986.

Neuritic transport of herpes simplex virus in rat sensory neurons *in vitro*. Effects of substances interacting with microtubular function and axonal flow [nocodazole, taxol and erythro-9-3-(2-hydroxynonyl)adenine]. Journal of General Virology **67:**2023-2028.

52. **Lee, E. C., D. Yu, J. Martinez de Velasco, L. Tessarollo, D. A. Swing, D. L. Court, N. A. Jenkins, and N. G. Copeland.** 2001. A Highly Efficient Escherichia coli-Based Chromosome Engineering System Adapted for Recombinogenic Targeting and Subcloning of BAC DNA. Genomics **73:**56-65.

53. **Lee, G. E., J. W. Murray, A. W. Wolkoff, and D. W. Wilson.** 2006. Reconstitution of herpes simplex virus microtubule-dependent trafficking in vitro. J Virol **80:**4264-75.

54. **Lee, J. I., G. W. Luxton, and G. A. Smith.** 2006. Identification of an essential domain in the herpesvirus VP1/2 tegument protein: the carboxy terminus directs incorporation into capsid assemblons. J Virol **80:**12086-94.

55. **Luxton, G. W., S. Haverlock, K. E. Coller, S. E. Antinone, A. Pincetic, and G. A. Smith.** 2005. Targeting of herpesvirus capsid transport in axons is coupled to association with specific sets of tegument proteins. Proc Natl Acad Sci U S A **102:**5832-7.

56. **Luxton, G. W., J. I. Lee, S. Haverlock-Moyns, J. M. Schober, and G. A. Smith.** 2006. The Pseudorabies Virus VP1/2 Tegument Protein Is Required for Intracellular Capsid Transport. J Virol **80:**201-9.

57. **Lycke, E., B. Hamark, M. Johansson, A. Krotochwil, J. Lycke, and B.**

Svennerholm. 1988. Herpes simplex virus infection of the human sensory neuron. An electron microscopy study. Arch Virol **101:**87-104.

58. **Lycke, E., K. Kristensson, B. Svennerholm, A. Vahlne, and R. Ziegler.** 1984. Uptake and transport of herpes simplex virus in neurites of rat dorsal root ganglia cells in culture. J Gen Virol **65 (Pt 1):**55-64.

59. **Mabit, H., M. Y. Nakano, U. Prank, B. Saam, K. Dohner, B. Sodeik, and U. F. Greber.** 2002. Intact microtubules support adenovirus and herpes simplex virus infections. J Virol **76:**9962-71.

60. **Marchand, C. F., and M. E. Schwab.** 1986. Binding, uptake and retrograde axonal transport of herpes virus suis in sympathetic neurons. Brain Res **383:**262-70.

61. **Martinez-Moreno, M., I. Navarro-Lerida, F. Roncal, J. P. Albar, C. Alonso, F. Gavilanes, and I. Rodriguez-Crespo.** 2003. Recognition of novel viral sequences that associate with the dynein light chain LC8 identified through a pepscan technique. FEBS Lett **544:**262-7.

62. **McGeoch, D. J., S. Cook, A. Dolan, F. E. Jamieson, and E. A. Telford.** 1995. Molecular phylogeny and evolutionary timescale for the family of mammalian herpesviruses. J Mol Biol **247:**443-58.

63. **McGeoch, D. J., and A. J. Davison.** 1999. The molecular evolutionary history of the herpesviruses, First ed, vol. 1. Academic Press, San Diego.

64. **McGeoch, D. J., F. J. Rixon, and A. J. Davison.** 2006. Topics in herpesvirus genomics and evolution. Virus Res **117:**90-104.

65. **McNabb, D. S., and R. J. Courtney.** 1992. Analysis of the UL36 open reading frame encoding the large tegument protein (ICP1/2) of herpes simplex virus type 1. J Virol **66:**7581-4.

66. **Meckes, D. G., Jr., and J. W. Wills.** 2007. Dynamic Interactions of the UL16 Tegument Protein with the Capsid of Herpes Simplex Virus. J Virol.

67. **Mettenleiter, T. C.** 2004. Budding events in herpesvirus morphogenesis. Virus Res **106:**167-80.

68. **Mettenleiter, T. C.** 2006. Intriguing interplay between viral proteins during herpesvirus assembly or: the herpesvirus assembly puzzle. Vet Microbiol **113:**163-9.

69. **Mettenleiter, T. C., B. G. Klupp, and H. Granzow.** 2006. Herpesvirus assembly: a tale of two membranes. Curr Opin Microbiol **9:**423-9.

70. **Michael, K., S. Bottcher, B. G. Klupp, A. Karger, and T. C. Mettenleiter.** 2006. Pseudorabies virus particles lacking tegument proteins pUL11 or pUL16 incorporate less full-length pUL36 than wild-type virus, but specifically accumulate a pUL36 N-terminal fragment. J Gen Virol **87:**3503-7.

71. **Michael, K., B. G. Klupp, T. C. Mettenleiter, and A. Karger.** 2006. Composition of pseudorabies virus particles lacking tegument protein US3, UL47, or UL49 or envelope glycoprotein E. J Virol **80:**1332-9.

72. **Miranda-Saksena, M., P. Armati, R. A. Boadle, D. J. Holland, and A. L. Cunningham.** 2000. Anterograde transport of herpes simplex virus type 1 in cultured, dissociated human and rat dorsal root ganglion neurons. J Virol **74:**1827-

39.

73. **Nicola, A. V., J. Hou, E. O. Major, and S. E. Straus.** 2005. Herpes Simplex Virus Type 1 Enters Human Epidermal Keratinocytes, but Not Neurons, via a pH-Dependent Endocytic Pathway. J Virol **79:**7609-16.

74. **Nicola, A. V., A. M. McEvoy, and S. E. Straus.** 2003. Roles for endocytosis and low pH in herpes simplex virus entry into HeLa and Chinese hamster ovary cells. J Virol **77:**5324-32.

75. **Nii, S., C. Morgan, and H. M. Rose.** 1968. Electron microscopy of herpes simplex virus. II. Sequence of development. J Virol **2:**517-36.

76. **Ogawa-Goto, K., S. Irie, A. Omori, Y. Miura, H. Katano, H. Hasegawa, T. Kurata, T. Sata, and Y. Arao.** 2002. An endoplasmic reticulum protein, p180, is highly expressed in human cytomegalovirus-permissive cells and interacts with the tegument protein encoded by UL48. J Virol **76:**2350-62.

77. **Pickard, G. E.** 1982. The afferent connections of the suprachiasmatic nucleus of the golden hamster with emphasis on the retinohypothalamic projection. J Comp Neurol **211:**65-83.

78. **Pickard, G. E., C. A. Smeraski, C. C. Tomlinson, B. W. Banfield, J. Kaufman, C. L. Wilcox, L. W. Enquist, and P. J. Sollars.** 2002. Intravitreal injection of the attenuated pseudorabies virus PRV Bartha results in infection of the hamster suprachiasmatic nucleus only by retrograde transsynaptic transport via autonomic circuits. J Neurosci **22:**2701-10.

79. **Radtke, K., K. Dohner, and B. Sodeik.** 2006. Viral interactions with the

cytoskeleton: a hitchhiker's guide to the cell. Cell Microbiol **8:**387-400.

80. **Rassnick, S., L. W. Enquist, A. F. Sved, and J. P. Card.** 1998. Pseudorabies virus-induced leukocyte trafficking into the rat central nervous system. J Virol **72:**9181-91.

81. **Reynolds, A. E., L. Liang, and J. D. Baines.** 2004. Conformational changes in the nuclear lamina induced by herpes simplex virus type 1 require genes U(L)31 and U(L)34. J Virol **78:**5564-75.

82. **Schlieker, C., G. A. Korbel, L. M. Kattenhorn, and H. L. Ploegh.** 2005. A deubiquitinating activity is conserved in the large tegument protein of the herpesviridae. J Virol **79:**15582-5.

83. **Schlieker, C., G. A. Korbel, L. M. Kattenhorn, and H. L. Ploegh.** 2005. A Deubiquitinating Activity Is Conserved in the Large Tegument Protein of the Herpesviridae. J Virol **79:**15582-15585.

84. **Schlieker, C., W. A. Weihofen, E. Frijns, L. M. Kattenhorn, R. Gaudet, and H. L. Ploegh.** 2007. Structure of a herpesvirus-encoded cysteine protease reveals a unique class of deubiquitinating enzymes. Mol Cell **25:**677-87.

85. **Smeraski, C. A., P. J. Sollars, M. D. Ogilvie, L. W. Enquist, and G. E. Pickard.** 2004. Suprachiasmatic nucleus input to autonomic circuits identified by retrograde transsynaptic transport of pseudorabies virus from the eye. J Comp Neurol **471:**298-313.

86. **Smibert, C. A., B. Popova, P. Xiao, J. P. Capone, and J. R. Smiley.** 1994. Herpes simplex virus VP16 forms a complex with the virion host shutoff protein

vhs. J Virol **68:**2339-46.

87. **Smith, B. N., B. W. Banfield, C. A. Smeraski, C. L. Wilcox, F. E. Dudek, L. W. Enquist, and G. E. Pickard.** 2000. Pseudorabies virus expressing enhanced green fluorescent protein: A tool for in vitro electrophysiological analysis of transsynaptically labeled neurons in identified central nervous system circuits. Proc Natl Acad Sci U S A **97:**9264-9.

88. **Smith, C. L.** 1998. Cultures from chick peripheral ganglia, p. 261-287. *In* G. Banker and K. Goslin (ed.), Culturing Nerve Cells. MIT Press, Cambridge.

89. **Smith, G. A., and L. W. Enquist.** 2000. A self-recombining bacterial artificial chromosome and its application for analysis of herpesvirus pathogenesis. Proc Natl Acad Sci U S A **97:**4873-8.

90. **Smith, G. A., and L. W. Enquist.** 1999. Construction and transposon mutagenesis in Escherichia coli of a full- length infectious clone of pseudorabies virus, an alphaherpesvirus. J Virol **73:**6405-14.

91. **Smith, G. A., S. P. Gross, and L. W. Enquist.** 2001. Herpesviruses use bidirectional fast-axonal transport to spread in sensory neurons. Proceedings of the National Academy of Sciences **98:**3466-70.

92. **Smith, G. A., L. Pomeranz, S. P. Gross, and L. W. Enquist.** 2004. Local modulation of plus-end transport targets herpesvirus entry and egress in sensory axons. Proc Natl Acad Sci U S A **101:**16034-9.

93. **Smith, P. G., J. D. Warn, J. J. Steinle, D. Krizsan-Agbas, and W. Hasan.** 2002. Modulation of parasympathetic neuron phenotype and function by sympathetic

innervation. Auton Neurosci **96:**33-42.

94. **Sodeik, B., M. W. Ebersold, and A. Helenius.** 1997. Microtubule-mediated transport of incoming herpes simplex virus 1 capsids to the nucleus. J Cell Biol **136:**1007-21.

95. **Sodeik, B., M. W. Ebersold, and A. Helenius.** 1997. Microtubule-mediated transport of incoming herpes simplex virus 1 capsids to the nucleus. Journal of Cell Biology **136:**1007-1021.

96. **Sollars, P. J., C. A. Smeraski, J. D. Kaufman, M. D. Ogilvie, I. Provencio, and G. E. Pickard.** 2003. Melanopsin and non-melanopsin expressing retinal ganglion cells innervate the hypothalamic suprachiasmatic nucleus. Vis Neurosci **20:**601-10.

97. **Spear, P. G., and R. Longnecker.** 2003. Herpesvirus entry: an update. J Virol **77:**10179-85.

98. **Spear, P. G., and B. Roizman.** 1972. Proteins specified by herpes simplex virus. V. Purification and structural proteins of the herpesvirion. J Virol **9:**143-59.

99. **Stannard, L. M.** 1995, posting date. Herpesvirus. [Online.]

100. **Tirabassi, R. S., and L. W. Enquist.** 1998. Role of envelope protein gE endocytosis in the pseudorabies virus life cycle. J Virol **72:**4571-9.

101. **Tischer, B. K., J. von Einem, B. Kaufer, and N. Osterrieder.** 2006. Two-step red-mediated recombination for versatile high-efficiency markerless DNA manipulation in *Escherichia coli*. Biotechniques **40:**191-7.

102. **Tomishima, M. J., G. A. Smith, and L. W. Enquist.** 2001. Sorting and transport

of alpha herpesviruses in axons. Traffic **2:**429-36.

103. **van Leeuwen, H., G. Elliott, and P. O'Hare.** 2002. Evidence of a role for nonmuscle myosin II in herpes simplex virus type 1 egress. J Virol **76:**3471-81.

104. **Varnum, S. M., D. N. Streblow, M. E. Monroe, P. Smith, K. J. Auberry, L. Pasa-Tolic, D. Wang, D. G. Camp, 2nd, K. Rodland, S. Wiley, W. Britt, T. Shenk, R. D. Smith, and J. A. Nelson.** 2004. Identification of proteins in human cytomegalovirus (HCMV) particles: the HCMV proteome. J Virol **78:**10960-6.

105. **Verma, R., L. Aravind, R. Oania, W. H. McDonald, J. R. Yates, 3rd, E. V. Koonin, and R. J. Deshaies.** 2002. Role of Rpn11 metalloprotease in deubiquitination and degradation by the 26S proteasome. Science **298:**611-5.

106. **Vernon, S. K., W. C. Lawrence, C. A. Long, B. A. Rubin, and J. B. Sheffield.** 1982. Morphological components of herpesvirus. IV. Ultrastructural features of the envelope and tegument. J Ultrastruct Res **81:**163-71.

107. **Vittone, V., E. Diefenbach, D. Triffett, M. W. Douglas, A. L. Cunningham, and R. J. Diefenbach.** 2005. Determination of interactions between tegument proteins of herpes simplex virus type 1. J Virol **79:**9566-71.

108. **Wang, J., A. N. Loveland, L. M. Kattenhorn, H. L. Ploegh, and W. Gibson.** 2006. High-Molecular-Weight Protein (pUL48) of Human Cytomegalovirus Is a Competent Deubiquitinating Protease: Mutant Viruses Altered in Its Active-Site Cysteine or Histidine Are Viable. J Virol **80:**6003-12.

109. **Ward, P. L., W. O. Ogle, and B. Roizman.** 1996. Assemblons: nuclear structures defined by aggregation of immature capsids and some tegument proteins of

herpes simplex virus 1. J Virol **70:**4623-31.

110. **Whealy, M. E., J. P. Card, A. K. Robbins, J. R. Dubin, H. J. Rziha, and L. W. Enquist.** 1993. Specific pseudorabies virus infection of the rat visual system requires both gI and gp63 glycoproteins. J Virol **67:**3786-97.

111. **Wild, P., M. Engels, C. Senn, K. Tobler, U. Ziegler, E. M. Schraner, E. Loepfe, M. Ackermann, M. Mueller, and P. Walther.** 2005. Impairment of nuclear pores in bovine herpesvirus 1-infected MDBK cells. J Virol **79:**1071-83.

112. **Wong, M. L., and C. H. Chen.** 1998. Evidence for the internal location of actin in the pseudorabies virion. Virus Res **56:**191-7.

113. **Xu, F., M. R. Sternberg, B. J. Kottiri, G. M. McQuillan, F. K. Lee, A. J. Nahmias, S. M. Berman, and L. E. Markowitz.** 2006. Trends in herpes simplex virus type 1 and type 2 seroprevalence in the United States. Jama **296:**964-73.

114. **Ye, G. J., K. T. Vaughan, R. B. Vallee, and B. Roizman.** 2000. The herpes simplex virus 1 U(L)34 protein interacts with a cytoplasmic dynein intermediate chain and targets nuclear membrane. J Virol **74:**1355-63.

115. **Ye, G. J., K. T. Vaughan, R. B. Vallee, and B. Roizman.** 2000. The Herpes Simplex Virus 1 U(L)34 Protein Interacts with a Cytoplasmic Dynein Intermediate Chain and Targets Nuclear Membrane. J Virol **74:**1355-1363.

116. **Yu, D., H. M. Ellis, E. C. Lee, N. A. Jenkins, N. G. Copeland, and D. L. Court.** 2000. An efficient recombination system for chromosome engineering in escherichia coli. Proc Natl Acad Sci U S A **97:**5978-83.

117. **Zhou, Z. H., D. H. Chen, J. Jakana, F. J. Rixon, and W. Chiu.** 1999.

Visualization of tegument-capsid interactions and DNA in intact herpes simplex virus type 1 virions. J Virol **73:**3210-8.

118. **Zhu, F. X., J. M. Chong, L. Wu, and Y. Yuan.** 2005. Virion proteins of Kaposi's sarcoma-associated herpesvirus. J Virol **79:**800-11.